Dissertation

submitted to the

Combined Faculty of Natural Sciences and Mathematics

of the Ruperto Carola University Heidelberg, Germany

for the degree of

Doctor of Natural Sciences

Presented by

M.Sc. Nitya Mohan

born in: Bangalore, India

Oral examination: 31st August 2021

Investigation of the effect of hypoxia on antigen presentation and T cell-based cytotoxicity of HPV16-transformed cells

Referees Prof Dr. Matthias P. Mayer

PD Dr. Dr. Angelika Riemer

This work was performed from August 2016 –September 2021 under scientific supervision of PD Dr. Dr. Angelika Riemer in the Research Group Immunotherapy and Immunoprevention at the German Cancer Research Center, Heidelberg.

Peer-reviewed publication based on this study

Blatnik R*, Mohan N*, Bonsack M*, Falkenby LG, Hoppe S, Josef K, Steinbach A, Becker S, Nadler WM, Rucevic M, Larsen MR, Salek M, Riemer AB. *A targeted LC-MS strategy for low-abundant HLA class-I-presented peptide detection identifies novel human papillomavirus T-cell epitopes.*
Proteomics 2018, 18(11): e1700390. *Equal contribution

Conference and workshop presentations based on this study

Poster presentation titled "*Investigation of the effect of hypoxia on presentation of HPV16-derived antigens - implications for therapeutic vaccine design*". Nitya Mohan, Maria Bonsack, Jonas Förster, Alina Steinbach, Renata Blatnik, Mogjiborahman Salek, Angelika B. Riemer. *AACR Annual Meeting 2019*

Poster presentation titled "*Investigation of the effect of hypoxia on presentation of HPV16-derived antigens*". Nitya Mohan, Maria Bonsack, Jonas Förster, Alina Steinbach, Mogjiborahman Salek, Angelika B. Riemer. *CIMT-Cancer Immunotherapy 2019*

Poster presentation titled "*Detection of Novel HPV Epitopes by Targeted Mass Spectrometry*" Nitya Mohan, Maria Bonsack, Renata Blatnik, Mogjiborahman Salek, Angelika Riemer. *HUPO-HIPP (Human Proteome Project-Human Immunopeptidome Project) Summer School-2018*

Poster presentation titled "*Targeted LC-MS detection identifies novel immunogenic HLA-A2-restricted T cell epitopes derived from HPV16 E6 and E7*". Bonsack, Maria; Mohan, Nitya, Becker, Sara; Hoppe, Stefanie; Küpper, Marius; Dreßler, Lisa; Schessner, Julia; Blatnik, Renata; Salek, Mogjiborahman; Riemer, Angelika B. *CIMT Cancer Immunotherapy-2018*

Poster presentation titled "*Detection of low abundant HPV16-derived HLA-A2 epitopes on the tumor cell surface by mass spectrometry*". Renata Blatnik, Nitya Mohan, Stephanie Hoppe, Lasse G. Falkenby, Martin R. Larsen, Angelika B. Riemer. *HUPO (Human Proteome Organization) World Congress-2017*

Poster presentation titled "*Mass spectrometry-based identification of HPV16 E6 and E7 T-cell epitopes*". Nitya Mohan, Maria Bonsack, Stephanie Hoppe, Renata Blatnik, Angelika B. Riemer. *11th European Summer School Advanced Proteomics-2017*

Abstract

Human papillomavirus (HPV)-induced malignancies have long been considered the ideal scenario for the development of a therapeutic cancer vaccine, as viral proteins can serve as immune targets. However, the attempts to develop a therapeutic vaccine against HPV-induced malignancies have not been clinically successful to date. One possible reason may be the hypoxic microenvironment present in most tumors, including cervical cancer. Recent studies have shown that hypoxia leads to decreased levels of E6 and E7 proteins in HPV-transformed cells. Hypoxia is also known to dysregulate the levels of HLA I (human leukocyte antigen class I) molecules in the context of different tumors. Furthermore, hypoxia has been reported to both enhance and suppress cytotoxic $CD8^+$ T cell functions. Hence, the aim of this project is to investigate the effect of hypoxia on antigen presentation in HPV16-transformed cells as well as their targeting by $CD8^+$ T cells.

In this study, it was observed that hypoxia led to downregulation of the protein levels of HPV16 oncoproteins E6 and E7 in several cervical cancer cells transformed with different HPV16 variant lineages. More than 24 hours of hypoxia were needed for complete loss of expression of the E7 oncoprotein in HPV16-transformed CaSki cells. Presentation of E6 and E7-derived epitopes on the cell surface, in context of HLA class I (HLA-I) molecules, is essential for recognition and targeting of these cells by cytotoxic T cells. Peptide presentation occurs with the help of a repertoire of proteins (proteasome, transporters, chaperones and enzymes) known as the antigen processing and presentation machinery (APM). Any perturbations in the APM could result in an altered epitope repertoire on the cell surface. Thus, the effect of hypoxia on the APM was investigated in different HPV16-transformed cells, as well as two HPV negative control cells, using label free quantitation (LFQ) mass spectrometry. Next, using flow cytometry, the effect of hypoxia on the surface expression of the HLA-I (HLA-A2) molecule was assessed. Interestingly, no significant change was observed in the expression of any of the APM proteins. The surface levels of HLA-A2 were also not significantly affected by hypoxia in any of these cells. No effect of hypoxia on the APM is promising from the context of therapeutic vaccine design. However, for the success of the vaccines, it is essential that the HPV16-transformed cells are actually targeted by cytotoxic $CD8^+$ T cells. Interestingly, enhanced killing of CaSki cells by E6 and E7-derived peptide-specific $CD8^+$ T cells was observed in a majority of the cases, with the exception of one $CD8^+$ T cell line, which showed suppressed killing upon hypoxia. The contradictory results are however consistent with the contradictory results published about the effect of hypoxia on $CD8^+$ T cells, in the context of different tumors. Enhanced cytotoxicity in most cases was surprising given the results that the target proteins are decreased in hypoxia. Using hypoxia-

preincubated targets, it was demonstrated that the enhanced killing of CaSki cells under hypoxia is suppressed, with the likely reason being the decreased expression of the source oncoprotein under hypoxia. Thus, the inhibitory effect of hypoxia on the target cells seems to supersede the positive effect of hypoxia on the $CD8^+$ T cells. In summary, the results obtained in this thesis provide important insights into the effect of hypoxia on cervical cancer cells and their targeting by $CD8^+$ T cells. The study highlights the importance of considering the effect of the tumor microenvironment (TME), particularly hypoxia, while developing immunotherapies. Incorporating these insights into developing combination therapies will hopefully pave the way to making immunotherapies a mainstream standard of care for HPV-induced malignancies.

Zusammenfassung

Maligne Erkrankungen, ausgelöst durch humane Papillomviren (HPV) wurden lange als ideales Szenario für die Entwicklung von therapeutischen Krebsimpfstoffen angesehen, da virale Protein als Ziele für die Immunantwort dienen können. Allerdings waren die Bemühungen eine therapeutische Impfung gegen HPV-induzierte Krankheiten zu entwickeln bis jetzt nicht in der Klinik erfolgreich. Eine mögliche Erklärung könnte das hypoxische Mikromilieu vieler Tumoren, inklusive Gebärmutterhalskrebs, sein. Jüngste Studien zeigten, dass Hypoxie zu verringerten E6 und E7 Proteinleveln in HPV-transformierten Zellen führt. Ebenfalls ist bekannt, dass Hypoxie zu einer Dysregulation der humanen Leukozytenantigen Klasse I (HLA I) Moleküle in verschiedenen Tumoren führt. Außerdem wurde beobachtet, dass Hypoxie die zytotoxische CD8+ T-Zellfunktion sowohl verstärkt als auch unterdrückt. Daher ist das Ziel dieses Projekts, den Effekt von Hypoxie auf die Antigenpräsentation in HPV16-transformierten Zellen, als auch auf deren Erkennung als Ziele von CD8+ T-Zellen zu untersuchen.

In dieser Studie wurde beobachtet, dass Hypoxie zu einer Herabregulierung der Proteinlevel der HPV16 Onkoproteine E6 und E7 in verschiedenen, mit diversen HPV16 Varianten transformierten, Gebärmutterhalskrebszellen führt. Für einen kompletten Expressionsverlust des E7 Onkoproteins in HPV16-transformierten CaSki Zellen wurden mehr als 24 Stunden Hypoxie benötigt. Die Präsentation von E6 und E7 Epitopen auf der Zelloberfläche via HLA Klasse I (HLA-I) Molekülen ist unerlässlich für die Erkennung dieser Zellen durch zytotoxische T-Zellen. Die Peptidpräsentation geschieht mithilfe eines Proteinrepertoires (Proteasom, Transporter, Chaperone und Enzyme), das als Antigenprozessierungsmaschinerie (APM) bekannt ist. Jede Störung der APM kann in einem veränderten Antigenrepertoire auf der Zelloberfläche resultieren. Deshalb wurden die Auswirkungen von Hypoxie auf die APM in verschiedenen HPV16-transformierten Zellen, als auch in zwei HPV-negativen Kontrollzelllinien mithilfe von markierungsfreier massenspektrometrischer Quantifizierung (LFQ) untersucht. Danach wurde mithilfe von Durchflusszytometrie der Effekt von Hypoxie auf die Oberflächenexpression der HLA-I (HLA-A2) Moleküle gemessen. Interessanterweise konnte keine signifikante Veränderung der Expression jeglicher APM Proteine festgestellt werden. Auch die Oberflächenexpression von HLA-A2 war in diesen Zellen nicht signifikant von Hypoxie betroffen. Kein Effekt von Hypoxie auf die APM ist vielversprechend für das Design von therapeutischen Impfungen. Allerdings ist es für den Erfolg von Impfungen essentiell, dass die HPV16-transformierten Zellen tatsächlich von zytotoxischen CD8+ T-Zellen als Ziele erkannt werden. Interessanterweise konnte in den meisten Fällen eine vermehrte Abtötung von CaSki Zellen durch E6- und E7-peptidspezifische CD8+ T-Zellen beobachtet werden, mit Ausnahme einer CD8+ T-Zelllinie, die

weniger Tötungsaktivität unter Hypoxie zeigte. Diese Daten sind allerdings konsistent mit den widersprüchlichen Daten, die über den Effekt von Hypoxie auf CD8+ T-Zellen in verschiedenen Tumoren publiziert wurden. Die erhöhte Zytotoxizität war in den meisten Fällen überraschend aufgrund unserer Ergebnisse, dass die Zielproteine in Hypoxie vermindert sind. Unter Zuhilfenahme von Hypoxie-vorinkubierten Zielen konnte gezeigt werden, dass die vermehrte Abtötung von CaSki Zellen unter Hypoxie, wahrscheinlich durch verringerte Expression der ursprünglichen Onkoproteine, unterdrückt ist. Daher scheint der inhibitorische Effekt der Hypoxie auf die Zielzellen den positiven Effekt der Hypoxie auf die T-Zellen zu verdrängen. Zusammengefasst geben die Ergebnisse dieser Thesis wichtige Einblicke in den Effekt von Hypoxie auf Gebärmutterhalskrebszellen und deren Erkennung als Ziele von CD8+ T-Zellen. Diese Studie hebt hervor, wie wichtig die Berücksichtigung des Effekts des Tumor Mikromilieus (TME), vor allem der Hypoxie, für die Entwicklung von Immuntherapien ist. Das Integrieren dieser Einblicke in die Entwicklung von Kombinationstherapien wird hoffentlich den Weg bereiten, um Immuntherapien zur etablierten Standardbehandlung für HPV-induzierte maligne Erkrankungen zu machen.

Acknowledgements

I would like to thank PD Dr. Dr. Angelika Riemer, for giving me the opportunity to work in her lab. Her encouragement and support through my PhD have been really helpful. I also like to offer her a special thanks for the opportunities of attending the various conferences and summer schools, where I got my scientific high!

I would also like to acknowledge my TAC members, Prof Dr. Matthias Mayer and Prof. Dr. Jeroen Krijgsveld and thank them for the inspiring discussions and valuable suggestions during the TAC meetings. I would also like to thank Prof. Dr. Ralf Bartenschlager and Prof. Dr. Nina Papavasiliou for being my PhD examiners.

I would like to thank Prof. Dr. Felix Hoppe-Seyler and Prof. Dr. Karin Hoppe-Seyler for their help and suggestions with the hypoxia aspect of the project. Dr. Thomas Ruppert, Roman, Wiebke and Sabine, get a special thanks for being extremely helpful emergency go-to people for any problems with the QTRAP6500 instrument.

I would also like to thank all the members of the group, present and past, who helped me during the various stages of my PhD. A special heartfelt thanks goes to late Monika Bock, who brought a very special warmth to the lab, which was precious. She is deeply missed. A special thanks to Alexandra Klevenz, for being there whenever I was in need of a listening ear to vent my stresses and her help with qPCRs and Western blots. E7 Western blots were performed by Alexandra Klevenz. It made things so much easier to have some help from Rebecca Köhler with some of the pesky HIF1α blots. Renata, thank you for being there during the infamous, inevitable 'Valley of doom' phase of my PhD. Her reminder to introspect on what I really want, and her conviction when she told me that if I really do want something, nothing can stop me, really helped me get through to the other side. Thanks to Christoph, Patrick and Jonas for the spontaneous scientific discussions, sometimes at odd hours, which made it even more fun for the scientist in me! All the other lab members Maria, Sam, Jonas, Sebastian, Mogjib and Nika for the fun and nice times we shared, and your valuable inputs in the lab meetings, especially when I was switching between projects. I would particularly like to appreciate all my students, especially Kathrin Öhlenschläger, Ceren Özerdem and Nisha Veits, for being quick to learn, willing to work at the sometimes odd hours I had, and their valuable contribution to speeding up my project. Internship students Kathrin Öhlenschläger, Ceren Özerdem and Nisha Veits helped with T cell cultures, ELISpot assays and VITAL-FR assays shown in this thesis.

A warm thanks to Anja Reimann, from the Heidelberg Life Science lab, for inviting me to set up the AG Immunology and Vaccination; and then to be a mentor in the AG Immunology and Virology, which was an extremely interesting and fun experience. Interacting with the enthusiastic school students reminded me of my own passion for science, which is sometimes forgotten during a PhD.

I would also like to offer a warm thanks to Millie Baker, with whom I've been on a delightful journey of learning about building authentic self confidence in public speaking. As an introvert, I honestly never imagined I would enjoy public speaking. Thanks a lot to her, and DKFZ for organizing her courses.

Another heartfelt thanks goes to Heike Langlotz from the international office, for making visa extension matters seems like such a breeze.

Outside the lab, I would like to thank Gabriella, for being a delightful friend, having coffee (red wine, lieblich!) with whom was all the therapy one needed. Sunee, Madhura, Damaris, Dikshya, Andrea, Anna-Chiara and Gayatri, a warm thanks to all of you for being such great friends to spend fun times with (mostly eating!). Thanks also to Kai for all the encouraging daily chitchats. A particularly warm thanks to my really precious circle of friends, who despite being spread through the world, provide me with such positive energy to believe in myself, and encouragement to carry on towards my dreams. Thanks for always being there for me! Sometimes the people far away from you can make you feel better than those right beside you. A big warm hug goes to my extended family, for encouraging me to stay strong and not quit even while the rather apocalyptic Covid19 crisis was going on in India. Their reassurances that they would be fine, despite their own stress, are what kept me going. Without their love and support during the various phases of my scientific journey so far, I would probably not be where I am today.

Table of contents

1 Introduction 1

1.1 Human papillomavirus and cancer 1

1.1.1 HPV genome organization and classification 1

1.1.2 Factors influencing differential disease association amongst closely related types 3

1.1.3 Disease burden 3

1.1.4 Infection and life cycle 4

1.2 Immune reactions to viruses and HPV immune evasion 8

1.2.1 Innate immunity to viruses 9

1.2.2 Adaptive immunity to viruses 10

1.2.3 Immunity to HPV 14

1.2.4 Evasion of immune responses by HPV 17

1.3 Preventive and therapeutic approaches to HPV-based malignancies 19

1.3.1 Preventive approaches: preventive vaccines and screening. 19

1.3.2 Therapeutic strategies: chemotherapy, surgery, and therapeutic vaccines. 20

1.4 Tumor microenviroment and hypoxia 25

1.4.1 Aspects of the cervical cancer TME 28

2 Aims 31

3 Materials 33

4 Methods 45

4.1 Cell culture 45

4.1.1 Culturing of cervical cancer cells and controls. 45

4.1.2 PBMC isolation 46

4.1.3 Short-term T cell cultures 47

4.1.4 Autologous DC cultures 48

4.1.5 Semi long-term T cell cultures 49

4.2 Hypoxia treatment of cells 50
4.3 Western Blotting 51
4.3.1 Preparation of protein lysates 51
4.3.2 Protein concentration estimation 51
4.3.3 SDS-PAGE and Western blotting 51
4.4 Flow cytometry 53
4.4.1 FACS staining of cervical cancer cells 53
4.4.2 FACS staining of buffy coats 53
4.5 Mass spectrometry 54
4.5.1 Label free quantification (LFQ) mass spectrometry-based detection of APM components 54
4.5.2 Targeted epitope detection strategy 55
4.6 ELISpot assay 57
4.7 Cytotoxicity assays 58
4.7.1 Labelling of target cells 58
4.7.2 $CD8^+$ T cell isolation 58
4.7.3 Setting up the assay 59
4.7.4 FACS analysis 60
5 Results 63
5.1 HPV16-transformed cells are responsive to hypoxia. 63
5.2 Decrease in HPV16 oncoproteins E6 and E7 upon 24h hypoxia treatment. 65
5.3 Timeline of E7 decrease upon hypoxia in CaSki cells. 67
5.4 Investigating the effect of hypoxia on the APM components 69
5.5 Hypoxia treatment does not affect HLA-A2 expression levels 74
5.6 Mass spectrometry-based detection of HPV16-derived peptides 76
5.7 Selection of HLA-A2 positive donors 81

5.8 Effect of hypoxia T cell memory responses towards HPV16 E6- and E7-derived peptides. 82
5.9 Screening of donors for memory responses against HPV16 E6 and E7-derived peptides 85
5.10 Effect of hypoxia on $CD8^+$ T cell-mediated killing of HPV16-transformed cells. 87
6 Discussion 91
6.1 Hypoxia as a challenge to therapies 91
6.1.1 Importance of targeting hypoxia for successful therapies 92
6.2 Effect of hypoxia on HPV16-transformed cells 92
6.2.1 Hypoxia decreases HPV oncoproteins expression 92
6.2.2 No effect of hypoxia on the APM 93
6.2.3 Effect of hypoxia on $CD8^+$ T cell-mediated killing of HPV16-transformed cells 95
6.3 Conclusion 96
6.4 Open questions 97
6.4.1 Effect of hypoxia on other HLA-I allotypes 97
6.4.2 Irreversible effects of hypoxia on $CD8^+$ T cells 97
6.4.3 Effect of hypoxia on other immune cell subsets in the cervical cancer TME 97
7 References 99
8 Supplementary Figures 106

List of Figures

Figure 1. HPV16 genome..... 1
Figure 2. Antigen processing and presentation to $CD8^+$ T cells. 13
Figure 3. Innate immunity to HPV..... 15
Figure 4. Adaptive immunity to HPV..... 16
Figure 5. Layout for culturing of short-term T cell lines. 47
Figure 6. Layout for culturing DCs..... 49
Figure 7. Layout for culturing of semi-long term T cell lines. 50
Figure 8. Hypoxia treatment of cells..... 50
Figure 9. Layout of VITAL-FR assay. 59
Figure 10. Layout of cultures for normoxic and hypoxic VITAL-FR cytotoxicity assays. 61
Figure 11. HPV16-transformed cells are responsive to hypoxia..... 64
Figure 12. CaSki and C33A cells are responsive to 48h hypoxia. 65
Figure 13. Decrease in E6 protein levels upon hypoxia. 66
Figure 14. Decrease in E7 protein levels upon hypoxia 67
Figure 15. Timeline of E7 expression upon hypoxia in CaSki cells 68
Figure 16 Comparison of sample preparation methods (Sophia Fohr). 70
Figure 17. APM upon 24h hypoxia in selected cells..... 71
Figure 18. APM upon 24h hypoxia in other cells 72
Figure 19. APM upon 48h hypoxia in selected cells..... 73
Figure 20. Effect of 24h hypoxia on HLA-A2 75
Figure 21. Effect of 48h hypoxia on HLA-A2 levels. 76
Figure 22. Comparison of on-column IP with in-solution IP. 77
Figure 23. Optimizing the in-solution IP. 79
Figure 24. Peptides detected in HPV16-transformed cells. 80
Figure 25. Flow cytometry-based selection of HLA-A2+ donors..... 82
Figure 26. Effect of hypoxia on T cell memory responses. 84
Figure 27. Screening donors for memory responses against HPV16 E6- and E7-derived peptides.86
Figure 28. Hypoxia leads to increased killing of target cells. 88
Figure 29. Hypoxia leads to decreased killing of target cells. 88
Figure 30. Pre-incubation of target cells in hypoxia leads to decreased killing under hypoxia..... 89

List of tables

Table 1. List of abbreviations XVIII
Table 2. HPV16 variant lineages and sub-lineages 2
Table 3. List of materials 33
Table 4. List of reagents 36
Table 5. List of cell lines and culture medium 40
Table 6. List of buffers 41
Table 7. List of HLA-A2 binding peptides and control peptides. 42
Table 8. List of peptide pools. 44
Table 9. VITAL-FR assay cell numbers. 60
Table 10. APM components 69

Table 1. List of abbreviations

ALR	AIM-like receptors
APC	Antigen presenting cells
APM	Antigen processing and presentation machinery
ATM	Ataxia telangiectasia mutated kinase
ATR	Ataxia telangiectasia and Rad3 related
B_2M	β 2 microglobulin
BPE	Bovine pituitary extract
BSA	Bovine serum albumin
CALR	Calreticulin
CANX	Calnexin
CARs	Chimaeric antigen receptor
CCL	CC-chemokine ligand
CD	Cluster of differentiation
CDK1	Cyclin-dependent kinase 1
CEF	CMV-EBV-Flu
CFSE	Carboxyfluorescein succinimidyl ester
CIN	Cervical intraepithelial neoplasia
CMV	Cytomegalovirus
ConA	ConcavalinA
COX	Cyclooxygenase
CXCL	Chemokine (C-X-C motif) ligand
DCs	Dendritic cells
DC assay	Detergent-free assay
DMSO	Dimethyl sulfoxide
DNA	Deoxy ribonucleic acid
dsDNA	Double-stranded DNA
EBV	Epstein-Barr Virus
ECL	Enhanced chemiluminescence
ECM	Extracellular matrix
EGF	Epidermal growth factor

EGFR	Epidermal growth factor receptor
EMT	Epithelial to mesenchymal transition
ER	Endoplasmic reticulum
ERAP	Endoplasmic reticulum associated aminopeptidase
FA	Fanconi Anemia
FBS/FCS	Fetal bovine serum/Fetal calf serum
FDR	False discovery rate
FITC	Fluorescein isothiocyanate
Flt3L	Fms-related tyrosine kinase 3 ligand
FR	Far Red
GM-CSF	Granulocyte monocyte-colony stimulating factor
HIF1α	Hypoxia inducible factor 1 α
HIV	Human Immunodeficiency Virus
HLA	Human leukocyte antigen
HPV	Human papillomavirus
HR	High-risk
HRP	Horse radish peroxidase
HSPGs	Heparan sulphate proteoglycans
IDA	Information Dependent Acquisition
IFN	Interferon
Ig	Immunoglobulin
IL	Interleukin
iNKT	invariant natural killer T cell
IP	Immunoprecipitation
JAK-STAT	Janus kinase-signal transducer and activator of transcription
kDa	kilo Daltons
K-SFM	Keratinocyte serum free medium
LBC	Liquid based cytology
LC	Langerhans cells
LC-MS	Liquid chromatography-mass spectrometry
LCR	Long control region

LFQ	Label-free quantitation
LPS	Lipopolysaccharide
LR	Low-risk
MACS	Magnetic-activated cell sorting
MFI	Mean fluorescence intensity
MHC	Major histocompatibility complex
miRNA	microRNA
MRM	Multiple reaction monitoring
MS^3	Tandem mass spectrometry (3 mass analyzers in tandem; MS/MS/MS)
MDSCs	Myeloid-derived suppressor cells
MVA	Modified Vaccinia virus Ankara
MW	Molecular weight
MyD88	Myeloid differentiation primary response 88
NBT/BCIP	Nitro blue tetrazolium/5-Bromo-4-chloro-3-indolyl phosphate
NFκB	Nuclear factor kappa light chain enhancer of activated B cells
NK	Natural Killer
NLR	NOD-like receptor
ORF	Open reading frame
P/S	Penicillin/Streptomycin
PAMPs	Pathogen associated molecular patterns
Pap smear	Papanicolou smear
PBMC	Peripheral blood mononuclear cells
PBS	Phosphate buffered saline
PGE2	Prostaglandin E2
PHD2	Prolyl hydroxylase domain containing protein 2
PIDCs	Pre-immune dendritic cells
pRb	Retinoblastoma protein
PRR	Pattern recognition receptors
PV	Papillomaviridae
pVHL	Von Hippel-Lindau tumor suppressor protein
RANKL	Receptor activator of nuclear factor kappa-B ligand

RLR	RIG-like receptor
RNA	Ribonucleic acid
SD	Standard deviation
SFU	Spot forming units
SI	Stimulation index
SLP	Synthetic long peptide
ssDNA	Single-stranded DNA
TAAs	Tumor associated antigens
TAMs	Tumor associated macrophages
TAP	Transporter associated with antigen processing
TAPBP	TAP binding protein
TCR	T cell receptor
TGF	Transforming growth factor
TILs	Tumor-infiltrating lymphocytes
TLR	Toll-like receptors
TME	Tumor microenvironment
TNF	Tumor necrosis factor
TORC1	Target of Rapamycin complex 1
VIA	Visual inspection with acetic acid
VILI	Visual inspection with Lugol's iodine
VLP	Virus like protein
WHO	World Health Organisation

1 Introduction

1.1 Human papillomavirus and cancer

Human papillomaviruses (HPVs) are non-enveloped double-stranded DNA viruses belonging to the Papillomaviridae (PV) family. Several studies, dating back to as early as the 1970s, showed a causal link between HPV and cancer. However, the recognition of the discovery of the causal link between HPV and cancers by awarding the Nobel prize in 2008 to Prof. Harald zur Hausen revived interest in a major alternative therapeutic avenue for these cancers [1, 2], other than the prevalently used chemotherapy and surgery which have severe side effects.

1.1.1 HPV genome organization and classification

HPV has a genome consisting of 8000 base pairs, which is divided into the early region, the late region, and the long control region (LCR). The early (E) region consists of seven open reading frames (ORFs) E1, E2, E4, E5, E6, E7 and E8, which encode regulatory proteins. The late (L) region encodes the minor and major capsid proteins (L1 and L2). The LCR contains the origin of replication and the transcription control sequences [3]. Out of the ORFs, E1, E2, L1 and L2 are essential for ensuring viral replication and shedding of the matured virus. These are present in all PVs. The E5 and rarely the E6 ORFs can be missing from certain HPV genomes [4]. The E8 ORF is an alternative reading frame in the E1 region of the genome. This region encodes a repressor protein for viral transcription and is present in all PVs [4, 5] (Figure 1).

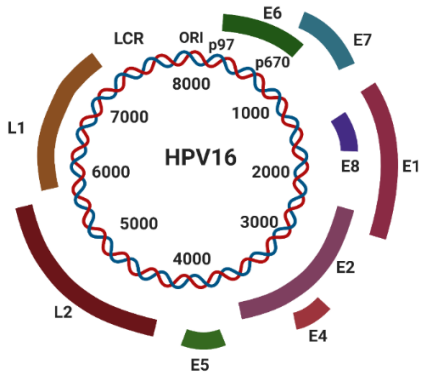

Figure 1. HPV16 genome.
The HPV16 has an 8000bp genome. It comprises of early genes (E1, E2, E4, E5, E6, E7 and an alternative ORF E8), late genes (L1 and L2) and the long control region (LCR). The origin of replication (ORI), and the early promoter (p97) and late promoter (p670) are marked. The early genes encode regulatory proteins, which play a role in the early phase of the viral life cycle, required for viral genome replication. The late genes encode the capsid proteins and are only required during the later stages of virus assembly and maturation. The LCR encodes the origin of replication and the transcription control sequences. Created with BioRender.com.

The L1 ORF is the most conserved gene within the PV genome and can be aligned for all known PV types. Thus, the L1 ORF is used for the classification of these viruses. PVs having less than 60% similarity within the L1 part of their genome are classified into different genera. A letter from the Greek alphabet is used to define each genus, with the prefix dyo- being added once all the letters are used. Within each genus, a species shares an L1 sequence similarity between 60-70%, and derives from a common ancestor. Currently identified HPV types are classified into 5 genera (α, β, γ, μ and η) and 49 species. An HPV type is defined as having a variation of at least 10% in the L1 sequence, from other known types [6, 7]. Due to advances in metagenomics sequencing, new HPV types are being discovered rapidly. Newly discovered types are identified by a unique number once they have been successfully cloned and re-sequenced by the HPV reference center [8]. An efficient analysis of the genome sequences of the PV family is achieved with the help of the Papillomavirus Episteme, a web-based tool that enables efficient storage, analysis and exchange of information. Currently, there are 65 HPV types in the α genus, 52 types in the β genus, 97 types belonging to the γ genus, 3 types belonging to the μ genus and 1 type in the η genus [9]. Within a type, a variation between 1-10% in the whole genome leads to the classification of different variant lineages, previously called subtypes. Sublineages are a further subgroup within the variant lineages characterized by a difference of a minimum of 0.5% to a maximum of 1% in the whole genome alignment amongst each other (Table 2). Recent studies have used complete genome alignment, along with phylogenetic classification, to define variant lineages and sublineages. Since there are more than 200 HPV types, classification has been useful in studying patterns of disease association [10].

Table 2. HPV16 variant lineages and sub-lineages

HPV16 variant lineage	HPV16 variant sub-lineage	Other names
A	A1	European (E)
	A2	European (E)
	A3	European (E)
	A4	Asian (EA)
B	B1	African 1
	B2	African 1
C	-	African 2
D	D1	North American 1
	D2	Asian American 2
	D3	Asian American 1

1.1.2 Factors influencing differential disease association amongst closely related types

Apart from the genotype of the virus, other factors play a role in determining HPV pathogenicity. One of the important factors includes the site of viral infection (tissue tropism). Different PV types have developed different life cycle strategies to survive at different epithelial sites. This is rooted in the long term coevolution of these viruses with their host species [11] since their origin 450 years ago [4]. Such a long, gentle evolution, in combination with the ecological niches created by tissue tropism [12, 13], resulted in differences in the oncogenicity of related HPV types. Based on tissue tropism, HPV types belonging to the α genus are classified into cutaneous and mucosal types. The mucosal types are further subdivided into low-risk (LR) and high-risk (HR) types. The LR types are associated with benign skin warts and are not associated with neoplasia, except in some immunocompromised individuals. The HR HPV types are responsible for a large proportion of oropharyngeal and anogenital cancers [11]. Out of the 218 currently known HPV types which have been sequenced [9], twelve types (HPV16, 18, 31, 33, 35, 39, 45, 51, 52, 56, 58, 59) have been defined as carcinogenic [14]. Also, eight types (HPV26, 53, 66, 67, 68, 70, 73, and 82) have been classified as probably or possibly carcinogenic [4, 14]. In addition, different pathogenicity has been observed for different HPV16 variants. These variants show a different geographical distribution throughout the world [15].

1.1.3 Disease burden

It is estimated that more than 80% of men and women in the U.S. are infected by at least one HR HPV type under the age of 45 [16]. Most HPV infections are spontaneously cleared or result in 'silent' infections where the viral genes are not expressed. Progression from HR HPV infection to cancer can occur over decades and is dependent on the regulation of the viral gene expression [11]. During this time, cancer development occurs via a progression through early to late/advanced stages. Non-malignant, early-stage lesions are termed CIN1 (cervical intraepithelial neoplasia grade 1), while higher-grade lesions are called CIN2 or CIN3 (cervical intraepithelial neoplasia grade 2 and 3, respectively), which can ultimately progress to cervical cancer. [11]

HPV is responsible for as many as 4.5% of all new cancer cases worldwide per year. As per a survey in 2012, 54% (630,000/1,200,000) of anogenital (cervical, anal, vulvar, vaginal, and penile) and oropharyngeal (oropharyngeal, laryngeal, and oral) cancer cases were associated with HPV infection globally, with cervical cancer accounting for the largest number of cases (530,000). Out of the over 200 HPV types [9], HPV 16 and 18 together are responsible for 70.8% of cervical cancers (370,000/530,000) [14]. As of 2018, cervical cancer was the 4th most common cancer in women worldwide and causes over 300,000 deaths annually [17].

According to the latest WHO GLOBOCAN survey based on 185 countries, the average age of incidence of cervical cancer was estimated at 53 years, and the average age of mortality was 59 years [17]. The preventive vaccines and screening strategies have led to a decline in incidence and mortality worldwide, with exceptions in some geographical regions. However, despite the decline, with 7.5% cervical cancer deaths amongst all cancer deaths, it remains notorious as the fourth most common cause of cancer-related deaths [17].

Contradictory reports exist regarding differences between HPV16 variant lineages regarding contribution to CIN3 development [10, 18-20]. A study based in Denmark showed not much of a difference between lineages, in terms of risk of progression to CIN3 [18]. However, other studies, based in Central and North America have shown an increased risk of progression to CIN3 associated with HPV16 NE lineages (lineages B, C and D), as compared to European lineages (lineage A) (Table 2) [19, 20]. Taken together, closely related lineages might differ in their pathogenicity and prevalence, and it is of interest to study these differences more closely.

Irrespective of these differences, what is established is that there is an intricate regulation between viral life cycle and the development of cancer. The interplay between viral gene regulation and the stages of cervical neoplasia is further explained in the following section.

1.1.4 Infection and life cycle

1.1.4.1 Productive infection

Productive infection is a feature of both HR and LR HPV infections. It is characterized by an ongoing virus replicative life cycle, with regulated expression of viral genes, and – in the case of HR types – leads only to early lesions (CIN1 or equivalent) [11]. Given its long-term coevolution with the host, it is not surprising that the life cycle of HPV is closely adapted to the growth of the infected host squamous epithelial cells. While HPV can only infect the dividing basal cells in the squamous epithelium, the viral progeny is produced in differentiated daughter cells in the uppermost layers of the epithelium [11, 21]. As reviewed by Harden & Münger . [3], the life cycle of HPV consists of stepwise regulated expression of viral genes and regulation of host genes. The **first stage** is the entry of HPV into the host cells. Infection occurs through micro-abrasions that expose the basal epithelial cells, which are otherwise protected by several layers of differentiated cells. These are the only cells in the epithelium capable of proliferation, hence infecting these is crucial for persistent infection [3]. Besides, cells with a unique morphology and gene expression signature located in the squamocolumnar transformation zone in the cervix and anus are exceptionally vulnerable to HPV infection [22].

Upon exposure of the basal cells or the exposed basement membrane, the viral L1 capsid protein binds to heparan sulfate proteoglycans (HSPGs) on the basement membrane, which serve as the primary attachment receptors [3]. This binding leads to a conformational change in the virus capsid, followed by endocytosis of the virus into the host cell by a mechanism similar to macropinocytosis. Once inside the acidified endosomes, the viral L1 protein is targeted for degradation. Subsequently, the minor capsid protein L2 helps in the exit of the viral genome from the endosomes and its transport from the cytosol to the nucleus by interaction with host sorting proteins (sorting nexin 17 and 27) and a motor protein (dynein). The L2 protein also helps in the entry of the viral genome complex into the nucleus as well as initial genome amplification and transcription [3, 4]. Entry into the nucleus is considered the critical point in the establishment of infection. However, this is only sufficient for genome maintenance, and 'silent' infection. The regulation of viral gene expression in 'silent' infection is not well elucidated [11]. The early viral proteins are crucial for vegetative viral DNA replication, which is needed to produce genomes for the production of new virions [3, 21]

HPV early proteins E1 and E2 are involved in viral genome replication, which is the **second stage** of the HPV life cycle [3]. The E1 protein is the only enzyme encoded by the PVs [23]. It functions as an ATP dependent helicase. It binds to AT-rich sequences at the origin of replication and is involved in the initiation and elongation phases of viral DNA synthesis. It is required for viral episome replication and maintenance during all phases of the viral replicative cycle [3, 23]. Two splice forms of the E2 protein are encoded by all PVs with different functions [5]. The full-length E2 protein stabilizes the interaction of E1 to the origin of replication, leading to high affinity binding of the E1/E2 complex to the viral origin of replication. HPV does not encode any other replication enzymes and depends on hijacking the host DNA synthesis machinery for replicating the viral genome. To enable this, E1 and E2 recruit host DNA polymerases and other essential accessory enzymes [3]. The short length E2 transcript functions as a repressor of full-length E2. Repression of full-length E2 has been observed to increase the expression of E6 and E7 early proteins, the main viral oncoproteins. In the context of a productive life cycle, the viral proteins E6 and E7 are responsible for reactivating the host DNA replication machinery in differentiating cells of the epithelium as these usually withdraw from the cell cycle after their exit from the basal layer of the epithelium. Early proteins E6 and E7 help maintain these cells in the proliferative state needed for viral replication [3].The E6 protein can bind to a variety of cellular proteins via interaction with the LXXLL peptide motifs and the PDZ domain on the target proteins [24]. Repression of pro-apoptotic p53, the main target of E6, helps maintaining cells in the proliferative state.

The global cellular transcription downstream of p53 is also regulated by E6. Apart from this, E6 proteins regulate numerous other cellular pathways, namely: cellular metabolism (primarily via the mTORC1 pathway), cellular apoptosis (regulated by Bax, Bak, and Bcl2 proteins), the immune response (by regulation of NFκB activation) as well as the expression profile of several microRNAs [24]. Most of the functions of E6 occur in close coordination with the E7 protein [3, 24]. The main target of the HPV E7 proteins are the pocket proteins p107 and p130 and the retinoblastoma tumor suppressor protein pRb. Inhibition of the pocket proteins leads to the release of the host transcription factor E2F from the pocket protein-bound transcription repressor complexes. This leads to constitutive activation of DNA synthesis and loss of pRb-mediated control of the cell cycle and uncontrolled cell proliferation . HPV E7 also inhibits CDK1 inhibitors, thereby avoiding triggering the G1-cycle arrest in epithelial cell differentiation. This allows the viral proliferation to continue in differentiating cells [3, 11, 25]. In the context of avoiding apoptosis in these constantly proliferating cells, another crucial function of the early proteins E1, E2, and E7 is the hijacking the host DNA damage repair pathways. These viral proteins regulate the ATM (ataxia telangiectasia mutated) pathway, the ATR (ataxia telangiectasia and Rad3 related) pathway, and the FA (Fanconi anemia) pathway to recruit DNA replication and repair factors and enable cell proliferation and subsequently viral genome maintenance [26, 27]. The transcription and translation of the E6 and E7 proteins from HR and LR HPVs are regulated differently. In LR HPVs, both E6 and E7 are regulated by an upstream promoter each[28]. However, in HR HPVs, both E6 and E7 are regulated by a single promoter upstream of E6, and a polycistronic mRNA is transcribed. The relative levels of E6 and E7 proteins in HR HPVs are dependent on the used splice site [29]. Functionally, interestingly only LR HPV E6 inhibits the NOTCH signaling pathway, which is essential for keratinocyte differentiation [30, 31], and not the HR HPV E6 [11]. Major consequences of the regulation of various cellular pathways by E6 and E7 are sustained cell proliferation and successful replication of viral genomes. The late stage of the viral development is regulated by the viral major late promoter, which is situated in the *E7* gene region. Activation leads to the upregulated expression of E1, E2, E3, and E4 proteins, and the late proteins E4 proteins are involved in genome amplification in HR HPV types, but not in LR HPV [26]. Given its activation only in the later stages of the viral life cycle, it has been observed that the absence of E4 protein does not perturb the ability of HR HPVs (HPV16, 18 and 31) to maintain a basal proliferative state and drive host cell proliferation [32]

The **last stage** of HPV infection is the assembly of viruses and the release of mature viruses from the cells. This step occurs in terminally differentiated keratinocytes after viral genome replication and expression of viral proteins are complete. The maturation of virus particles involves the accumulation of a disulfide bond between the L1 proteins, leading to increased stability of the capsid.

This process is relatively slower compared to other viruses [33]. The viral genome is packaged into capsids comprised of L1 and L2 capsid proteins in the nucleus [4, 11]. L1 proteins can form capsid-like structures (virus-like particles, VLPs) on their own, but the process is enhanced by L2 [3].

E4 proteins contribute to the release of the virus by binding to and disrupting host cells cytokeratin filaments [4, 32]. Once assembly is completed, HPV does not cause lysis of host cells but mature viruses are released naturally upon shedding dead, terminally differentiated host keratinocytes from the epithelial surface [3, 21].

1.1.4.2 Non-productive infection and HPV-induced cancer

Chronic infection of cells with HR HPV can lead to high-grade lesions, termed CIN2 and CIN3, and eventually to cervical cancer [11] and the other cancers mentioned above. These are a consequence of the dysregulated expression of HPV proteins, where no virus particles are produced. This is termed a non-productive infection [3]. Such dysregulation of gene expression is frequently associated with the integration of the viral DNA into the host genome [3, 4]. The integration of an HR HPV is associated with 83% of cervical cancers. The frequency of integration varies with the HPV type. HPV16 can be present as episomal DNA, integrated DNA, or both, while HPV18 is almost always present in the integrated form [4]. Amongst the five most common HR types, HPV16, 18, and 45 were seen to have a much higher frequency of integration compared to HPV31 and 33 [34]. Integration of viral DNA has also been seen to increase with the severity of disease [35], with precancerous lesions more frequently having episomal viral DNA [34]. Integration mostly occurs in the E1/E2 region, leading to disruption of the E2 sequence. As mentioned earlier, the full-length E2 protein is an inhibitor of E6 and E7 expression. In the absence of this regulation, E6 and E7 are overexpressed [36]. It is considered that E6 and E7 expression increases with the progression of cervical intraepithelial neoplasia from the CIN1 to the CIN3 stage [3, 37]. The higher expression levels of E6 and E7 oncoproteins contribute to cellular transformation only in non-productive HR HPV infections [11].

As alluded to previously, the functional difference between LR and HR HPV E6 and E7 proteins is considered to contribute to the higher transforming ability of the HR HPV types [28]. The stronger and irreversible suppression of p53, solely by HR HPV E6, allows the cell cycle to proceed despite accumulating DNA damage and cellular stress caused by aberrant entry into the S phase. In addition, only HR HPV E6 upregulates telomerase activity, thus leading to the maintenance of telomere length despite repeated cell proliferation. Also, cell contact and signaling pathways are regulated by HR HPV E6 protein [3, 11]. HR HPV E7 also displays a stronger inhibition of pRb than LR HPV E7 as detailed above [28].

HR HPV E7 is involved in the dysregulation of the cell cycle via the regulation of multiple cellular pathways. It dysregulates the cell cycle by mitigating cell cycle arrest and promoting mitosis by interaction with various regulatory proteins. It also abrogates apoptosis via several pathways. It additionally modulates cytokine signaling pathways including the TNFα, TGFβ and IFNα pathways. Unlike the LR HPVs, HR HPV E7 has also been shown to alter the metabolism of the host cells [25]. The continuous cell cycle, accumulation of DNA damage and resistance to apoptosis are all key contributors to the transformation of host cells. The transforming ability of E6 and E7 is further enhanced by the E5 protein, which is relatively less studied [3, 38]. The E5 ORF is absent in certain HPV types, and this site is also frequently disrupted during genome integration. This indicates that the role of E5 is in the early stages of carcinogenesis rather than in maintenance or progression of infection. The best studied E5 protein is that of HPV16. Via regulation of EGFR (epidermal growth factor receptor), the E5 protein regulates cell cycle progression and potentiates the immortalization effects of E6 and E7. It also inhibits apoptosis by downregulating miR196a, which is required for cell proliferation, decreasing levels of proapoptotic proteins Bak and Bax and increasing expression of anti-apoptotic Bcl2 [4, 39]. The non-productive pathway is generally considered the classical route for the transformation of HPV-infected cells and the progression of malignancies. However, in light of the fact that integration is a not a prerequisite in all HPV-induced cancers [34], some recent studies have elucidated alternative pathways dependent on E2/E4 and E5 proteins. [40]. For this thesis, I will focus mainly on the E6 and E7-driven classical non-productive pathway.

In addition to viral infection and the dysregulation of host cellular pathways, other factors play an important role in disease progression. One factor involves the site of infection or tissue tropism (section 1.1.2). Another important factor is the interaction of the virus with the immune system, which is of interest in the development of immunotherapies.

1.2 Immune reactions to viruses and HPV immune evasion

Our immune system is a key factor that protects us from numerous pathogens surrounding us. As a brief introduction, the immune system can be thought of as comprising two arms, the innate immunity, which is non-specific, and the adaptive immunity, which is pathogen-specific. While categorization into these arms helps with understanding the complex immune response, it is important to note that they act in concert with each other, and not independently [41]. For this thesis, I will focus on introducing immunity in an antiviral context.

1.2.1 Innate immunity to viruses

Innate immune defences are the initial defence mechanism against infectious diseases. The first line of defence is represented by non-specific barriers which prevent the entry of pathogens into the body. A physical barrier can be provided in the form of an impenetrable epithelial surface or by preventing entry through mucous secretions or cilia. Another preventive mechanism is the natural flora of the host, which prevents infection by outcompeting the invading pathogen. Physiological barriers which prevent infection include body temperature and pH levels. Alterations in either of these can inhibit or slow down the growth of the invading pathogen [41]. The complement system, the humoral part of the innate immune system, is composed of an array of soluble proteins and plays an important role in both innate and adaptive immunity, and can provide another line of defense against pathogens [41]. Infection can trigger inflammation, which leads to the recruitment of innate immune cells, including phagocytes and antigen-presenting cells (APCs), which help to control infection [41, 42]. Most components of innate immunity recognize infection through non-specific pattern recognition receptors (PRRs). These are receptors that recognize molecular patterns present commonly across a range of pathogens as signals for activation. These molecular signals are called pathogen-associated molecular patterns (PAMPs), some examples of which include ss/dsRNA, ssDNA, or CpG DNA motifs, in the context of viruses. The toll-like receptor (TLR) family represents the main category of PRRs. It comprises several proteins, which have different cellular localizations. These PRRs work through downstream pathways, which include either transcription factors named interferon regulatory factors (IRFs) or a myeloid differentiation primary response gene 88 (MyD88) dependent pathway. The role of TLR3 is best characterized in the recognition of most RNA viruses [42]. TLR7 and TLR8 are expressed on different dendritic cell populations in humans, and recognize ssRNA. TLR9 recognizes ssDNA genomes [43]. Via different downstream mechanisms, the activation of these TLR signaling pathways leads to the production of type I interferon, which is a type of cytokine. Type I interferons (IFN-α and IFN-β) are key players in the innate immune response against viruses [43]. They are produced majorly by monocytes, macrophages and fibroblasts, as well as infected cells. IFNα/IFNβ bind to their corresponding receptors and activate the JAK-STAT signaling pathway, which leads to the inhibition of viral replication by the degradation of viral RNA or inhibiting viral protein synthesis, or by enhancing the recognition and thus killing of virally infected cells. Another pathway downstream of TLR signalling is the NFκB pathway, which is dependent on MyD88 activation. The NFκB pathway is an important pathway involved in regulating the transcription of cytokines in response to cellular stress [41]. Other classes of PRRs, such as NOD-like receptors (NLRs), RIG-like receptors (RLRs), and AIM-like receptors (ALRs) can detect by-products of viral replication [43]. The activation of these pathways leads to the secretion of

interleukins IL-1β and IL-18, apart from the activation of the type I IFN pathway [43]. Innate immune cells, such as macrophages, natural killer (NK) cells and neutrophils, contribute to the prevention of viral infection. Macrophages are phagocytes generated from monocytes. Based on their differentiation mode, they are classified into M1 (classically activated) or M2 (alternatively activated) macrophages. M1 macrophages secrete pro-inflammatory cytokines, while M2 macrophages are anti-inflammatory [44]. NK cells are activated by IFN-α, IFN-β, IL-12 and IL-18, and they constitutively express perforin and granzyme B, which help kill target cells. They also produce IFN-γ, which helps activate the cellular components of the adaptive immune system[42] [41]

Epithelial cells, as well as phagocytic cells, produce antimicrobial peptides called defensins. These are 29-35 amino acids containing cysteine-rich structures, which have an inhibitory effect against viruses [41, 42]. NK cells recognize decreased MHC I surface presentation and damage signals on virally infected cells and can secrete molecules leading to the killing of target cells [42].

1.2.2 Adaptive immunity to viruses

The adaptive immune response is the second stage of antiviral immunity. It is characterized by higher specificity for the virus than the non-specific innate immune responses. It again includes two types of immunity, humoral and cell-mediated. Humoral adaptive immune responses are mediated by antibodies, which are generated by B lymphocytes. There are 5 classes of antibodies (IgA, IgD, IgE, IgG, and IgM). Out of these, secretory IgA plays a role against some viruses, since it is secreted into the mucus, thereby protecting the epithelial barriers. IgA is the first antibody type to be secreted in an antiviral immune response and is crucial for the defence against polioviruses, influenza viruses, etc [42]. Other antibody classes such as IgG and IgM also play a crucial role in protection against viruses, dependant on the cytopathic nature of the invading virus. Viruses which are acutely cytopathic (such as vesicular stomatitis virus) induce high titres of neutralizing IgG and IgM early during infection (0 - 4 days post infection). In contrast, poorly cytopathic viruses only induce weak antibody responses much later (60 days post infection) [45]. Antibodies are important in long term antiviral responses, which is evidenced in the fact that individuals suffering from X-linked agammaglobulinemia (a disease characterized by the inability to synthesize all classes of antibodies) have defective long term antiviral responses [42]. Antibodies also provide a link with the innate immune system. E.g., macrophages can bind to certain classes of antibodies and thus can target antibody-coated viruses [41]. Antibodies, however, are unable to eliminate an invading virus. This is where cell-mediated immunity becomes crucial. Three cell types function as professional antigen-presenting cells (APCs), which are dendritic cells (DC), macrophages, and B-lymphocytes. These are innate immune cells which act as a bridge between innate and adaptive immune systems [41, 42].

It is of note that an initial innate immune response is a prerequisite before the adaptive immune system can be activated via APCs. Out of the different types of APCs, DCs are the most efficient [42]. Professional APCs in the skin include Langerhans cells (LCs) in the epidermis and three other classes of DCs in the dermis. LCs differ functionally and phenotypically from the other DCs in the dermis [41].

The LCs express a limited repertoire of TLRs (TLR 1, 2, 3, 6, and 10), and they release IL-15, thereby promoting a T cell response. Dermal DCs have a wider repertoire of TLRs and secrete a wider repertoire of cytokines (IL-1α, TGFβ, IL-10, IL-12, GM-CSF, IL-6 and IL-8 secreted by the $CD14^+$ DCs). An effective immune response in the skin requires both LCs and other DC repertoires. The APCs are responsible for the presentation of viral antigens to T lymphocytes (also called T cells) [41]. LCs are particularly important in this role, since they are able to interact with keratinocytes through tight junctions, and sample antigens. Upon maturation, these cells then travel to the lymph nodes and can prime T lymphocytes [46]. T lymphocytes are responsible for releasing cytokines that regulate innate and adaptive immunity and are the main cell type responsible for killing virally-infected cells. T lymphocytes are primarily divided into two types based on the expression of CD (cluster of differentiation) molecules on their surface. There are $CD4^+$ T helper cells and $CD8^+$ cytotoxic T cells. Both these populations can be further differentiated into effector cells or memory cells. Depending upon which cytokines they are exposed to, naïve $CD4^+$ T cells can differentiate into different effector cell populations (Th1, Th2, Th9, Th17, Th22, Tregs, and Tfh). Each of these has a specific cytokine signature and characteristic roles in the inflammatory process [47]. Memory cells can be further classified as tissue-resident, central memory, and effector memory cells [48]. Continued activation of cytotoxic T lymphocytes requires the simultaneous activation of helper T lymphocytes ($CD4^+$ T cells), which produce cytokines required to activate killing by cytotoxic T lymphocytes [49].

1.2.2.1 Antigen presentation.

Viral antigens can be presented on the cell surface of APCs or infected cells by various antigen presentation pathways. Endogenously produced antigens from viruses that directly infect APCs can be presented on the cell surface in the context of the MHC I (major histocompatibility complex class I) molecule. This is important for antigen recognition by $CD8^+$ T cells. The other pathway involves the presentation of extracellular antigens. These can either be directly presented on the MHC II molecule to $CD4^+$ T cells or cross-presented via the MHC I pathway to $CD8^+$ T cells [41, 50]. The latter is termed as cross-presentation because usually only endogenous antigens are presented via the MHC I pathway. MHC I is expressed on all nucleated cells, and thus viral antigens are also presented on infected cells via this pathway. The MHC in humans is called the HLA (human leukocyte antigen) complex . Thus the terms MHC I and HLA I are used

interchangeable in the text. The genes encoding the HLA I are highly polymorphic and each individual can express up to 6 HLA allotypes, 2 of each of the major genes HLA-A, B and C [41].

Since most of the polymorphism occurs in the peptide-binding groove of the MHC molecule, this leads to variations in the repertoire of peptides depending on the alleles expressed. However, despite the polymorphism, the different allotypes can be clustered into supertypes, which are largely similar in the characteristics of the bound peptides [51, 52].

The MHC I antigen presentation and processing pathway consists of the proteasome, the enzymes involved in peptide trimming, transporters, and chaperone proteins, and the MHC class I molecule. Together, these components comprise the antigen processing and presentation machinery (APM). The process of presentation of an antigen on the cell surface in the context of MHC I can be summarized in three steps, as described below (Figure 2) [41]

Proteasomal degradation

The proteasome is a cylindrically shaped multimeric protein, comprised of a catalytic core and regulatory subunits. Its function is to degrade proteins into peptide fragments [41]. In conditions of an intensified immune response, some of the proteolytic core subunits (PSMB 5, 6 and 7) are replaced by functionally different counterparts, namely PSMB 8, 9, 10 (also referred to as LMP7, LMP2 and LMP10, respectively [53]) [54]. Proteasomes incorporating the PSMB 8, 9 and 10 are called immunoproteasomes. They are induced in most cells in response to type I and type II IFNs, and other immune signals [53, 55] and are expressed constitutively in some immune cells. Immature DCs have equal amounts of proteasome and immunoproteasome, while mature DCs have only immunoproteasomes [56]. Immunoproteasomes have a chymotryptic-like activity and thus produce peptides which better fit the MHC I peptide binding site, leading to more optimal sensitization of T cells [55].

Peptide trimming and transport into the ER

Once a protein has been degraded into peptides by the proteasome, these peptides are trimmed to the right size for loading on the MHC molecule by various cytosolic peptidases. The next step is the transport of these peptides into the endoplasmic reticulum. This is done with the help of the TAP (transporter associated with antigen processing) proteins (TAP1 and TAP2). TAP transports peptides between 8 - 12 residues most efficiently into the endoplasmic reticulum (ER).

Within the ER, the peptides are further trimmed. This is done by aminopeptidases (ERAP1, ERAP2). ERAP1 (ER aminopeptidase associated with antigen processing 1) is called the molecular ruler because of its

specific trimming of peptides of 10 - 16 residues while sparing peptides between 8 - 9 residues, which is the optimal length for MHC I binding [56, 57].

MHC I loading in the ER and transport to the cell surface

The final step is the assembly of the peptide-MHC I complex. This requires the help of various chaperone proteins (tapasin, calnexin, calreticulin, and ERp57), which together form the MHC I loading complex. Calnexin and ERp57 facilitate completion of the folding and correct oxidation of the MHC I heavy chain. Binding β-2-microglobulin to the heavy chain then leads to the release of calnexin and binding of the MHC I/β-2-microglobulin complex to calreticulin. Tapasin aids the entry of peptides into the ER by bridging MHC I molecules to TAP. It also stabilizes the peptide-MHC I complex. After peptide binding, the chaperones are released and the peptide-loaded MHC I is transported to the cell surface for the presentation of the peptide to $CD8^+$ T cells [56].

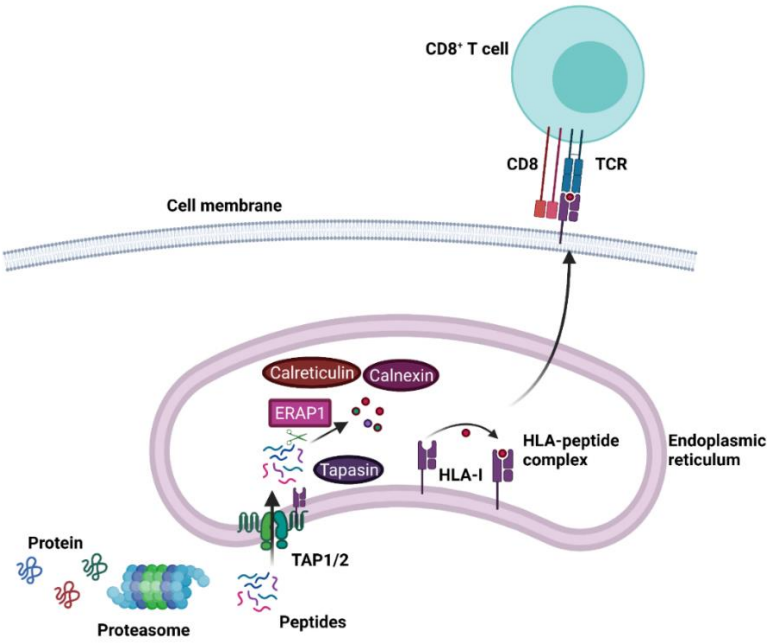

Figure 2. Antigen processing and presentation to $CD8^+$ T cells.
Peptide loading onto HLA-I molecules is done with the help of a repertoire of proteins collectively called the antigen processing and presentation machinery. Proteins are degraded into peptides by the proteasome., transported into the endoplasmic reticulum (ER) with the help of transporter proteins (TAP1 and TAP2). This entry is facilitated by a chaperone protein named tapasin. Within the ER, the peptides are trimmed to the correct size to fit into the HLA-I molecule's peptide binding groove with the help of aminopeptidases (ERAP). Loading onto the HLA-I molecule requires the help of other chaperone proteins (calnexin, calreticulin). The peptide-HLA-I complex is then transported to the cell surface, where it can be recognized by $CD8^+$ T cells. Created with BioRender.com.

1.2.2.2 Activation of T lymphocytes

Antigen uptake and presentation by professional APCs with appropriate costimulatory signals is essential for a primary adaptive immune response. When presented with an antigen in the absence of costimulatory signals, T cells become anergic and subsequently unable to be activated even in the presence of professional APCs[42]. $CD4^+$ T cells play an essential role in the activation of $CD8^+$ T cells. Antigen presentation by MHC II in APCs occurs by a similar pathway with the help of a slightly different APM. This leads to the activation of $CD4^+$ T cells. Once activated, $CD4^+$ cells activate DCs, leading to an upregulation of the maturation markers CD80/86 on the DCs. CD80/86 interaction with CD28 on naïve $CD8^+$ T cells leads to the priming of these T cells. Once primed in the lymph node, the $CD8^+$ T cells differentiate into effector cells, which are capable of recognizing the same peptide-MHC I complex on any cell and of killing the target cell [50]. Both $CD4^+$ and $CD8^+$ T lymphocytes are involved in the elimination of virally infected cells [41]. $CD8^+$ T cells secrete IFN-γ and induce target cell lysis through the secretion of granzyme B and perforin [41]. While also secreting IFN-γ, accumulating evidence suggests that also $CD4^+$ helper T cells can mediate cytotoxicity by activating caspase-mediated apoptosis in target cells [58].

Another special population of T cells are invariant natural killer T cells (iNKT), which express an invariant α chain in their TCR. These cells are restricted to the CD1d molecule (instead of MHC), and their main function is the rapid production of cytokines (IFN-γ, and interleukins IL-4 and IL-10) in response to stimulation by viral glycoproteins, which can be presented on CD1 proteins on host cells [41]

1.2.3 Immunity to HPV

Almost 90% of anogenital HPV infections are cleared within 2 years in immunocompetent individuals [59]. This indicates that a successful immune response is capable of controlling the infection. Both innate (Figure 3) and adaptive immunity (Figure 4) play a role in clearing HPV infections [60]. The first line of defense against HPV is the skin/mucosa. As HPV enters the epithelium through micro-abrasions, tissue damage is the first initiating signal for innate immune defences against HPV. Tissue damage leads to the infiltration of innate immune cells such as neutrophils and macrophages [61]. Within keratinocytes, HPV infection is blocked by α defensin5 [62]. The absence of this defensin in the squamocolumnar junction of the cervix may be the reason why this region is more susceptible to infection by HPV [63]. It has been demonstrated that this defensin, also called HD5 (human defensin 5), binds to and stabilizes the HPV capsid. It inhibits the endosomal exit of the L2-viral genome complex (see section 1.1.3.1), and directs it instead to the lysosome where it is rapidly degraded [64, 65].

In addition, keratinocytes contain TLRs (TLR3, TLR7, TLR8, and TLR9) and NLRs, which recognize PAMPs such as the viral capsid proteins L1 and L2, the dsDNA viral genome and CpG motifs in the genome. Activated keratinocytes can moreover, release pro-inflammatory mediators such as IFNα, IFNβ, TNFα, TGFβ as well as interleukins, amongst them, IL-12. Acute inflammation has been observed to be beneficial in the clearing of HPV infection [60]. Fibroblasts are also activated by keratinocytes, which promotes initial inflammatory reactions by increasing the expression of various chemokines (CCL2, CXCL1, CXCL2, CXCL5, CCL20) and other pro-inflammatory molecules (COX-2, IL-1β, IL-6, and IL-8) [61]. Keratinocytes additionally play a role in the recruitment and activation of cellular mediators of immunity via secretion of chemokines (CCL2, CCL20, CXCL9) [61] (Figure 3).

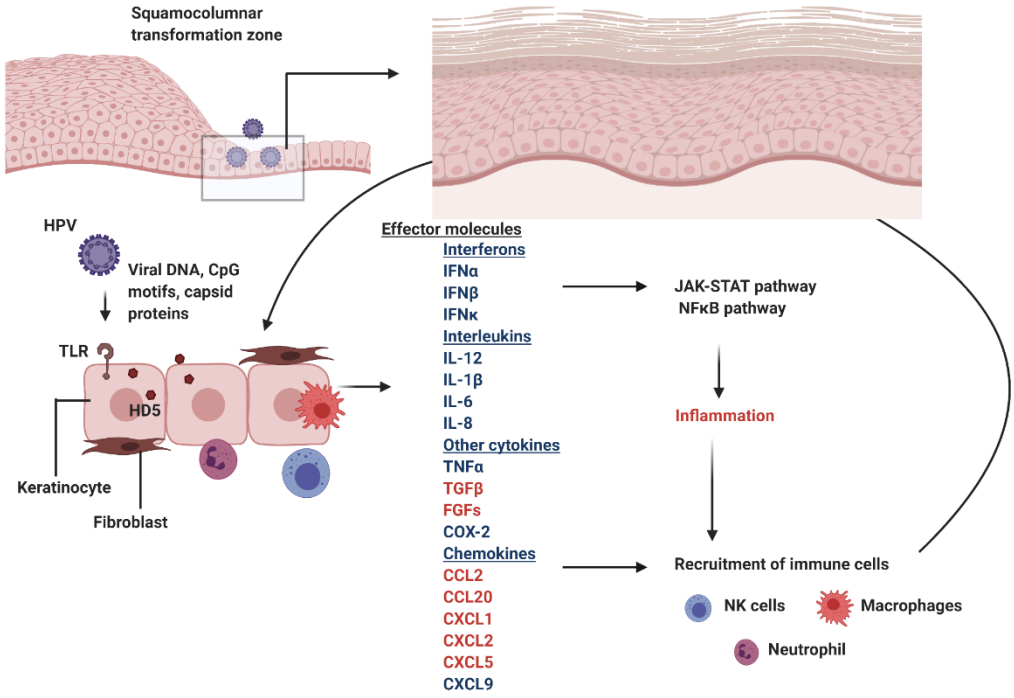

Figure 3. Innate immunity to HPV.
HPV infects the squamocolumnar transformation zone in the cervix. Innate immunity is triggered by the recognition of PAMPs (viral DNA, CpG motifs, capsid proteins), followed by the activation of the TLR signalling pathway. This leads to the secretion of several effector molecules (pro-inflammatory molecules marked in red), such as interferons and interleukins. The activation of JAK-STAT pathway as well as the NF-kB pathway contribute to the inflammation and recruitment of immune cells. Additionally, the defensin HD5, produced by keratinocytes prevents HPV infection. The absence of this defensin makes the squamocolumnar transformation zone more susceptible to HPV infection. Created with BioRender.com

Several immune cell populations are involved in promoting an adaptive immune response against HPV. These include DCs, Langerhans cells (LCs), NK cells, NKT cells, and keratinocytes. Keratinocytes are the main targets of HPV and, given their suggested role as non-professional APCs, they activate both memory $CD4^+$ and $CD8^+$ T cells into active cytokine-secreting and cytotoxic states [60, 66, 67]. Sources of antigen for APCs include free virus particles or cell debris. Viral antigens taken up by APCs are presented to $CD4^+$ T cells in the context of MHC II. Since there is no evidence supporting the productive infection of APCs by HPV, antigen presentation to $CD8^+$ T cells occurs most likely by cross-presentation on MHC I molecules (Figure 4)[60].

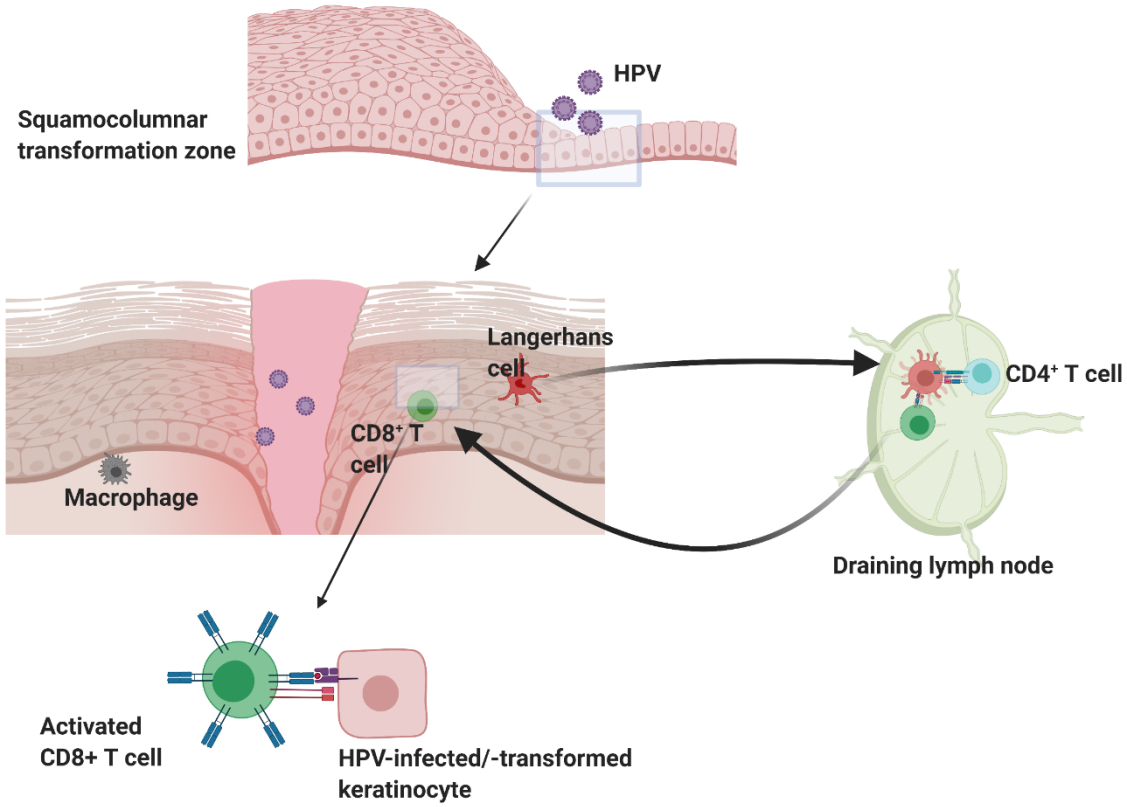

Figure 4. Adaptive immunity to HPV.
The main APCs involved in the antigen presentation of HPV16 antigens are DCs (professional APCs) and keratinocytes (non-professional APCs). HPV does not infect APCs, thus the source of antigens is considered to be cellular debris or free virus particles. The APCs then translocate to the draining lymph nodes, where antigens are presented to $CD4^+$ T cells (via the MHC II pathway) and cross-presented to $CD8^+$ T cells (via MHC I). These primed $CD8^+$ T cells then return to the infected epithelium, and can target HPV-infected cells, leading to their killing. Created with BioRender.com.

Immunity to HPV-induced malignancies

While acute inflammation is beneficial in clearance of HPV infection, chronic inflammation has been associated with promotion of carcinogenesis [60]. Immunity also plays a major role in the context of HPV-induced malignancies. M1 macrophages contribute to lesion regression and tumor cell lysis, through secretion of TNFα and NO (nitric oxide) [61]. A paucity of NK cells in the epidermis in direct contact with the keratinocytes initially suggested a limited role of these cells in immunity against HPV [60]. However, more recent studies have shown NK cells are essential for the clearance of HPV-mediated cancers [61]. The role of NKT cells in immunity against HPV is not fully elucidated. Some studies have shown that NKT cells play a role in early but not late tumor regression [68]. As for the adaptive immunity, it has been observed that 30 - 50% of those infected with genital HR and LR HPV types do not develop antibodies to HPV [69, 70]. The humoral response through antibodies is not considered a requirement for the regression of HPV-induced lesions. Instead, infiltration of $CD4^+$ and $CD8^+$ T lymphocytes into the site of a cervical lesion is associated with regression, as shown in various studies using animal regression models [60].

1.2.4 Evasion of immune responses by HPV

To persist in the host epithelial cells for the purpose of replication, HPV has evolved effective strategies for immune evasion. The persistence of HPV in the host cells is longer than that of most viruses, and hence, its immune evasion strategies are quite comprehensive and act at multiple levels.

First, its life cycle passively favors immune evasion. There is no viremia or virus-induced cell death in the host cells. Instead, the virus is released from the outer layers of the epithelium with the shedding of naturally dying cells. Thus, there is minimal damage signaling to activate the immune system. Also, the viral gene expression is maintained at a low level throughout the life cycle of the HPV, and expression of E6 and E7 is only seen to increase progressively in high-grade lesions and cancer [71].

HPV regulates the innate immune system at multiple levels including downregulation of TLR9 expression [71], inhibition of inflammation [59] and interfering with keratinocyte IFN signaling by inhibiting the synthesis of interferons [71, 72]. Only as the infection progresses to cancer, paracrine IL-6 signaling leads to chronic inflammation [59]. Dysregulation of the NFκB pathway may be involved in chronic inflammation and cancer development [71, 72], as contradictory reports show enhancement of NFkB signalling by HPV16 E6 proteins via regulation of the TLR pathway [73] as well as its inhibition by HPV oncoproteins [72].

HPV actively avoids the adaptive immune response, which is the reason why infection can persist for over 10 years.

The HPV E7 protein leads to promoter methylation of the E-cadherin adhesion molecule, thereby decreasing its concentration. The E-cadherin protein is essential for Langerhan cells movement through the epithelium, and its loss leads to LC leaving the epithelium [60].

Apart from this, the APM is majorly dysregulated by the HPV oncoproteins at various levels. The immunoproteasome components PSMB8 and PSMB9 have decreased expression levels in HPV16 infected cells. Expression of TAP1 and TAP2 is repressed by E7 and a partial loss of the other APM components including the chaperones has been observed. ERAP1 variants have been correlated with increased metastasis and decreased survival. ERAP1 expression was seen to be increased in cervical cancer and was observed to decrease HPV16-specific $CD8^+$ T cell killing [57]. Suppression of ERAP1 expression was observed to enhance the killing of HPV16-transformed CaSki cells but not 866 cells [57]. Defects in the APM in cervical cancer cells have also been shown to prevent the presentation of E6-derived T cell epitope ($E6_{29-28}$) and prevent killing by epitope-specific T cells [74]. Given the importance of the APM in the presentation of epitopes to $CD8^+$ T cells, its regulation by the virus is quite a masterful scheme of immune evasion. Yet another method to regulate the immune system is to alter the cytokine and chemokine milieu, thereby affecting immune cell recruitment. Both E6 and E7 alter the gene expression of cytokines and chemokines, such as IFN-κ and CXCL-14, respectively, through DNA methylation. This hinders the recruitment of NK cells, DCs, and T cells. HPV can also affect the helper T cell polarization between Th1/Th2 types. High expression levels of TNF-α, and both Th1- and Th2-favouring cytokines in high grade lesions, suggest a dysregulated immune response in advanced disease[71]. HPV16-transformed cells have also been shown to negatively affect the maturation of DCs by secretion of receptor activator of NFκ B ligand (RANKL). This, is turn, limits the ability of DCs to activate T cells, leading to tolerization instead of activation of T cells [75]. Additionally, like other tumors, immunosuppressive cells are recruited by HPV-mediated tumors, including tumor associated macrophages (TAMs) [71]. TAMs have been shown to have a positive correlation with HR HPV infection, and cervical carcinogenesis [76]. TAMs attract Tregs and secrete immunosuppressive cytokines. Another immunosuppressive cell population are myeloid-derived suppressor cells (MDSCs), which produce reactive oxygen species (ROS). The activation of T cells is believed to be inhibited by ROS species [71]. NKT cells have been shown to have increased infiltration into E7-expressing transgenic skin grafts and mediate a local immunosuppressive environment, preventing graft rejection [77]. In addition, in this HPV-E7 skin-grafted mouse model, it was shown that antigen-specific $CD8^+$ T cell activation and cytotoxicity were impaired due to defective cross-priming by DCs in skin draining lymph nodes. In the absence of direct evidence of the role of NKT cells in HPV-mediated cancer, these studies suggest their contribution towards an immunosuppressive microenvironment [78].

1.3 Preventive and therapeutic approaches to HPV-based malignancies

1.3.1 Preventive approaches: preventive vaccines and screening.

Despite these elegant immunosuppressive mechanisms, HPV-induced malignancies are attractive targets for immunotherapies, since they are virus-induced, and thus provide a repertoire of potential non-self-target proteins. The development of preventive vaccines against HPV-induced cancers was made possible by the study from Kirnbauer et al., which revealed that the viral L1 protein can self-assemble into virus-like particles (VLPs). It was shown that these VLPs mimic virions and they are capable of producing 1000-times higher antibody titers than previously achieved with bacterially expressed L1 and L2 [79]. Subsequently, preventive vaccines based on VLPs were developed against the most important HPV types. A bivalent vaccine against HPV16 and 18 (Cervarix©) provided effective protection against incident and persistent infections in the fully vaccinated group. The vaccine also offered protection to women who did not complete the vaccination schedule[80]. Subsequently, a quadrivalent vaccine (Gardasil©) was developed, which provided protection against HPV6 and 11 in addition to HPV16 and 18. HPV6 and 11 are responsible for 90% of benign anogenital warts. It was shown that the lowest dose of the vaccine was as effective as the intermediate or high doses in terms of antibody titers produced as well as protection from incident and persistent infection [81]. This vaccine was then expanded to include VLPs from 5 more HR HPV types (Gardasil9©)[82] Currently, there are three approved preventive vaccines against HPV-induced cervical malignancies, namely Cervarix (bivalent), Gardasil (quadrivalent), and Gardasil9 (nonavalent). The efficacy endpoint is defined as prevention from HPV16 and 18 infections. Cervarix protects for 10 years while Gardasil for 5 years [83]. Since it is efficacious in a single dose, unlike Gardasil or Gardasil9, Cervarix could be the most cost-effective option for developing countries. However, the WHO currently still recommends 2 doses of either Gardasil9 or Cervarix for women younger than 15 years, and three doses for those older. This also takes into account the efficacy of prevention of high-grade lesions (CIN2 or CIN3). The prevention efficacy of three doses of either vaccine is 62% for CIN2, and 93% for CIN3 with Cervarix [83]. Preventive vaccines, however, are only effective in the case of uninfected individuals and do not aid the clearance of the virus in pre-infected women, as was shown for the bivalent vaccine [84].

An analysis of global vaccine coverage from 2006 to 2014 has revealed great disparities in the vaccine implementation and the number of vaccinated women depending on the income levels of the various countries. High-income countries (based on the World Bank classification), while accounting for only 14% of annual cervical cancer cases, included 70% of the vaccinated women. The main reason for this disparity was the high initial cost of the vaccines, but social norms and values related to sexual activity also played a key role.

Based on these coverage data, using a projection up to the year 2080, it was predicted that worldwide around 380,000 cervical cancer cases will be prevented in the 118 million women vaccinated between 2006 and 2014, assuming life-long protection. In the same projection study, in these 118 million women, an additional approximately 65,000 prevented cases can be attributed to those who only received a single-dose vaccination. However, this is only a small percentage of the total 1,100,000 total projected cases by 2080. A total of 675,000 projected cases worldwide, by the year 2080, can be attributed to the lack of vaccination, or to HPV types not included in the vaccines [85], which is a concerningly high number of women.

For pre-infected women, for whom the existing vaccines would not be helpful, the main methods for prevention of development of cervical cancer include extensive screening and treatment of precancerous lesions, using the Papanicolaou smear (Pap smear). It involves the examination of a cervical smear under the microscope for abnormal cells. In developed countries, cytology-based testing methods have shown great success and have led to a 70% decline in cervical cancer mortality rates [86]. However, the Pap smear has also faced some criticism regarding its high cost [87], and it has met with only limited success in developing countries . Major challenges include the dependence on scarce resources such as electricity and limited patient follow-up, with patients being unable to travel repeatedly to the site where screening is happening. Other less resource intensive approaches, such as HPV testing by genotyping (using home-based kits), visualization (visualization of the cervix with acetic acid (VIA) or visualization with Lugol's iodine (VILI)) and colposcopy (30x magnification of the cervix, with a colposcope) to allow differentiation of normal tissue and a lesion, hold promise in low-resource settings [86, 88]. Despite the promise of these preventive approaches, the large numbers of already infected women, the lack of accessibility of the screening methods as well as the costs associated highlight the need for improving effective therapeutic strategies for HPV-induced premalignant lesions as well as advanced cancers.

1.3.2 Therapeutic strategies: chemotherapy, surgery, and therapeutic vaccines.

Following diagnosis by screening methods, treatment for advanced stages of precancerous lesions (CIN2 and CIN3), is by cryotherapy, thermoablation or surgery. Cryotherapy uses compressed gas to freeze cervical tissue and cause necrosis. As suggested by the name, thermoablation uses heat instead of cold. This is followed by the surgical excision of the lesion. Cryotherapy is associated with drawbacks for low resource countries, such as high cost and low availability of compressed gas [86].

Since cell-mediated immunity has been observed in HPV infected individuals and is associated with clearance of infection and negatively associated with progression towards advanced cancer, there is a lot of research focused on the development of a therapeutic vaccine against HPV ([89]. These therapeutic vaccines aim to target both early as well as advanced stages of cervical cancer. A variety of strategies have been tried with somewhat promising results in clinical trials . Attractive targets are the early E1 and E2 proteins, as these are expressed at higher levels than E6 and E7 early in the viral infection [89, 90]. However, strategies targeting E2 would be limited to targeting only early infections, where E2 is being expressed [91]. The early protein E5 has also been the focus of some earlier studies, but with limited success. Most studies, however, have focused on the E6 and E7 proteins. They are the main target proteins of interest for therapeutic vaccines since they are constitutively expressed, from early infection until advanced cancer. Additionally, the essential role of these proteins in the life cycle of the virus and malignant transformation of the host cell decreases the chances of these proteins being mutated or their expression being drastically altered [90]. Safety concerns have been addressed by using mutated versions of E6 and E7, which are unable to bind to their main downstream target proteins p53 and pRb [92]. Another way to ensure the safety of the vaccines is to minimize the dosage of the antigen which however negatively affects its immunogenicity [93]. To circumvent these negative effects, certain additional compounds can be used to enhance the immunogenicity of the vaccine. Such additional compounds are called adjuvants [41]. Several vaccination strategies have been explored for therapeutic vaccine development, including live vector-based vaccines, nucleic acid-based vaccines, cell-based vaccines, and subunit vaccines.

Live vector-based vaccines

Live vector-based vaccines are based on recombinant viral or bacterial vectors, encoding a viral antigen that replicates within the host. Antigen presentation can occur via both MHC class I and class II pathways, leading to the activation of $CD8^+$ and $CD4^+$ T cells, respectively [90]. One example of such a vaccine is **TA-HPV**, a live recombinant **vaccinia virus**-based HPV candidate vaccine (encoding modified forms of HPV16 and 18 **E6** and **E7** proteins). The safety of this vaccine was approved and its immunogenicity confirmed in a study with twenty-nine early-stage cervical cancer patients. HPV-specific cytotoxic T cells were observed in 4 patients [94]. A phase II clinical trial of TA-HPV showed limited success in the treatment of advanced stage HPV positive anogenital intraepithelial neoplasia (vulvar or vaginal intraepithelial neoplasia). Out of twelve women included in the trial, 5 patients showed a 50% regression of the lesion over 24 weeks and one patient showed complete regression [95]. Another phase III clinical trial that showed promise was one using **MVA-E2**, which is a **vaccinia virus** encoding the **E2 protein**.

This trial included 1176 female participants with HPV positive CIN (stage 1 to 3) or condyloma, and 180 male participants with HPV positive anal lesions or urethral condyloma. Lesion regression was seen in 89.3% of female participants and 100% of male participants [96]. However, the commercialization of these vaccines still faces challenges.

The main issues associated with the use of live vector-based vaccines include the generation of neutralizing antibodies, the risk of a dominant immune response to the vector instead of the antigen, pre-existing immunity to the vector, and potential pathogenicity to immunocompromised individuals [90].

Nucleic acid-based vaccines

Nucleic acid-based vaccines are either DNA-based, RNA replicon-based DNA vaccines or mRNA vaccines encoding the viral antigen. Once it enters the cells, the viral antigen encoded by the DNA or RNA is transcribed and translated into a viral protein. This is followed by antigen presentation via the MHC I pathway. However, DNA vaccines alone were seen to be poorly immunogenic. Hence, they have been used in combination with strategies to enhance antigen processing and presentation and interaction between DCs and T cells [90]. One example of a DNA vaccine for HPV is **GX-188E** (Genexine Inc.). This vaccine co-expresses HPV16/18 **E6** and **E7**, along with a DC activator Fms-like tyrosine kinase-3 ligand (**Flt3L**). A phase I study with nine patients with HPV16/18 positive CIN3, showed complete lesion regression in seven patients. The enhanced function of cytotoxic T cells was also observed in terms of the cytotoxicity, proliferation, and secretion of effector molecules [97]. **VGX-3100** (Inovio Pharmaceuticals Inc.) is another DNA vaccine against HPV that has shown promising results. In a phase II double-blind, placebo-controlled study, women with HPV16/18 positive CIN2/3, showed higher lesion regression in the treated group (49.5%) compared to the placebo group (30%) [98]. DNA vaccines have the advantage of being safe and easy to manufacture. The main advantage of nucleic acid-based vaccines is the absence of neutralizing antibodies, which allows them to be administered repeatedly.

RNA replicon-based vaccines are similar to DNA vaccines, except that they include an RNA replicon encoded into the DNA, which leads to apoptosis of the target cell upon transcription. However, the main challenge seen here was the induction of apoptosis in APCs, leading to decreased immunogenicity. RNA-based HPV vaccines still face some technical challenges. [90].

Cell-based vaccines.

Cell-based vaccines involve the *ex-vivo* manipulation of cells isolated from the patient followed by their injection back into the patient.

A phase I study has demonstrated that DC-based vaccines generated by pulsing **DCs with HPV16/18 full-length E7** are capable of generating E7-specific $CD8^+$ T cells in 8 out of 10 patients with early stage cervical cancer. All patients developed $CD4^+$ T cell responses [99]. The large-scale production capacity of DC-based vaccines is restricted by the need to harvest sufficient DCs from the patients and the need for high technical competence for *ex-vivo* manipulation of the DCs.

Additionally, the process is time-, labor- and cost-intensive. This, once again, would limit the accessibility of these vaccines in areas most needed, such as economically weaker countries where resources are limited [90]. A more recent approach using *in vitro* maturation of PBMCs may have the potential to address this challenge. These *in vitro* generated DCs were termed pre-immune dendritic cells (PIDCs). **PIDCs pulsed with HPV16 E6/18-26 or E7/12-20** peptides were able to induce specific immune responses in 63% and 57% patients with advanced cervical cancer, respectively [100]. However, more clinical trials are needed before DC-based therapies can reach the clinic.

A recently published study showed promising results using a **E7/11-19 targeting TCR**, with objective responses observed in 6 out of 12 patients with HPV-induced cancers [101]. However, tumor heterogeneity, antigen escape and the presence of an immunosuppressive microenvironment are major challenges, which need to be resolved before T cell therapy can become a standard treatment for HPV-induced malignancies [90].

Subunit-based vaccines

Subunit-based vaccines represent the fourth major strategy used for therapeutic vaccines. Subunit-based vaccines can be of two types, either protein-based or peptide-based. Protein-based vaccines are made from proteins mutated so that their oncogenicity is lost. These vaccines have the major advantage of not being restricted to a patient's HLA type since the entire protein is available for proteasomal degradation and antigen presentation. However, due to presentation via the MHC II pathway, they primarily induce activation of $CD4^+$ T cells, which promote antibody production by B lymphocytes. Adjuvants have been used to bypass this problem with promising results [90]. Due to it being more conserved and due to its higher expression level, the E7 protein has commonly been used alone. However, being a small protein (11kDa), its immunogenicity is limited. This was resolved by the use of suitable adjuvants [92]. Amongst others, a phase II clinical trial using **TA-CIN**, a **subunit vaccine** comprised of a **fusion protein** of **HPV16 L2,**

E6 and E7 proteins, showed regression in 63% (12/19) of patients with VIN2/3 (Vulvar intraepithelial neoplasia grade 2 and grade 3) [102].

Peptide-based vaccines overcome the limitation of HLA polymorphism (see section 1.2.2.1) and HLA-restriction by the use of synthetic long peptides (SLPs). SLPs are 15-35 amino acid long overlapping peptides, which can cover the entire protein sequence.

In a phase II study of an HPV16 SLP-based vaccine, with 20 patients with VIN3, 9 out of 19 patients showed a completed response at 24 months post vaccine [103]. Apart from this study, multiple others have successfully demonstrated the immunogenicity and generation HPV-specific cytotoxic T cell responses by SLP-based vaccines against HPV16 [92]. The major advantage of subunit-based vaccines is their safety, particularly of peptide-based vaccines, and their relative ease of production compared to other strategies [90, 92]. The use of SLPs, however, has a drawback. Because of its exogenous delivery, the SLP may not be processed through the APM the same way as the native pathogen. This might lead to unwanted immune responses or insufficient anti-tumor responses.

The alternative is to use synthetic short (8-11 amino acid long) specific $CD8^+$ T cell epitopes. Clinical trials using peptide-specific vaccination against HPV-induced malignancies have shown promise. Different epitopes such as E7/11-20, E7/12-20, and E7/86-93 have been used in combination with different adjuvants [92]. In a phase I trial of patients with advanced grade CIN/VIN, treated with **E7/12-20 and/or E7/86-93 peptide-based** vaccines, 3 out of 17 patients were seen to show complete regression, and 6 showed partial regression of >50% [104]. One of the major drawbacks of peptide-based vaccines for the clinical setting is the need for HLA-typing of the patients. This can be overcome by the use of a combination of peptides, binding to several HLA-supertypes. [51, 52]. Given the important role of $CD4^+$ T cells in long-term $CD8^+$ T cell responses [49], MHC II-restricted epitopes are good candidates for inclusion into a peptide-based therapeutic vaccine [90]. In this context, a study from our group identified promiscuous $CD4^+$ T cell epitopes, which were capable of inducing an IFNγ response in $CD4^+$ T cells from CIN2 and CIN3 patients [105]. Another main challenge in the use of $CD8^+$ specific epitopes for therapeutic vaccination is the detection of specific immunogenic epitopes for effective vaccine design. This has been recently addressed using a combination of *in silico* prediction and mass spectrometry-based techniques. This methodology was successful in the detection of HPV16 E7-derived epitopes, also partially as a part of this thesis [106].

1.3.2.1 Detection of peptides for use as potential epitopes for therapeutic vaccine design

The best candidates for the development of a therapeutic vaccine are peptides that are presented on the surface of tumor cells and that induce a cytotoxic immune response. In the past, only indirect methods were used to detect these peptides, such as *in silico* prediction combined with immunogenicity or killing assays. The actual validation of the surface presentation of peptides was achieved using tandem mass spectrometry combined with bioinformatics tools. However, the first study of this kind was able to detect only one HPV16-derived MHC I epitope, E7/11-19, despite its high resolution and sensitivity [107].

The successful mass spectrometry-based detection of HPV-derived peptides is associated with various challenges. Due to the immune evasion strategies of the virus, the expression of E6 and E7 is low compared to other cellular proteins.

Thus, detection by the commonly used untargeted information dependent acquisition (IDA) mass spectrometry approach, which picks the top n most abundant ions for further analysis, is not possible. Further, these peptides are not tryptic peptides, for which most mass spectrometry approaches have been optimized. Instead, MHC I-restricted peptides have diverse chemical characteristics, such as hydrophobicity and surface charge, for which sample preparation strategies need to be optimized and standard procedures need to be followed across different labs to ensure reproducibility [108], such that effective vaccines can be designed, targeting the truly presented peptides.

Despite several immunotherapies having reached clinical trials and shown promising results, as summarized above [90], and more reported as ongoing last year [89, 109], there are as of yet no commercially available therapeutic vaccines. This suggests that there is a need to investigate other aspects of cervical cancer pathophysiology before the development of a successful therapeutic vaccine is possible. One very important parameter, which has not received much attention from the clinical perspective, is the tumor microenvironment.

1.4 Tumor microenviroment and hypoxia

As early as the year 2000, Hanahan and Weinberg defined a set of six hallmarks defining capabilities that must be acquired by cells to successfully progress to a cancerous state [110]. The contribution of the TME to the hallmarks of cancer development was later added by them in 2011 [111]. A more comprehensive investigation into the interactions of the cancer cell and each of the TME components has since replaced the earlier cell-centric approach to understanding cancers [112, 113]. Apart from the cancer cells, the extracellular matrix (ECM), the vasculature, the stromal cells and the immune cells, play a key role in cancer

progression. These factors, together with the altered nutrient levels, oxygen concentration and pH levels of the surrounding tissue constitute the TME [112-115].

Solid epithelial tumors derived from different anatomical sites share features in their microenvironment. The defining features of the TME arise from reciprocal interactions between the cancer cells and their environment. Uncontrolled proliferation of cancer cells leads to decreased nutrients and a decreased partial pressure of oxygen in the surrounding tissue [114]. As tumor proliferation outgrows its surrounding vasculature, the oxygen concentration drops below 2%, a condition that is termed hypoxia [115].

Hypoxia is a prevalent feature in most rapidly growing solid tumors, and responsible for a further dysregulation of each of the TME components [116]. Hypoxia leads to an increase in levels of hypoxia-inducible factor 1 α (HIF1α) levels, which is the main regulator of most pathways regulated by hypoxia. Under normoxic conditions, HIF1α is hydroxylated by the prolyl hydroxylase enzyme 2 (PHD2). This hydroxylation allows for interaction with the von Hippel-Lindau tumor suppressor protein (pVHL), resulting in subsequent ubiquitination and degradation. In hypoxic conditions, the hydroxylation of HIF1α is reduced, due to the decreased activity of PHD2 [114], leading to its stabilization in cancer cells and other cells in the TME [115, 116]. HIF1α regulates hundreds of downstream target genes. Thus, the interaction of HIF1α with its upstream regulatory proteins and its targets in cancer cells can play a role in determining tumor prognosis, [117]. Hypoxia plays a central role in regulating the other aspects of the TME [115], and is a central regulator of all the hallmarks of cancer, in particular tumor vasculature and angiogenesis; invasion and metastasis; and metabolic switch, and evasion of the immune response, as reviewed by Wigerup et al.[118]. As tumors grow in size, they need to enhance the development of the surrounding vasculature to improve blood flow. This process of development of new blood vessels is termed angiogenesis. Hypoxia promotes angiogenesis by enhancing the secretion of the growth factor VEGF from tumor cells and stromal cells [115]. However, highly increased VEGF concentrations lead to immature vascularization, thereby further enhancing hypoxia [114]. Another hallmark of cancer is invasion and metastasis to other sites [111]. Hypoxia promotes the conversion of precursor cells into cancer-associated fibroblasts [116], which release proteolytic enzymes that damage the integrity of the ECM [114]. Hypoxia directly promotes the disorganization of the ECM structure via various mechanisms, mainly including the degradation of collagen, its main structural component [116]. A structurally damaged ECM and the immature and leaky vasculature permit the escape of cancer cells from the primary tumor site. This contributes to the invasiveness and metastasis of several tumor types [113, 114]. Epithelial to mesenchymal transition (EMT) is the initial step required for metastasis. Upregulation of various transcription factors playing a key role in EMT, by HIF1α, promotes EMT under hypoxic conditions [118].

Metabolic reprogramming, one of the main hallmarks of cancer, is intrinsically linked with hypoxia. Cancer cells adapt to decreased oxygen availability by switching to glycolytic metabolism, a phenomenon called the Warburg effect. This metabolic shift leads to intracellular accumulation of lactic acid and carbonic acid. To prevent the cytotoxic effect of decreased intracellular pH levels, cellular proton extrusion methods are activated causing acidification of the TME [114]. Also, HIFs promote a switch from glucose to glutamine metabolism, to produce acetyl-CoA for fatty acid synthesis in cancer cells [118]. One of the major hallmarks of cancer added to the six original cancer hallmarks is escape from immune surveillance [111].

The component of the TME differing highly amongst most solid tumors is the extent of the inflammation and the repertoire of immune cells. The hypoxic and acidic TME plays a major role in suppressing the activities of the immune cells infiltrating the tumor, aiding the immune escape of tumors [114, 115, 119]. There exists a bidirectional interplay between hypoxia and the chronic inflammation in the tumor microenvironment. The synthesis of inflammatory enzymes and cytokines by immune cells is associated with enhanced metabolism, leading to a high demand for oxygen. The elevated oxygen consumption further promotes the creation of a hypoxic environment. On the other hand, NFκB, a transcription factor key to downstream signaling in response to inflammation, is regulated by hypoxia. The effect of hypoxia on the immune cells in the TME of different tumors is dependent on which inflammatory cytokines are present in the TME of the specific tumor [120]. The effect of hypoxia on different immune cells has been elaborately investigated as recently reviewed by Vito et al [119].

Regarding myeloid cells, MDSCs develop into TAMs in a hypoxic environment [114] and TAMs localize preferentially in a hypoxic environment [115]. The majority of TAMs in the TME display the M2 phenotype, which is pro-tumorigenic [119]. Various aspects of DC functions are also regulated by hypoxia. Antigen uptake, as well as differentiation and activation of DCs, was inhibited in hypoxia [121]. Hypoxic DCs also showed an altered chemokine profile and suppressed maturation [122]. Both short (16h) and long term (96h) hypoxia in combination with IL-2 treatment affected the cytokine expression and chemokine receptor expression profile, leading to altered migration of NK cells [123]. In another study, deletion of HIF1α in NK cells led to decreased tumor growth. Hypoxic NK cells were seen to be promoting tumor growth by allowing more mature blood vessel formation, via inhibition of VEGF [124]. In general, hypoxia seems to be playing an immunosuppressive role in all cell types as elaborated above. Regarding lymphoid cells, the role of HIF1α in B cells is poorly understood, though HIF1α plays a critical role in B cell development [119]. There is some controversy concerning the effect of hypoxia on $CD8^+$ T cells. Vuillefroy de Silly et al. have shown that exposure of $CD8^+$ TILs (tumor-infiltrating lymphocytes) to hypoxia led to their decreased proliferation. Also, these hypoxic TILs secreted the immunosuppressive cytokine IL-10

[125]. However, some recent studies have demonstrated a positive effect of hypoxia on $CD8^+$ T cells. Cytotoxic $CD8^+$ T cells, precultured in hypoxia, led to a higher tumor rejection and improved survival in B16-OVA tumor-bearing mice than $CD8^+$ T cells precultured in normoxia [126]. Regarding antigen presentation by tumor cells, hypoxia has been observed to regulate the expression of the MHC I molecule in a tumor-specific manner. Some studies have shown an upregulation of MHC I upon hypoxia, in melanoma and colorectal cancer cell lines [127, 128].

Other studies, however, have shown downregulation of MHC I upon hypoxia using 3D culture systems, *in vivo* sarcoma, and pulmonary mouse models. The protein levels of the APM components TAP1, TAP2, LMP2 and LMP7 were also decreased upon hypoxia *in vitro* as well as *in vivo* [129]. Regulation of the immune cells and tumor cell antigen presentation by the hypoxic TME has prompted an investigation into its effect on immunotherapies.

Vaccination with cell lysates generated under 5% O_2 was observed to lead to enhanced cytolytic function of $CD8^+$ T cells in mice models of breast cancer and glioma [130]. This was confirmed to be related to more efficient antigen uptake and presentation by DCs under physiological oxygen conditions, compared to 20% atmospheric oxygen, in glioma cultures [131].

Despite the central role of hypoxia in regulating the various hallmarks of cancer, the effect of hypoxia has only been considered in a countable number of clinical studies so far. The NCT03003637 trial is investigating the effect of hypoxia on the efficiency of PD-L1 and CTLA4 blockade therapy. NCT03575598 is examining the effect of hypoxia on immunotherapy of head and neck cancer with tyrosine kinase inhibition in combination with PD-1 blockade. Methods such as relieving ECM pressure or normalizing tumor vasculature may hold promise in enhancing the efficacy of immunotherapies[132].

1.4.1 Aspects of the cervical cancer TME

A recently explored component of the TME in certain tissues is the resident flora, also known as the microbiome. The cervical microbiome composition is associated with either HPV clearance or progression to cervical cancer. Recent studies have elucidated the importance of the cervical microbiome in regulating the cervical microenvironment via the secretion of bacterial bioproducts. The other possibility is that the bacteria themselves regulate host gene expression, thereby affecting the prognosis of HPV infection and cervical cancer development [133]. Another important factor in cervical cancer development is angiogenesis. Several regulatory proteins of angiogenesis have been shown to be associated with cervical cancer progression [134]. The clinical importance of the microenvironment is highlighted by the positive

results observed upon the combination of the anti-angiogenic drug bevacizumab with prevalent chemotherapeutic protocols [134, 135].

The best-studied aspect of the cervical cancer microenvironment is the enrichment of immunosuppressive innate and adaptive immune cells, such as tumor-associated macrophages (TAMs), MSDCs, NKT cells, and Tregs. Besides, there is a depletion of APCs, such as LCs. Cells with the potential to detect and eliminate tumors, such as NK cells and $CD8^+$ T cells, are also reduced.

Moreover, the pro-inflammatory cytokine milieu leads to chronic inflammation. This is primarily the outcome of the elaborate mechanisms employed by HPV to evade the immune system (See section 1.2.4) [61, 71, 75-78, 136].

However, the most prevalent aspect of the cervical cancer microenvironment, like with most other tumors, is the presence of hypoxia. The effect of hypoxia on cervical cancers has, however, not been investigated in detail. It has been recently shown that hypoxia induces a state of dormancy in cervical cancer cells, which was reversible upon reoxygenation. Mechanistically, this was due to a downregulation of E6 and E7 mRNA and protein levels upon exposure to hypoxia [137-139].

HPV E6 and E7 are the prime targets of most therapeutic vaccines. Thus, it is relevant to investigate the effect of hypoxia on the presentation of epitopes from these proteins, and the subsequent effect on the adaptive immune response.

2 Aims

HPV-induced malignancies are an attractive target for immunotherapies, since these belong to the few cancers where non-self targets can easily be found. This is especially true for cervical cancers, 100% of which are linked to HPV infection. However, despite promising results, no immunotherapies have reached the stage to become the standard treatment for these malignancies. A potential hindrance to the success of immunotherapies might be the hypoxic tumor microenvironment. While hypoxia is a key feature of the TME of most solid tumors, including cervical cancer, the effects of hypoxia in the context of immunotherapies have been surprisingly little explored. The main target proteins of interest for generating a therapeutic vaccine against HPV are the oncoproteins E6 and E7. Given their pleiotropic functions during the life cycle of the virus, they are expressed through the early stages of infection, and their expression rises with integration of the virus, followed by the transformation of the cells. However, it has been recently reported that hypoxia downregulates the expression of E6 and E7 proteins.

Different HPV16 variant lineages have been reported to have differential pathogenicity (section 1.1.3). Thus, the **first aim** of this thesis was to investigate whether hypoxia downregulates the oncoprotein expression in different cell lines, transformed with different variant lineages of HPV16.

For the effective targeting of HPV16-infected cells by $CD8^+$ T cells, epitopes must be presented in the context of HLA-I molecules. This involves the processing of the antigen via an elaborate APM (section 1.2.2.1). In the context of different tumors, hypoxia has been reported to up- or down-regulate HLA-I surface expression and decrease the expression of certain APM components (section 1.4.1). Thus, the **second aim** of this thesis was to investigate the effect of hypoxia on the APM as well as surface expression levels of HLA-A2 in cervical cancer cells transformed with different HPV16 variant lineages.

For the design of a therapeutic vaccine, it is important to determine peptides that are truly presented on the surface of HPV16-transformed cells. Thus, the **third aim** of this thesis was the optimization of the targeted epitope detection workflow developed previously in the group [106] and analysis of HPV peptides on normoxic and hypoxic target cells.

Finally, from the context of developing successful immunotherapies, the most concerning feature of the hypoxic microenvironment is its immunosuppressive effect. Interestingly, however, some recent studies have shown that hypoxic $CD8^+$ T cells have enhanced cytotoxicity. Conversely, there are also reports of hypoxia suppressing cytotoxic T cell functions. Thus, the **last aim** of this thesis was to investigate the effect of hypoxia on the killing of cervical cancer cells by HPV16-specific $CD8^+$ T cells.

3 Materials

Table 3. List of materials

Material	Manufacturer	Location
Automated cell counter	Countess™, Thermo Fisher Scientific	Waltham, MA, USA
Cell freezing container	Nalgene® Mr. Frosty® Cryo 1°C Freezing Container, Thermo Fisher Scientific,	Waltham, MA, USA
Centrifuge rotor for plates	M-20, 75003624, Thermo Fisher Scientific	Waltham, MA, USA
Centrifuge rotor for swinging buckets	TX-400, 75003629, Thermo Fisher Scientific	Waltham, MA, USA
Countess Chamber slides	LifeTechnologies	Waltham, MA, USA
Econocolumn 1.5 x 10cm ,	BioRad	Hercules, CA, USA
Enzyme-linked immunospot (ELISpot) plate reader	CTL-Immunospot® S6 Ultra-UV, CTL Europe	Bonn, Germany
Eppendorf tubes (Protein LoBind^{R})	Eppendorf	Hamburg, Germany
Falcon tube (15ml and 50ml)	Nerbe Plus,	Winsen, Germany
Flow cytometer	Fluorescence activated cell scanner (FACS) Canto II™ (Michael), BD Biosciences	Franklin Lakes, NJ, USA
Flow cytometer	BD Accuri™ C6 with BD CSampler™ accessory kit, BD Biosciences	Franklin Lakes, NJ, USA
Gloves	Microflex	Reno, NV, USA
Hypoxia chamber	Baker Ruskinn, InVivo2	Maine, USA
Laminar flow hood	SterilGard® Class II laminar flow hood, The Baker Company	Sanford, USA
Laminar flow hood	Maxisafe 2020, Thermo Fisher Scientific	Waltham, MA, USA

LC column	nanoEase M/Z Peptide BEH C18 Column	Waters, Milford, MA, USA
Light microscope	Wilovert Standard 30 microscope, Hund Wetzlar	Wetzlar, Germany
Light microscope	Axiovert 25, Carl Zeiss Microscopy GmbH,	Jena, Germany
Liquid nitrogen tank	Locator 8 plus, Barnstead/Thermolyne	Dubuque, IA, USA
Liquid nitrogen tank	ARPEGE110 NU, Cryopal,	Bussy-Saint-Georges, France
Magnet for MACS	Quadro MACS, Miltenyi Biotech,	Bergisch Gladbach, Germany
Magnetic stand for PCR tubes	In house	DKFZ, Germany
Magnetic stirrer	RSM-01S, Phoenix Instrument GmbH	Garbsen, Germany
Magnetic stirrer, heatable	MR-Hel Standard Heidolph Instruments	Schwabach, Germany
Mass spectrometer	QTRAP 6500, AbSciex LLC	Foster city, CA, USA
Mass spectrometer	Q-Exactive HF-X, Thermo Fisher Scientific,	Waltham, MA, USA
Mass spectrometer	Orbitrap Exploris, Thermo Fisher Scientific	Waltham, MA, USA
Multichannel pipetting reservoir	Trifill reservoir	Roth, Karlsruhe
Multiskan™ GO Microplate Spectrophotometer -	Thermo Fisher Scientific	Waltham, MA, USA
Nano Drop	ND-2000, Thermo Fisher Scientific	Waltham, MA, USA
NanoAcquity UPLC system	Waters,	Milford, MA, USA
PCR tubes	Biozym Scientific	Oldendorf, Germany
Peristaltic Pump	1322 Pharmacia P1 P-1, Scientific support, Inc.	Hayward, CA, USA
pH Meter	SevenCompact™ pH/Ionmeters S220 with pH Electrode	Glostrup, Denmark
Pipette tips	Starlab	Hamburg, Germany

Pipettes (2µl, 20µl, 200µl, 1000µl, 50µl multichannel and 300µl multichannel)	Finnpipette F2, Thermo Fisher Scientific	Waltham, MA, USA
Pipettes, glass	Hirschmann Labortechnik	Eberstadt, Germany
Pipetting controller Pipetboy	Integra Biosciences	Biebertal, Germany
Power supply	EPS3500Pharmacia	Uppsala, Sweden
Reaction tubes (0.2mL, 0.5mL, 1.5mL and 2mL)	Eppendorf	Hamburg, Germany
Refrigerator (4°C, -20°C)	Mediline, Liebherr	Biberach an der Riss, Germany
Sep-Pak 96 well desalting plate	Sep-Pak; Waters	Milford, MA, USA
Sep-Pak tC18 cartridges (1ml)	Sep-Pak; Waters	Milford, MA, USA
Ultimate^{TM} 3000 HPLC	Thermo Fisher Scientific	Waltham, MA,USA
Vortexer	Vortex Genie-2, Scientific Industries	Bohemia, USA
Vacuum concentrator Plus	Eppendorf	Hamburg, Germany
Water bath	GFL	Burgwedel, Germany

Table 4. List of reagents

Reagent	Product. Number	Company
Cell Culture		
D-MEM medium	D5796	Sigma-Aldrich
RPMI-1640	E15-840	PAA
Trypsin/EDTA	T3924	Sigma-Aldrich
L-Glutamine 100x	25030024	Thermo Fisher Scientific
Fetal Bovine Serum (FBS)	16140071	Gibco/ Thermo Fisher Scientific
Human serum	H4522	Sigma-Aldrich
Penicilin-Streptomycin Solution	P0781	Sigma-Aldrich
Incidin	22170	EcoLab
DMSO	D8418	GE Healthcare
β-Mercaptoethanol (sterile)	31350-010	Gibco
Recombinant human Interleukin 7 (rhIL-7)	207-IL	R&D Systems
Recombinant human Interleukin 2 (rhIL-2)	200-02	PeproTech
Rh-GM-CSF	215-GM	R&D Systems
IL-4	204-IL	R&D Systems
TNFα	210-TA	R&D Systems
IL-6	206-IL	R&D Systems
PGE_2	14010	Cayman Chemical
DMSO	D8418	GE Healthcare
Peptides	-	DKFZ, synthesized by Mario Koch
CEF Peptide Pool	PA-CEF-001	PanaTecs
Keratinocyte SFM 500ml	17005	Gibco
F12 medium	21765	Gibco
Hydrocortizone	H0396	Sigma-Aldrich
Cholera toxin	C3012	Sigma-Aldrich
Insulin	I6634	Sigma-Aldrich
Adenine	A8626	Sigma-Aldrich
E.G.F.	13247-051	Invitrogen

SDS-PAGE and Western blotting		
Anti-E6 primary antibody	E6-6F4	EUROMEDEX
Anti-E7 primary antibody	NM2	Kindly provided by Prof M. Müller, DKFZ
Anti-HIF1α primary antibody	ab179483	Abcam
Anti-Tubulin primary antibody	T5168	Sigma-Aldrich
AffiniPure Goat Anti-Mouse IgG (H+L) Peroxidase	115-035-003	Dianova (Jackson IR)
Goat anti-rabbit IgG (H&L) Ab Peroxidase	611-1302	Rockland / Biotrend
MiniProtean TGX™ Any kD™ SDS-PAGE gels	4569036 (15 wells), 4569036 (10 wells)	BioRad
Precision Plus Protein Kaleidoscop Standards	161-0375	BioRad
NuPAGE LDS Sample Buffer (4x)	NP0007	Invitrogen
2-Mercaptoethanol	4227.3	ROTH
Tween 20	Tween201	MP Biomedicals
Methanol	32213	Sigma-Aldrich
Peroxidase-conjugated Goat Anti-Mouse IgG (H+L)	115-035-003	Jackson IR
Peroxidase-conjugated Goat Anti-Mouse IgG Light Chain Specific	115-035-174	Jackson IR
PVDF	88518	Thermo Scientific
Western Blotting Filter Paper	88600	Thermo Scientific
Pierce ECL Western Blotting Substrate (normal)	32209	Thermo Scientific
Amersham ECL Prime Western Blotting Detection Reagent	RPN2232	GE Healthcare
Sodium phosphate dibasic dehydrate (Na_2HPO_4 $2H_20$)	30412	Sigma-Aldrich

Potassium dihydrogen phosphate (KH_2PO_4)	3904.1	Roth
Potassium chloride (KCl)	6781.1	Roth
Sodium chloride	31434	Sigma-Aldrich
DC protein assay	500-0116	BioRad
BSA (protein standard)	500-0007-MSDS	BioRad
FACS		
Anti-HLA-A2 antibody-FITC	551285	BD Biosciences
FITC Mouse IgG2b, κ Isotype Ctrl Antibody	401205	BioLegend
Immunoprecipitation and sample preparation for analysis by mass spectrometry		
GammaBind Plus Sepharose	17-0886-01	Roche
Protease inhibitor cocktail	11 836 153 001	Roth
Zorbax SB-C18	899999-777	Agilent technologies
Anti-HLA-A2 antibody (BB7.2)	-	In house
IGE-PAL-630	A1099	Sigma-Aldrich
CNBr activated sepharose 4B	17-0430-01	VWR International, LLC
Acetic acid LC/MS grade	01074101	Biosolve
ddH_20 LC/MS grade	23210601	Biosolve
Trifluoroacetic acid LC/MS grade	80457-10X1ML	Sigma-Aldrich
Methanol LC/MS grade	13687801	Biosolve
Acetonitrile LC/MS grade	01204101	Biosolve
Sera-Mag Speed Beads A, Slurry at 50 ug/ul	24152105050250,	Fisher Scientific;
Sera-Mag Spead Beads B Slurry at 50 ug/ul.	44152105050250	Fisher Scientific
Trypsin Sequencing Grade	V5111	Promega
TEAB buffer	T7408	Sigma-Aldrich
PBMC isolation		
Ficoll-Paque ™PLUS	17-1440-02	Roth
Ammonium chloride (NH_4Cl)	K298.1	Roth

Potassium bicarbonate ($KHCO_3$)	298-14-6	Sigma-Aldrich
Ethylenediaminetetraacetic acid (EDTA)	E6758	Sigma-Aldrich
ELISpot		
Mab anti-human IFNγ clone 1-D1K	3420-3	MABtech
Mab anti-human IFNγ clone 7 B6-1 Biotin	3420-6	MABtech
Streptavidin-ALP	3310-10	Mabtech
NBT/BCIP	34042	Millipore
Millipore Multiscreen HA membrane plate	MAHAS4510	Millipore
MILLEX GS Filter 0.22µm	SLGS033SS	GE Healthcare
GammaBind Plus Sepharose	17-0886-01	Sigma-Aldrich
Concavalin A	C5275	Sigma-Aldrich
Cytotoxicity assay (VITAL-FR)		
CFSE	C1157	Life Technologies
Far Red	C34564	Life Technologies
$CD8^+$ T cell isolation kit	130-096-495	Miltenyi Biotec
LS columns	130-042-401	Miltenyi Biotec

Table 5. List of cell lines and culture medium.

Cervical cancer cells and controls		
Cell line	**Culture medium** **(materials in bold, freshly added before use)**	**HP16 variant**
NOK	Keratinocyte SFM + EGF(5ng/ml) + BPE (50µg/ml)	-
C33A	DMEM + FCS (10%) + P/S (1%) + L-Glutamine (1%)	-
CaSki	DMEM + FCS (10%) + P/S (1%) + L-Glutamine (1%)	European (E2)
SNU17	RPMI-1640 + FBS (10%) + P/S (1%) + L-Glutamine (1%) + HEPES (1%)	European (EA)
SNU703	RPMI-1640 + FBS (10%) + P/S (1%) + L-Glutamine (1%) + HEPES (1%)	European (EA)
SNU1299	RPMI-1640 + FBS (10%) + P/S (1%) + L-Glutamine (1%) + HEPES (1%)	Asian American (AA1)
866	F12-medium (375ml) + D-MEM (125ml) + FBS (5%) +P/S (1%) + hydrocortisone (0.4 mg/ml)+ insulin (5 mg/ml), + cholera toxin (0.01 mg/ml) + adenine (24.2µg/ml) + **epidermal growth factor (0.1 mg/ml)**	African-2
MRI-H-196	DMEM + FCS (10%) + P/S (1%) + L-Glutamine (1%)	European (E1)
Marqu (CxCa)	DMEM + FBS (15%) + P/S (1%) + L-Glutamin (1%) + HEPES (1%)	European (E1)
Other cells		
Cell line	**Medium**	
Human T cells	RPMI-1640+ 10% human serum (10%, heat-inactivated) + P/S (1%) + L-Glutamine (1%) HEPES (12.5mM) + β-Mercaptoethanol (0.05mM)	
Human DCs	DMEM + human serum (10%, heat-inactivated) +L-Glutamine (1%) + P/S (1%) HEPES (10mM)	

Table 6. List of buffers.

Buffer	**Composition** **(materials in bold freshly added before use)**
10x PBS	1.37 M NaCl 27 mM KCl 100 mM $Na_2HPO_4*2H_2O$ 18 mM KH_2PO_4 10g
RIPA lysis buffer	1% Na-DOC (Sodium Deoxycholate) 0,1% SDS 0,15 M NaCl 0,01 M Na-Phosphate 2 mM EDTA **1 mM PMSF** **2x protease inhibitor cocktail mix (Roche)** **1% NP-40**
E6 and E7 lysis buffer	10 mM Tris-HCl pH 7.5 50 mM KCl 2 mM $MgCl_2$ 1% Triton® X-100
SDS-PAGE running buffer (10x)	0.25 M Tris 1.92 M Glycine 1% SDS
Western blot transfer buffer	25 mM Tris 192 mM Glycine pH 8.3 **20% Methanol**
Western blot washing buffer (0.2% PBST)	0,2 % Tween 20 in 1xPBS
Western blot blocking buffer	5 % non-fat milk 1 % BSA In 0.2 % PBST (= washing buffer)
FACS staining buffer	1% FCS In 1x PBS

ELISpot wash buffer	0.05 % Tween20 In 1x PBS
Fixative buffer for FACS	0.2% PFA in PBS
ACK RBC lysis buffer	150mM NH_4Cl + 10mM $KHCO_3$+0.1mM EDTA
Lysis buffer for immunoprecipitation	1% IGEPAL-630 in 1xPBS
Medium	
ELISpot blocking medium	RPMI + FCS (5%) + P/S (1%)+ L-Glutamine (1%) HEPES (12.5mM) + β-mercaptoethanol (0.05mM)

Table 7. List of HLA-A2 binding peptides and control peptides.

Peptide	**Sequence**
HPV16 E6 R17I/9-17	FQDPQERPI
HPV16 E6 R17I/9-19	FQDPQERPIKL
HPV16 E6/18-26	KLPQLCTEL
HPV16 E6 Q21D/18-26	KLPDLCTEL
HPV16 E6/18-28	KLPQLCTELQT
HPV16 E6 Q21D/18-28	KLPDLCTELQT
HPV16 E6/25-33	ELQTTIHDI
HPV16 E6 D32E/25-33	ELQTTIHEI
HPV16 E6/28-38	TTIHDIILECV
HPV16 E6 D32E/28-38	TTIHEIILECV
HPV16 E6 D32E, I34R/28-38	TTIHEIRLECV
HPV16 E6/29-38	TIHDIILECV
HPV16 E6 D32E/29-38	TIHEIILECV
HPV16 E6 D32E, I34R /29-38	TIHEIRLECV
HPV16 E6/34-44	ILECVYCKQQL
HPV16 E6/52-60	FAFRDLCIV
HPV16 E6/79-87	KISEYRHYC
HPV16 E6 H85Y/79-89	KISEYRYYCYS
HPV16 E6 H85Y, L90V/81-90	SEYRYYCYSV
HPV16 E6 H85Y/81-90	SEYRYYCYSL

HPV16 E6 H85Y/83-90	YRYYCYSL
HPV16 E6 H85Y, L90V/83-90	YRYYCYSV
HPV16 E6 H85Y, L90V/84-93	RYYCYSLYGT
HPV16 E7/7-15	TLHEYMLDL
HPV16 E7/7-17	TLHEYMLDLQP
HPV16 E7/11-18	YMLDLQPE
HPV16 E7/11-19	YMLDLQPET
HPV16 E7/11-20	YMLDLQPETT
HPV16 E7/11-21	YMLDLQPETTD
HPV16 E7/12-19	MLDLQPET
HPV16 E7/12-20	MLDLQPETT
HPV16 E7/66-74	RLCVQSTHV
HPV16 E7/76-86	IRTLEDLLMGT
HPV16 E7/77-86	RTLEDLLMGT
HPV16 E7/77-87	RTLEDLLMGTL
HPV16 E7/80-90	EDLLMGTLGIV
HPV16 E7/81-90	DLLMGTLGIV
HPV16 E7/81-91	DLLMGTLGIVC
HPV16 E7/82-90	LLMGTLGIV
HPV16 E7/82-91	LLMGTLGIVC
HPV16 E7/82-92	LLMGTLGIVCP
HPV16 E7/83-93	LMGTLGIVCPI
HPV16 E7/84-93	MGTLGIVCPI
HPV16 E7/85-93	GTLGIVCPI
HPV16 E7/86-93	TLGIVCPI
Endogenous controls	
DEAD box polypeptide 17 isoform p82 variant/227-235	YLLPAIVHI
Coatomer subunit γ/1147-155	AIVDKVPSV
Spiked-in mouse peptides	
Cyclin-dependent kinase inhibitor 1B/33-41	FGPVNHEEL

Spectrin α chain non-erythrocytic (isoform X1)/393-401	KALINADEL
Cytosolic iron-sulphur assembly component 2B/144-152	AALENTHLL
ELISpot controls	
HIV Nef/137-145	LTFGWCFKL
CEF peptide pool	CMV, EBV and Flu peptides (PA-CEF-001)

Table 8. List of peptide pools.

Pool 1	**Pool 2**	**Pool 3**	**Pool 4**	**Pool 5**	**Pool 6**	**Pool 7**
E6/18-26	E6 Q21D/18-28	E6 Q21D/18-26	E6 R17I/9-19	E6 R17I/9-17	E6 D32E/25-33	E6/28-38
E6 D32E, I34R/28-38	E6 D32E/29-38	E6/29-38	E6/18-28	E6/79-89	E6 D32E/28-38	E6 H85Y/81-90
E6/34-44	E6 H85Y,L90V/81-90	E6H85Y, L90V/83-90	E6/25-33	E7/7-15	E6 H85Y/83-90	E7/11-19
E6/52-60	E7/11-18	E6 H85Y/84-93	E6 D32E, I34R/28-38	E7/12-20	E7/12-19	E7/76-86
E7/11-20	E7/66-74	E7/7-17	E6/79-87	E7/77-86	E7/82-90	E7/80-90
E7/81-90	E7/77-87	E7/11-21	E7/81-91	E7/84-93	E7/86-94	E7/86-93
E7/83-93	E7/82-91	E7/82-92	E7/85-93			

4 Methods

4.1 Cell culture

4.1.1 Culturing of cervical cancer cells and controls.

Cells were cultured in their respective medium (Table 5). For culturing, the cells were seeded according to their doubling time. Especially for SNU1299, 866, MRI-H-196 and Marqu cells, it is important to seed initially at high density (30% confluency) to maintain the cells in proliferative state. For C33A on the other hand, a low initial seeding density is required to avoid overconfluence, since these are rapidly proliferating cells (doubling time 12 hours). All the cells used are adherent cells.

Thawing cells

Cells were removed from liquid nitrogen, and placed in a water bath preheated to 37°C. Thawed cells were diluted 1:10 in complete medium. An aliquot was taken for cell counting and cells were centrifuged at 300xg for 5min at room temperature. The medium was removed and the cells were resuspended in around 5ml medium. Cells were seeded in appropriate flasks according to the cell numbers, to maintain optimal seeding density.

Sub-culturing

Cells were monitored regularly under a microscope for their confluency. At a maximum confluency of 70%, the cells were washed with PBS and harvested by addition of trypsin, followed by incubation for 5-7 minutes. When the cells were detached from the flask, trypisinization was stopped by addition of the respective cell medium, containing serum, and the cells were collected into a 50ml falcon tube. Cells were centrifuged at 300xg for 5 min and resuspended in fresh medium. Reseeding was performed according to the doubling time of the cells and when they were needed. Cells should not be reseeded below a 1:10 seeding density, since a minimum confluence is required for cells to survive and proliferate. For cells grown in serum free medium, it is essential to wash with PBS after harvesting, before reseeding to ensure complete removal of trace amounts of trypsin.

During culture, the cells were regularly monitored for adherence to the bottom of the flask, as well as their normal appearance as refractory, rounded cells under a light microscope. Cells which were not proliferating, appearing unhealthy or dying were discarded, and fresh aliquots were brought into culture.

Cell counting

Cells were counted using the Countess Automated cell counter. Briefly, cells were diluted 1:1 with 0.4% Trypan Blue and 10µl added onto the cell counting slide and counted using the counting chamber.

Freezing cells

Cryovials were pre-labelled, and freezing medium (complete cell medium + 40% FBS + 10% DMSO) was prepared and chilled on ice. The cells were washed, then harvested by trypsinization, and counted. The cells were resuspended in freezing medium at a concentration of $5x10^6$ cells/ml, and transferred to cryovials. These were placed in a −80°C freezer in a Cryo-Safe Cooler overnight and then transferred to liquid nitrogen.

4.1.2 PBMC isolation

Peripheral blood mononuclear cells (PBMCs) were isolated from buffy coats of healthy blood donors. These were ordered from DRK Blutspendedienst Mannheim. Prior to PBMC isolation, 1:5 diluted buffy coats were FACS stained to assess whether they are HLA-A2 positive (see 4.4.2). PBMC isolation was continued only for HLA-A2 positive donors. 15 ml Ficoll-Paque ^{TM}PLUS was added to each 50ml sterile Leucosep tube and centrifuged at 300g for 1 minute at 20° C (±2°C). The diluted blood from one donor was distributed amongst six Ficoll-filled Leucosep tubes and centrifuged at 600xg for 25 minutes at room temperature in a swinging bucket rotor with acceleration set to 5/9 and deceleration set to 0/9. The upper plasma fractions were discarded, and the buffy layer, enriched in leukocytes, was collected in three 50ml falcons. Tubes were filled with sterile 1xPBS and centrifuged at 300xg for 15 minutes at room temperature (acc 9/9, dec 5/9). The supernatant was discarded. If a red pellet was observed, 5ml ACK lysis buffer was added to the tubes, mixed vigorously, and incubated for 5 minutes at room temperature with continuous gentle shaking. Lysis was stopped by filling the tubes with sterile 1xPBS and centrifugation at 300xg for 10 minutes at room temperature (acc 9/9, dec 9/9). The supernatant was discarded, and the cells were pooled into one 50ml falcon. Washing was repeated twice more with 1x PBS. 50-80 million cells per donor were resuspended per 1ml of cold freezing medium (human serum with 10% DMSO) and were transferred into cryovials labelled with donor number, number of cells, date and initials. The vials were placed in a −80°C freezer in a Cryo-Safe Cooler overnight and then transferred to liquid nitrogen. To thaw the PBMCs, vials were placed in 37°C water bath for 1 minute and 1 ml cell suspension was added to 9 ml 1xPBS. The cells were diluted 1:10 and counted. Cell were plated in either DC or T cell medium, according to the subsequent assay.

4.1.3 Short-term T cell cultures

Short-term T cell cultures were set up for assessment of immunogenicity of HPV16 E6 and E7-derived peptides by assessing memory T cell responses to these, by subsequent ELISpot assays. The scheme of culturing is depicted in Figure 5. 1ml of human Interleukin 7 (rhIL-7; 50µg/ml, final concentration 10ng/ml) supplemented T cell medium was distributed per well into alternate wells of four 24-well plates. To each pre-labelled well, 2µl of either one of 46 HLA-A2-binding HPV 16-derived E6 and E7 synthetic short peptides (10mg/ml, final concentration 10µg/ml) was added. To the control wells, 50µl of CEF peptide pool that is a cocktail of viral peptides of cytomegalovirus (CMV/C), Epstein-Barr-Virus (EBV/E) and influenza (flu/F) (40µg/ml, final concentration 1µg/ml) as positive control or 2µl of a HLA-A2-binding human immunodeficiency virus-derived peptide (HIV-A2; 10mg/ml, final concentration 10µg/ml) as negative control was added. One vial of previously isolated PBMCs, containing at least 50 million cells, was thawed, counted with the Countess Automated Cell Counter and centrifuged at 300xg for 5 minutes. PBMCs were resuspended in 50 ml of the rhIL-7-supplemented T cell medium and 1 ml of the solution was distributed into each well containing the different peptides (1-2x10^6cells/well). Plates were placed in a 37°C humidified CO_2 incubator. On day 3 on setting up the cultures, 10µl of recombinant human Interleukin 2 (rhIL-2) (stock 10^5U/ml, final concentration 20U/ml) was added to each well. On the seventh day after starting the cultures, a half-medium change was performed. The plates were centrifuged at 300g for 5 minutes, followed by replacing half the medium per well with fresh T cell medium containing 2x IL2 (stock 10^5U/ml, final concentration 40U/ml). Twelve days after setting up the assay, the cultures were used to set up the ELISpot assay.

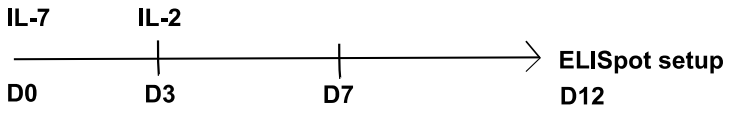

Figure 5. Layout for culturing of short-term T cell lines.
Prior to ELISpot setup, the PMBCs were cultured for 12 days, with HPV16 E6- and E7-derived HLA-A2 binding peptides, and controls (see Table 7) to expand memory T cells present in the donors from prior HPV16 exposure. To enhance the survival of T cells, PBMCs were cultured in the presence of IL-7 (10ng/ml) and supplemented with IL-2 (20U/ml) on the third and seventh day of culturing (marked vertical lines). On day 12, the cultures were used for setting up the ELISpot assay.

4.1.4 Autologous DC cultures

Autologous DCs were generated for use in generating semi-long-term peptide-specific $CD8^+$ T cell lines as per the scheme outlined in Figure 6. PBMCs were thawed, counted and seeded at a density of $1x10^7$ cells per well in a 6-well plate in DC medium. After incubation for a minimum of 3 hours in a 37°C humidified CO_2 incubator, the cells were observed under a microscope for adherent monocytes. After adherence, the supernatant was removed, and 2ml DC medium supplemented with GM-CSF (Granulocyte-macrophage colony-stimulating factor; 100µg/ml = $1x10^6$U/ml, final concentration 0.1µg/ml = 1000U/ml) and rhIL-4 (recombinant human Interleukin 4; 100µg/ml = $1x10^6$U/ml, final concentration 0.05µg/ml 500U/ml) was added to the wells, for the differentiation of monocytes to DCs. The supernatant was centrifuged and the cells contained therein were frozen for generation of T cell lines. Three days after setting up the assay, 0.5ml fresh DC medium supplemented with GM-CSF (100µg/ml = $1x10^6$U/ml, final concentration 0.1µg/ml = 1000U/ml) and rhIL-4 (100µg/ml = $1x10^6$U/ml, final concentration 0.05µg/ml 500U/ml) was added per well. On the sixth day, a maturation cocktail was added to each well. This consisted of TNF-α (Tumor Necrosis Factor α; 100µg/ml = $1x10^7$U/ml, final concentration 0.01µg/ml = 1000U/ml), IL-1β (Interleukin 1 β; 50µg/ml, final concentration 10ng/ml), IL-6 (Interleukin 6; 100µg/ml, final concentration 10ng/ml), PGE_2 (Prostaglandin E_2; 10mg/ml, final concentration 1µg/ml) and LPS (Lipopolysaccharides; 5mg/ml = $5x10^4$U/ml, final concentration 1µg/ml = 10U/ml). On day eight, DCs in suspension were collected into a 15ml or 50ml falcon tube (depending on number of wells seeded) and used for peptide loading. Immature DCs were also collected by gentle scraping.

Peptide-loading of DCs

Harvested DCs were centrifuged at 300xg for 5 minutes at room temperature, and resuspended in serum free DC medium at a concentration of $1x10^6$ cells/ml. These were distributed 1 ml per 15 ml falcon tube. The peptide of choice was added (10mg/ml stock, final concentration of 10µg/ml) and the tubes were incubated for 3 hours in a 37°C humidified CO_2 incubator with slightly unscrewed caps. Tubes were shaken gently every hour. After 3 hours, peptide loaded DCs were washed in cold DC medium and centrifuged at 300xg for 5 minutes at room temperature. Cells were resuspended in T cell medium, counted and used for generation of semi-long term peptide-specific $CD8^+$ T cells. For each peptide-specific semi-long term T cell line, 2 generations of DCs were generated.

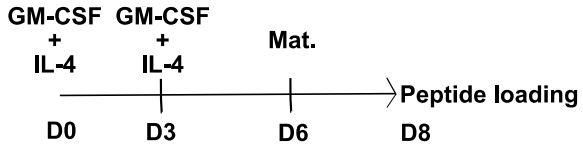

Figure 6. Layout for culturing DCs.
DCs were generated from PBMCs by allowing monocytes to adhere to cell culture plates, followed by culturing for 3 days in the presence of GM-CSF (100µg/ml) and IL4 (0.05µg/ml) for promoting differentiation to DCs. GM-CSF and IL-4 were again added on day 3. On day 6, DC maturation was induced by addition of a maturation cocktail composed of TNF-α (0.01µg/ml), IL-1β (10ng/ml), IL-6 (10ng/ml), PGE_2 (1µg/ml) and LPS (1µg/ml). DCs were harvested 48 hours after maturation and loaded with respective peptides.

4.1.5 Semi long-term T cell cultures

Semi long-term T cell cultures were generated as per the scheme outlined in Figure 7. To generate the peptide-specific T cell lines, all remaining PBMCs from a donor were thawed and combined with the supernatant of the 2nd generation of the DCs, containing all non-adhering PBMCs. To enable this, the DC generation 2 and the semi-long term T cell line generation were started on the same day. The PBMCs were counted, and $2x10^7$ PBMCs per well (at least 5 wells in total per peptide were needed for sufficient $CD8^+$ T cells at the end) were seeded in a 12-well plate in 2ml T-cell medium supplemented with 2x concentrated rhIL-7 (50µg/ml, final concentration 10ng/ml). To these, peptide-loaded DCs (from the 1st DC generation) resuspended in 2 ml T-cell medium were added. The PBMC/DC ratio was maintained at ideally 50:1, or minimum 200:1 depending on the sufficiency of cell numbers. Cells were placed in a 37°C humidified CO_2 incubator. Every second day until day 14, IL-2 (10^5U/ml, final concentration 50U/ml) was added to the wells. If the media turned a yellowish orange, a half medium change was performed. On day 8, cells were stimulated again with peptide loaded DCs from the 2nd DC generation (Figure 6) On day 12, each culture was divided equally into two 24-well plates. One of the plates was moved to the hypoxia chamber with 1% O_2 and 5% CO_2, whereas the other plate remained at the incubator with 20% O_2 and 5% CO_2 (see section 4.2). Cells were collected on day 14 and used for $CD8^+$ T cell isolation and subsequent cytotoxicity assay setup.

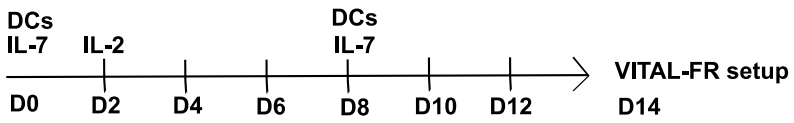

Figure 7. Layout for culturing of semi-long term T cell lines.
To generate $CD8^+$ T cells for use in cytotoxic T cell assays (VITAL-FR), the PBMCs were cultured for 14 days. PBMCs were cultured with IL-7 (10ng/ml), which was added again on day 8. The cultures were supplemented with IL-2 (50U/ml) every second day (marked with vertical lines). Peptide-loaded DCs (labelled DCs in figure) were added on day zero and day 8. These were generated as described in the previous section (4.1.4).

4.2 Hypoxia treatment of cells

Biological replicates of plated cells were simultaneously treated to hypoxia and normoxia (Figure 8). For hypoxia treatment, the cells were placed in a hypoxia chamber (Baker Ruskinn, InVivo2 workstation) for the intended duration, as mentioned in the specific figure legends. The cells were harvested by taking them out of the chamber in airtight boxes, followed by rapid processing for downstream purposes, to minimize re-exposure to 21% oxygen.

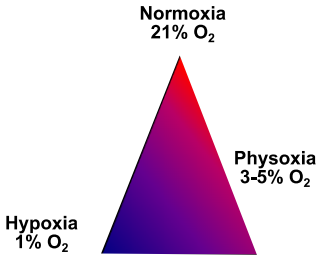

Figure 8. Hypoxia treatment of cells
Oxygen concentrations vary widely amongst cell culture (normoxia), healthy tissue (physoxia) and the TME (hypoxia). Most cell culture studies are performed at normoxia, which is defined as 21% O_2. Healthy tissues have oxygen ranging between 3-5%, varying on the tissue. This is termed as physoxia. The oxygen concentration in the TME, particularly for cervical cancer is 1%. For this thesis, normoxia and hypoxia were compared.

4.3 Western Blotting

4.3.1 Preparation of protein lysates

Protein lysates for the detection of HIF1α were made using RIPA lysis buffer (Table 6). Specifically, 400µl of buffer was used per one 60mm dish, and cells were harvested by scraping the dishes. This was done within the hypoxia chamber for hypoxia-treated cells. The lysate was transferred into pre-labelled Eppendorf tubes. These tubes were incubated on ice for 10 minutes, with intermediate vortexing. Then the lysates were centrifuged at 12,000xg for 5 minutes. The supernatant was transferred to fresh pre-labelled Eppendorf tubes. Lysates intended for use in detection of HIF1α Western blots were aliquoted into 100µl aliquots, to avoid repeated thawing and refreezing. The E6 and E7 lysis buffer was used to prepare cell lysates intended for detection of E6 and E7 proteins.

4.3.2 Protein concentration estimation

Protein concentration estimation was done using the DC assay kit, observing the manufacturer's instructions. The DC protein assay is a colorimetric assay, based on a principle similar to the Lowry assay. Briefly, a 1:5 dilution of the protein lysate was prepared, and 2µl of this were pipetted in triplicate wells of a flat-bottomed 96-well plate. Serial dilutions of BSA protein standard (Table 4) were used for the calculation of protein concentrations, ranging between 1.5mg/ml to 0.2mg/ml. Triplicates of 2µl of each dilution of the protein standard were also added to the plate. Solutions A, S and B are provided in the kit. 20µl of AS solution (20µl of solution S per 1ml of solution A) was added to each well. Then 200µl of solution B was pipetted into each well, and the plates were incubated in the dark for 15min. The plates were read using a Multiscan GO spectrophotometric plate reader, at 750nm excitation wavelength. Calculations were performed using an MS Excel template, where a standard curve is generated using the absorbance values and the known concentrations of the protein standards. Using this standard curve and the absorbance values of the samples, their protein concentrations were calculated.

4.3.3 SDS-PAGE and Western blotting

For the detection of HIF1α (MW 110kDa), 50µg of protein was loaded per well on a MiniProtean TGX ™ Any kD™ SDS-PAGE gel. The gels were run in a BioRad electrophoresis chamber in 1% SDS running buffer at 120V for 10min, followed by 90V for 1 hour. A prestained Kaleidioscope™ molecular weight marker (10-250kDa) was run alongside, in a separate well. Then the gels were removed from the apparatus and blotted onto a PVDF membrane using wet transfer, using 1x Transfer buffer, containing 20% freshly added methanol. Before the transfer, the PVDF membrane was activated by 30s incubation in absolute methanol. The gel and the membrane were arranged in a wet transfer cassette, with the membrane towards the

positive electrode. Bubbles were removed, and on both sides Western blot filter paper, and the foam pads provided with the transfer apparatus, were placed. Electrophoretic transfer was done by placing the transfer chamber in ice to keep it cool. Transfer was done for 90min at 90V.

For detection of E6 and E7 proteins, 30µg of total protein was loaded into the wells. SDS-PAGE running conditions were identical to those described above. However, these proteins were transferred onto the PVDF membrane using semi-dry transfer. This is more suitable for low MW weight proteins like E6 and E7 (around 21kDa). Electrophoretic transfer was done for 1 hour at 150mA.

The blots were then blocked for 1 hour in blocking buffer consisting of 5% milk in PBST (1x PBS containing 0.5% Tween-20). Then the blots were cut at an appropriate marker position, so that one of the strips could be probed for the protein of interest (HIF1α, E6 or E7), and the other for the loading control (α-Tubulin). Incubation with the primary antibody was done overnight at a shaker at 4°C. A 1:1000 dilution was used for all primary antibodies. The following day, the blots were washed thrice with 0.2% PBST buffer, for 10 minutes each, followed by incubation with anti-rabbit or anti-mouse HRP (horse radish peroxidase)-coupled secondary antibody (1:5000 dilution). All antibodies used are listed in the Materials section in Table 4. Incubation with secondary antibody was performed for 1 hour at room temperature. Following incubation, the blots were washed with 0.2% PBST for three times, and developed using ECL detection reagents. The Pierce ECL has lower sensitivity, and was thus used for detection of the highly abundant protein loading control α-Tubulin. HIF1α, E6 and E7 bands were detected using higher sensitivity ECL Prime Western Blot Detection Reagent (GE Healthcare). The blots were scanned in the GelDoc^{TM} EZ Imager. The full membrane and marker bands were imaged using the colorimetric mode, followed by the chemiluminescence mode for the detection of protein bands. Multiple images were taken in a preset time of 15 minutes, especially for the hard to detect HIF1α bands.

Controls

Treatment of cells to hypoxia, by placing within a hypoxia chamber, was considered an intrinsic control for HIF1αinduction. For E7 detection across cells, lysates from PAP-A2 cell line, established previously in our lab were used as a positive control given their high level of E7 expression, and their parental cell line 2277NS was used as a negative control [140]. The controls were checked in all cells, but are only depicted in the supplementary figure 1.

4.4 Flow cytometry

4.4.1 FACS staining of cervical cancer cells

Cells were harvested by trypsinization into individual Eppendorf tubes, pre-labelled with normoxic or hypoxic. Cells from one of the replicates for both normoxia and hypoxia were also collected for unstained controls as well as isotype control. Anti HLA-A2-FITC antibody was added to the cells at a dilution of 1:100, followed by incubation in the dark for 20 minutes, and the isotype control-FITC to the isotype controls. For certain cells, first staining revealed lower levels of HLA-A2, so the staining was repeated with a 1:50 dilution of the antibody.

Subsequently, cells were washed, and then fixed with 1% PFA in PBS for 10 minutes in the dark. FACS acquisition was done at the BD FACS Canto, at the FACS core facility, DFKZ, using the BD FACSDiva™ software. Photomultiplier tube (PMT) voltages for the forward scatter (FSC) and side scatter (SSC) were optimized for each cell line using unstained controls. Gating for target cells was done using FSC-A and SSC-A. Then the isotype control was used to set the PMT voltages for the FITC channel, as well as HLA-A2 positive and HLA-A2 negative gates. Within these gates, the statistic 'geometric mean of the FITC+ population' was added. This was used to calculate the fold change in HLA-A2, in hypoxia normalized to normoxia. Analysis was done using FlowJo™ software.

4.4.2 FACS staining of buffy coats

An aliquot of up to 2ml of diluted buffy coats from each donor was transferred into a sterile 50 ml tube. RBCs were lysed using 10 ml ACK lysis buffer and incubated for 5 minutes at room temperature with gentle shaking. Lysis was stopped by filling the tubes with sterile 1xPBS followed by centrifugation at 300xg for 5 minutes at room temperature. The cells were resuspended in PBS and equally distributed into 3 pre-labelled Eppendorf tubes for unstained control, isotype control and anti-HLA-A2-FITC antibody. The corresponding antibodies were added to the cells at a dilution of 1:100, followed by incubation in the dark for 10 minutes. Cells were washed, and then fixed with 1% PFA in PBS. FACS analysis was performed with with the BD Accuri C6 flow cytometer. Gating was performed using the FSC-A and the SSC-A gates, on the lymphocytes. The isotype control was used to set the HLA-A2 positive and negative gates. Since HLA-A2 is an HLA-I molecule, it is presented by all nucleated cells. Thus, donors were considered HLA-A2+ when no overlap was seen between the antibody-stained and the isotype-stained populations.

4.5 Mass spectrometry

4.5.1 Label free quantification (LFQ) mass spectrometry-based detection of APM components

Samples were prepared using RIPA lysis buffer in 4 replicates from normoxia- and hypoxia-treated HPV16-transformed cells and controls. The further processing of the samples, as well as acquisition by LC-MS were done by Sophia Föhr. Sample preparation for mass spectrometry was done using the published SP3 method [141]. This procedure was compared with in-gel trypsin digestion (protocol used as by the proteomics core facility, DKFZ), using a test sample. For SP3 sample preparation, after equilibration to room temperature for 10min, Sera Mag A and B beads were combined in equal volumes, and the mixture diluted to 1:5 with water, in PCR tubes. 2µl beads mixture was used for a maximum of 20µg protein, per sample. The diluted beads were placed on the magnetic rack and allowed to settle for 2min. The supernatant was subsequently discarded. The beads were washed twice by removing from the magnetic stand, resuspending in 200µl water, placing on the magnetic stand again, and removing supernatant after the beads were settled. The beads were resuspended in water at a concentration of 100µg/µl.

RIPA lysates (same samples as used for HIF1α detection, Section 4.3.1) were used as input sample, containing 10µg protein, per sample (estimation by DC assay, Section 4.3.2). Per sample, 2µl of the Sera A and B bead mix were added in a PCR tube. Acetonitrile was subsequently added at a final concentration of 50%, and the sample was incubated at RT for 18minutes. Then the sample was placed on the magnetic stand for another 2min at RT. Supernatant was discarded. 200µl of 70% ethanol was added to the samples and they were incubated again for 15 seconds on the magnetic stand. Then 180µl of acetonitrile was added per sample, and the samples were incubated for another 15 seconds on the magnetic stand. Supernatant was discarded and the beads were air dried for 1 min. The samples were resuspended in 10µl of 100mM TEAB digestion buffer. The samples were sonicated for 5minutes. Trypsin was added (1:50 enzyme: substrate ratio) to the samples followed by overnight incubation at 37°C.

For peptide cleanup, acetonitrile was added at a concentration of 95%, to each sample and these were incubated at RT for 18min. Then the tubes were placed on the magnetic rack for another 2 minutes. Subsequently the supernatant was discarded. 180µl acetonitrile was added to the samples, followed by incubation on the 15 seconds on a magnetic stand, and the supernatant was discarded. This step was repeated, and the samples were air dried for 1min. The beads were reconstituted in 0.1% TFA and sonicate for 5 minutes. Recover supernatant while making sure not to recover any beads, and transfer to a clean PCR tube. Samples were centrifuged for 30 seconds at maximum speed, to remove any precipitates.

Samples were acquired using the Orbitrap Exploris 480 mass spectrometer, coupled with the Dionex Ultimate 3000 LC. LC separation of samples was performed using a nanoEase M/Z Peptide LC column (1.7µm BEH 130Å C18 material, 75µm inner diameter, 200mm length). Samples were separated using a gradient of solvent A (99.9%water, 0.1% formic acid) and solvent B (80% acetonitrile, 0.1% formic acid, 19.9% water), at a flow rate of 300 nl/min. The following LC gradient was used for separation 0min solvent B 2%, 3min solvent B 2%, 4min solvent B, 5%, ,106min solvent B 38%, 107min solvent B 95%, 109min solvent B 95%, 110min solvent B 2% and 120min solvent B 2%. After separation by LC, the samples were injected into the MS for acquisition. The scan range for MS1 (m/z) was 350-1500, with the Orbitrap resolution of 15,000, desired minimum points across the peak was 9, m/z isolation window 1.4, and fixed collision energy.

Data analysis was carried out by MaxQuant [142] using an organism specific database extracted from Uniprot.org under default settings. Identification FDR cutoffs were 0.01 on peptide level and 0.01 on protein level. Match between runs option was enabled to transfer peptide identifications across Raw files based on accurate retention time and m/z. Quantification was done using a label free quantification approach based on the MaxLFQ algorithm [143]. A minimum of 2 quantified peptides per protein was required for protein quantification. Data was further processed by in-house compiled R-scripts.

The **statistical analysis** was performed with the R-package limma [144]. Protein groups with non-zero intensity values in 70% of the samples of at least one of the conditions were used for statistical analysis. Missing value imputation was performed via random values drawn from a down shifted normal distribution of the corresponding sample. The setup with a down-shift of 1.8 standard deviation (SD) and a width of 0.3 SD was adapted from the default parameters of the Perseus software package [145]. The p-values were adjusted with the Benjamini–Hochberg method for FDR to adjust for multiple testing [146].

4.5.2 Targeted epitope detection strategy

Immunoprecipitation and desalting of samples

Immunoprecipation (IP) of HLA-A2-peptide complexes was performed as published [106]. Briefly, in-house produced anti-HLA-A2 antibody (clone BB7.2) was coupled onto Protein G GammaBind Plus Sepharose beads. Cells previously expanded up to 60 or 120 90% confluent 10cm cell culture dishes, were harvested using lysis buffer for IP (1% IGEPAL-630). 1ml buffer was used for harvesting cells from 4 dishes (approximately 10million cells per 1 10cm dish). The antibody-coupled beads were added to the cell lysate. IP was performed for 4 hours at 4°C on a rotor. After IP, the beads were thoroughly washed until they

were free of detergent. Supernatent was removed completely in the last wash. Elution of peptides from the IP sample was performed using 0.1% TFA.

In the context of this thesis, several detergents were compared (1% n-Octyl β-D-glucopyranoside (OGP), 1% Digitonin, 1% CHAPS, 1% n-Dodecyl-β-D-maltoside (DDM)/ 0.1% Cholesteryl hemisuccinate (CHM, 1% OGP/ 0.25% Sodium deoxycholate (SDC) and 1% DDM) for their efficiency of enrichment of HLA-A molecule as described in detail in the Masters thesis of Catharina Lotsch, supervised by me.

For the setup of an on-column IP, a peristaltic pump was set up and anti-HLA-A2 antibody (BB7.2) was coupled to CNBr-activated protein G Sepharose beads. The column was washed with lysis buffer, packed with antibody-coupled beads, then the cell lysate was run through the column overnight at 4°C, using the peristaltic pump. Different elution buffers such as 0.1% TFA, 0.2% TFA and 10% acetic acid.

Desalting was performed using reverse phase liquid chromatography with in-house assembled micro-columns with Zorbax SB-C18 5µm, filled in 200µl tips, followed by using 1 mL Sep-Pak tC18 cartridges [106]. In the context of this thesis, this technique was compared with several desalting approaches (ultrafiltration, 96-well SepPak plate), in several combinations.

Buffers were used for desalting using reverse phase separation of proteins and salts from peptides present in the IP sample, as published for in-house assembled Zorbax microcolumns or SepPak tC18 cartridges [106]. For ultrafiltration using the Amicon 3kDa filters, the manufacturer's instructions were followed. Briefly, the filter was washed with 50% methanol. Then, the sample was added, and centrifugation was performed for 1h at 12,000-13,000g. The flowthrough was collected. The filter was then washed in 50% methanol for 40min. Flow through was collected, and transferred to LoBind eppis.

Post desalting, samples were dried using a SpeedVac concentrator, and stored at -20°C till analysis by MS. For analysis by LC-MS resuspended in 3% acetonitrile with 0.1% Formic acid. Spiked-in peptides were added at a concentration of 10ng/ml (10pmol/ml final concentration).

A sample derived from 200 million cells was used per injection for LC-MS analysis.

Liquid chromatography and Mass spectrometry analysis

Reverse-phase nano-scale liquid chromatography coupled with tandem mass spectrometry (nanoLC-MS) was used to detect the HLA-A2-binding peptides on HPV16-transformed cells. This was done using the NanoAcquity UPLC (Waters), coupled with a QTRAP-6500 (AbSciex) mass spectrometer. Targeted MS^3 mass spectrometry was used as per the published protocol, which involves the analysis of the spectrum of a fragment of a fragment of a peptide, and is thus highly specific. Synthetic peptides were used to generate

reference spectra of each of the 17 Cys-free HPV16 E6- and E7-derived HLA-A2-binding peptides [106]. Data analysis was performed in the Analyst^{R} software, followed by exporting the raw data. This data was imported into MS Excel 2016 and MS^3 and MRM spectra figures were generated using GraphPad Prism software v7.

MRM (Multiple reaction monitoring) mass spectrometry was used for a quantitative approach to compare several sample preparation methods. The sample acquisition was done by Dr. Renata Blatnik. The MRM method used was previously setup using synthetic peptide mixture containing cysteine-free HLA-A2 binding peptides. Data analysis was done by exporting the data from the Analyst^{R} software, into MS Excel 2016, followed by generating graphs in the GraphPad Prism software v7. Here the total peptide count for the respective peptide, normalized to spiked-in control mouse peptides (Table 7), was used for quantification.

4.6 ELISpot assay

The INFγ ELISpot assay was used to screen the buffy coats for memory T cell responses against HPV16 E6- and E7-derived peptides. This was set up using the short-term T cell cultures (Section 4.1.3). Between the days 10-11 of the short-term cultures, before setting up the ELISpot assay, the ELISpot plates were coated with anti-human IFNγ (clone 1-D1K 1 mg/ml) antibody. The antibody was diluted 1:500 in sterile 1xPBS and 100µl per well was added to six 96-well Millipore Multiscreen-HA membrane sterile plates per donor. The plates were incubated overnight (or longer up to 48h) at 4°C. The following day, antibody was discarded and wells were washed 3 times with sterile 1xPBS using a sterile plate washer. Plates were blocked with 200µl ELISpot medium per well at 37°C for 1 hour. For each T cell culture, 100µl T cell medium containing HLA-A2-restricted HPV16 E6- or E7 -derived synthetic short peptides were used in six replicates (stock 10mg/ml, final concentration 10µg/ml). 100µl T cell medium containing DMSO (final concentration 1µl/ml) as negative control and Concanavalin A (ConA; 5mg/ml, final concentration 2µg/ml) as positive control were added to the plates in triplicates. Short-term T cell cultures were resuspended and 100µl (0.05 - 0.1 x 10^6 cells) was added on the wells containing the corresponding peptides. The plates were incubated for 24 hours at 37°C in a still incubator, without stacking and undisturbed. After a minimum duration of 20h, to maximum 24h, the plates were developed. The plates were washed twice with 1xPBS and twice with ELISpot washing buffer using a plate washer. 100µl of bioinylated anti-human IFNγ clone 7 B6-1-Biotin solution diluted 1:1000 in 1xPBS was added to each well and the plates were incubated in the dark for 2 hours at room temperature. Subsequently, the plates were washed 4 times with ELISpot washing buffer and 100µl of Streptavidin-Alkaline Phosphatase (ALP) solution diluted 1:2000 in 1xPBS was added

to each well. This was followed by incubation in the dark for 1.5 hours at room temperature. After 1.5 hours, the plates were washed 4 times with ELISpot washing buffer. 100µl of p-nitroblue tetrazolium chloride/5-bromo-4-chloro-3-indolyl phosphate (NBT/BCIP; equilibrated at room temperature and filtered through 0.22µm filter) was added to each well and incubated in the dark, covered with aluminium foil for 10-20 minutes until spot formation was observed. The timing was started from addition of the NBT/BCIP reagent to the first plate. The plates were monitored for spot development after 10min. The reaction was stopped by washing wells on both sides of the membrane with tap water. The plates were air-dried overnight in the laminar flow hood. Analysis was done using the automated CTL ImmunoSpot reader. Spot forming units (SFU) per one million cells were calculated by multiplying the spot count with number of cells seeded per well. Stimulation Index (SI) was calculated by dividing spot counts test wells to the mean spot count in DMSO background wells.

4.7 Cytotoxicity assays

4.7.1 Labelling of target cells

One day before setting up the assay (day 13 of semi-long-term T cell stimulation, section 4.1.5), target cells were labelled with respective fluorophores. CaSki and C33A cells (thawed fresh a few days before each assay), were harvested by trypsinization, and counted. Cells were diluted in RPMI medium without supplements at a concentration of $1x10^6$ cells/ml. Carboxyfluorescein succinimidyl ester (Stock 10mM, final concentration 5µM) dye was mixed with $2x10^6$ of CaSki cells, i.e. the specific targets. CellTrace™ Far Red stain (Stock 1mM, final concentration 0.25µM) was added to $2x10^6$ of C33A cells, i.e. the non-specific targets, in 50 ml tubes. The cells were incubated for 10 minutes in the water bath while shaking the tubes occasionally. The reactions were stopped by filling the tubes up to 50 ml with pre-warmed stopping medium (90 ml RPMI containing 10% FCS) and centrifugation at 300xg for 5 minutes at room temperature. Each cell line was resuspended in the respective medium (Table 5) and plated into at least two wells of a 6-well plate, and incubated overnight in a humidified cell culture incubator with 21% O_2 and 5% CO_2.

4.7.2 $CD8^+$ T cell isolation

After 14 days of culturing with stimulation with peptide-loaded DCs, peptide-specific $CD8^+$ T cells were isolated for the cytotoxicity assay. Isolation was performed using magnetic-activated cell sorting technology (MACS; by Miltenyi Biotec) for the T cell cultures in normoxia and hypoxia. T-cells were collected in a 15 ml falcon, counted and centrifuged at 300xg for 10 minutes. The cell pellet was resuspended in 40µl MACS buffer per 10^7 total cells, followed by addition of 10µl $CD8^+$ T Cell Biotin-Antibody Cocktail per 10^7 total cells. The suspension was mixed and incubated for 15 minutes at 4°C. 30µl

MACS buffer was subsequently added per 10^7 total cells, followed by 20µl $CD8^+$ T Cell MicroBead Cocktail per 10^7 total cells and incubation for 15 minutes at 4°C. Cells were washed by adding 2 ml MACS buffer and centrifuged at 300xg for 10 minutes. Cells were resuspended in 500µl MACS buffer, for up to $1x10^8$ cells. For hypoxic T cells, the rest of the procedure was performed outside the hypoxia chamber. An LS column was placed on the magnetic field of a suitable MACS Separator. The column was rinsed with 3ml MACS buffer. The cell suspension was applied onto the column with a new 15ml tube at the bottom. Since this is a negative selection protocol, the unlabeled cells that passed through without attachment to the LS column, were of interest and were collected. The column was washed 3 times with 3 ml buffer and the flow-through was collected in the same tube. Cells were counted and resuspended in T cell medium supplemented with 2x concentrated IL-2 (stock 10^5U/ml, final concentration 50U/ml) at a concentration of 1.4 million cells per 600µl medium. Hypoxic T cells were immediately transferred back into hypoxia, and let rest for at least 30min before encountering the targets.

4.7.3 Setting up the assay

The setup of the assay is outlined in Figure 9. Labelled CaSki and C33A target cells were harvested by trypsinization, counted and resuspended in T cell medium at a concentration of 0.12 million cells per ml (to have 3000 target cells/50µl, after mixing the targets together).

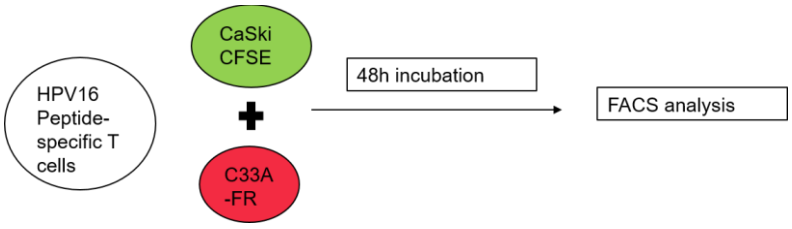

Figure 9. Layout of VITAL-FR assay.
The VITAL-FR assay is set up by incubating the peptide-specific $CD8^+$ T cells, with a mixed population of specific (CaSki) and non-specific (C33A) target cells for 48 hours. The target cells are labelled with different fluorescent dyes (CFSE for HPV16-transformed CaSki, and Far Red for HPV negative C33A) which enables their distinction during FACS analysis, for assessment of specific killing

Equal volumes of each cell line were mixed in a falcon tube. The isolated $CD8^+$ T cells were resuspended at a concentration of 2.3 x 10^6 $CD8^+$ T cells/ml, in 2x IL-2 (stock 10^5U/ml, final concentration 50U/ml) containing T cell medium. This was done to minimize differences amongst replicates caused due to pipetting errors, so that the replicates represent biological controls. Then, 100µl of the suspension of mixed target cells was added to each well to reach a final volume of 200µl per well. The final assay contained 3000 target cells from each cell line (CFSE and FarRed stained cells), resulting in a total of 6000

target cells per well and the appropriate $CD8^+$ T cell numbers were calculated so as to achieve the different E:T ratios as listed below (scheme of the plate: Table 9). As a control, mixed labelled target cells without $CD8^+$ T cells were seeded in 4 wells.

Separately, each of single stained target cells and mixed target cells were seeded on two wells of a 6-well plate for FACS gating. The assay was set up once for the normoxic $CD8^+$ T cells, which were incubated in a 37°C humidified CO_2 incubator and once for hypoxic $CD8^+$ T cells which were incubated in a 1% O_2 hypoxia chamber for 48 hours, since day 12. Another assay was also set up with hypoxia-preincubated target cells, where mentioned. Any remaining $CD8^+$ T-cells were frozen in cold freezing medium, and transferred to liquid nitrogen.

T cell:target cell ratio	**T cell number**
40:1	$2.4x10^5$
20:1	$1.2x10^5$
10:1	$6x10^4$
5:1	$3x10^4$
2.5:1	$1.5x10^4$
1.25:1	$7.5x10^3$
no T cells	

Table 9. VITAL-FR assay cell numbers.
The VITAL-FR cytotoxicity assay was set up with different effector: target (E:T) ratios. This table depicts the cell numbers required per E:T ratio. Each ratio was set up in triplicates. The controls with no T cells were used for normalization for the differential proliferation of the two target cells (CaSki and C33A). These cells were also used for gating during FACS analysis.

4.7.4 FACS analysis

After 48 hours, the cells from the plates were harvested for subsequent FACS analysis. Harvesting of normoxia and hypoxia VITAL-FR plates was timed so as to maintain the same duration of the cytotoxicity assay. The supernatants from the 48-well plates were transferred into pre-labelled Eppendorf tubes. The wells were rinsed with 200µl of PBS which was transferred into the same Eppendorf tubes. The non-adherent T cells were harvested so as to enable gating on target cells and exclusion of T cells during subsequent FACS analysis. 200µl Trypsin/EDTA solution was added to each well until all cells were detached, approximately 8 minutes. 200µl of 1xPBS containing 10% FCS was added to inactivate the

Trypsin and collect the cells. Finally, wells were rinsed with another 200µl of 1xPBS containing 10% FCS and transferred into the same Eppendorf tubes. Cells seeded in a 6-well plate for gating were also harvested by trypsinization. All harvested cells were centrifuged at 300g for 5 minutes at room temperature. Supernatants were discarded and cells were fixed with 100µl 1%PFA in PBS. The samples were washed and resuspended in FACS buffer. Cells were stored at 4°C in the dark until the analysis. FACS analysis was performed on the BD FACS-Canto instrument at the Flow Cytometry Core Facility, DKFZ. The singly stained controls were used for setting the PMT voltages and the gates, using the following channels: CFSE–FITC, FarRed – Alexa647. Raw FACS data was exported as .fcs files. Data analysis was done using FlowJo software v10. Analysis of specific killing was done using an in-house Excel sheet template based on the published VITAL-FR assay. Specific killing at each E:T ratio is calculated by the formula 100 - ((CFSE+)/(FR+)$_{E:T}$)/((CFSE+)/(FR+))$_{no\ T}$, where no T depicts the controls set up with no T cells, and CFSE+ and FR+ represent the cell count in the respective gates from flow cytometry analysis [147]. The assay was performed in hypoxia or normoxia, using different setups, regarding the target cells and the T cells as described in the respective figure legends, and depicted in Figure 10.

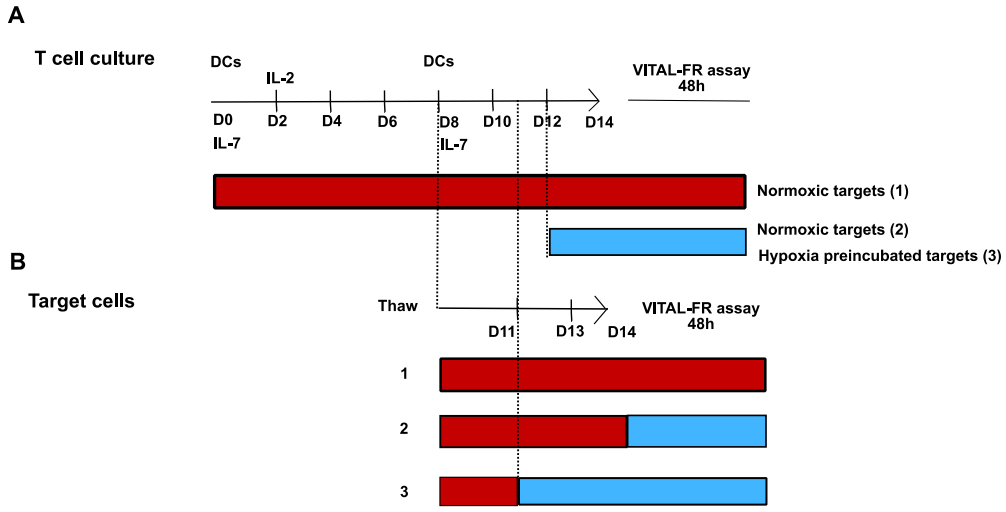

Figure 10. Layout of cultures for normoxic and hypoxic VITAL-FR cytotoxicity assays.
For comparison of cytotoxicity in normoxia versus hypoxia, different schemes for incubation of the T cells and/or the targets in normoxia and hypoxia were used. The figure describes the culturing of the different populations in normoxia (red) or hypoxia (blue). A) T cells were cultured in normoxia from day 0 of the semi-long term T cell cultures (see Figure 7). On day 12, the cultures were equally distributed into normoxia and hypoxia. Both normoxic (red) and hypoxic (blue) T cells were used against normoxia(-cultured target cells (1 and 2). The hypoxic T cells were additionally used against hypoxia-preincubated targets(3), where specified. B) Target cells were thawed on day 8 of the semi long term culture of T cells, and cultured in normoxia. For preincubation in hypoxia, cells were placed in hypoxia on day 11 of semi-long-term of T cells (3). The VITAL-FR assay was performed in normoxia for condition 1 (normoxic T cells and normoxic targets), and hypoxia for condition 2 (hypoxic T cells and normoxic targets), and where applicable in hypoxia for condition 3 (hypoxic T cells and hypoxia pre-incubated targets).

5 Results

5.1 HPV16-transformed cells are responsive to hypoxia.

For this study, seven cervical cancer cell lines (CaSki, SNU17, SNU703, SNU1299, 866, MRI-H-196 and Marqu(CxCa)) and 2 HPV negative controls (NOK and C33A) were used. The cervical cancer cells were transformed with different HPV16 variant lineages (Table 5). The control cells were HPV negative cervical cancer cells C33A and normal oral keratinocytes (NOK). Since HLA-A2 is the most frequently expressed HLA-I allele in the Caucasian population, as per the Allelefrequency.net website, cells that express this HLA-I allotype were selected. The first step towards assessing the effect of hypoxia on HPV16-transformed cells was to establish a model system for hypoxia treatment. To assess the effect of hypoxia on HPV16-transformed cells, It was decided to compare cells treated to hypoxia (1% O_2) with cells simultaneously treated to normoxia (21%) (Figure 8). Normoxia at 21% O_2 was selected as a point of comparison, since most *in-vitro* studies have studied cells cultured under these conditions. The hypoxic O_2 levels were chosen to be comparable to those reported for cervical cancer [137]. HIF1α protein levels are stabilized under hypoxia [148]. Thus, to assess whether the cell lines of interest are indeed responsive to hypoxia, HIF1α protein levels in normoxic and hypoxic HPV16-transformed cells and in HPV-negative control cells were assessed. HIF1α protein levels were observed to be increased in all the cell lines upon 24h hypoxia (Figure 11). as can be seen in the Western blots, and the respective quantification (Figure 11a). At least 2-fold increase in HIF1α was observed upon hypoxia in HPV negative control cells (NOK and C33A), as well as all the HPV16-transformed cells upon 24h hypoxia treatment (Figure 11b and Supplementary figure 1).

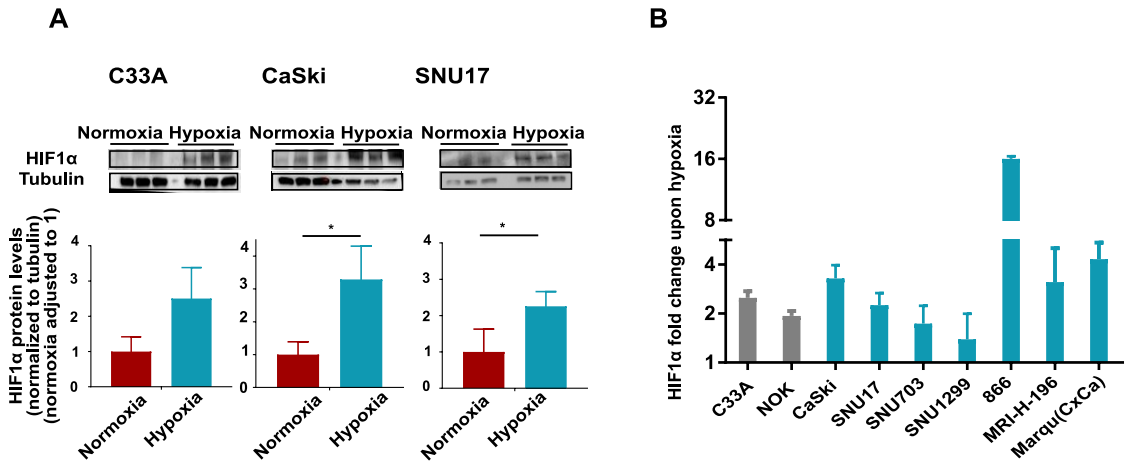

Figure 11. HPV16-transformed cells are responsive to hypoxia.
*Cells were cultured either in normoxia or hypoxia for 24 hours, in biological triplicates. The cells were lysed using RIPA lysis buffer, directly from the plates. HIF1α levels in the cells were assessed using SDS-PAGE and Western blotting with anti-HIF1α antibody. α-tubulin was used as the loading control. A) Western blot images (upper panel) and quantification (lower panel) of HIF1α levels upon hypoxia in C33A, CaSki and SNU17 cells. For quantification, the HIF1α band intensities (ImageJ software) were normalized to α-tubulin in the corresponding lane. Subsequently, the α-tubulin normalized band intensity for each lane (normoxia and hypoxia) was divided by mean intensity (normoxia), thus adjusting band intensities in normoxia to 1, and accordingly adjusting the hypoxia band intensities. The mean of biological triplicates +/- SD is depicted. Statistical testing was done using paired t tests using GraphPad Prism v7. * p value<0.05, n=3. (lower panels). B) Fold change in HIF1α levels upon hypoxia across different HPV16-transformed cell lines. Fold change was calculated as (mean α-tubulin normalized HIF1α band intensity hypoxia/normoxia). HPV negative cells are depicted with grey bars. Bars depict the fold change with error bars representing the error propagation. Calculations were done in MS Excel 2016 and the graphs were plotted in GraphPad Prism v7.*

In addition, in C33A and CaSki cells, we also observed an increase in HIF1α levels upon a longer 48h hypoxia treatment (Figure 12). It was thus concluded that all cell lines of interest are responsive to hypoxia. This also validated the hypoxia treatment regime, which was used for all subsequent experiments.

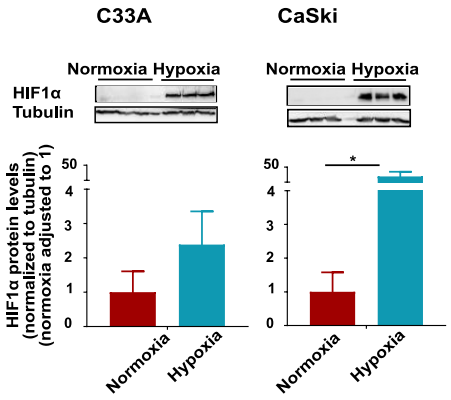

Figure 12. CaSki and C33A cells are responsive to 48h hypoxia.
*Cells were cultured either in normoxia or hypoxia for 48 hours, in biological triplicates. The cells were lysed using RIPA lysis buffer, directly from the plates. HIF1α levels in the cells were assessed using SDS-PAGE and Western blotting with anti-HIF1α antibody. α-tubulin was used as the loading control. Western blot images (upper panel) and quantification (lower panel) of HIF1α in C33A and CaSki cells. For quantification, the HIF1α band intensities (ImageJ software) were normalized to α-tubulin in the corresponding lane. Subsequently, the α-tubulin normalized band intensity for each lane (normoxia and hypoxia) was divided by mean intensity (normoxia), thus adjusting band intensities in normoxia to 1, and accordingly adjusting the hypoxia band intensities. The mean of biological triplicates +/- SD is depicted. Statistical testing was done using paired t tests using GraphPad Prism v7. * p value<0.05, n=3. (lower panels).*

5.2 Decrease in HPV16 oncoproteins E6 and E7 upon 24h hypoxia treatment.

As elaborated above, HPV16 E6 and E7 have important roles in the life cycle of the virus, as well as playing a key role in the transformation of cells into cancer (section 1.1.4). Given their importance as targets for immunotherapies (section 1.3.2), it was investigated whether the expression levels of these proteins are affected by hypoxia. Studies from another group have shown that E6 and E7 proteins levels are decreased in HPV16 (CaSki, SiHa, MRI-H-186) and HPV18-transformed cells upon hypoxia treatment [137, 139]. Thus, it was of interest to investigate if this is also true in the additional cell lines transformed with different HPV16 variant lineages. Thus, each cell line treated to normoxia and hypoxia, was assessed for E6 and E7 protein levels. A stark decrease in E6 levels can be observed upon 24h hypoxia in CaSki cells (Figure 13), consistent with previous literature [137], as well as SNU17 cells. Surprisingly, the levels of E6 protein were too low to be detected in normoxia by Western blotting in the other HPV16-transformed cell lines (data not shown).

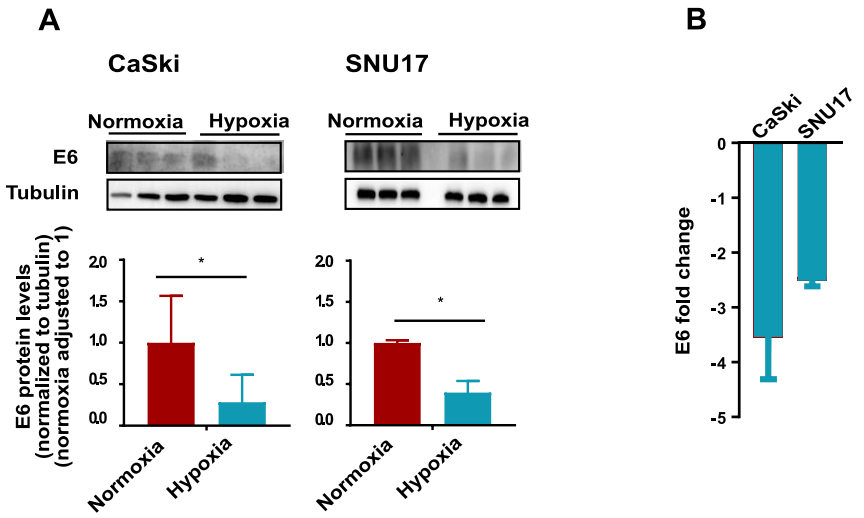

Figure 13. Decrease in E6 protein levels upon hypoxia.
*Cells were cultured either in normoxia or hypoxia for 24 hours, in biological triplicates. The cells were lysed using E6/E7 lysis buffer. E6 levels in the cells were assessed using SDS-PAGE and Western blotting with anti-E6 antibody. α-tubulin was used as the loading control. A) Western blot images (upper panel) and quantification (lower panel) of E6 levels upon hypoxia in CaSki and SNU17 cells. For quantification, the E6 band intensities were normalized to α-tubulin in the corresponding lane. Subsequently, the α-tubulin normalized band intensity for each lane (normoxia and hypoxia) was divided by mean intensity (normoxia), thus adjusting band intensities in normoxia to 1, and accordingly adjusting the hypoxia band intensities. The mean of biological triplicates +/- SD is depicted. Statistical testing was done using paired t tests using GraphPad Prism v7. * p value<0.05, n=3. (lower panels). B) Fold change in E6 levels in CaSki and SNU17. Fold change was calculated as (mean α-tubulin normalized E6 band intensity normoxia/hypoxia). For ease of visualization of decreased levels, the fold change is depicted on the negative axis. Bars depict the fold change with error bars representing the error propagation. Calculations were done in MS Excel 2016 and the graphs were plotted in GraphPad Prism v7.*

Thus, E7 the other HPV16 oncoprotein, was the focus for other cell lines. E7 protein levels were also seen to be starkly decreased upon 24h hypoxia in CaSki cells (consistent with previous literature, Figure 14), as well as in all other cell lines (Figure 14 and Supplementary figure 2). For all cell lines, a fold change in E7 protein levels upon hypoxia was calculated (Figure 14b). As for E6 fold change (Figure 13b), for better visualization, here too, the inverse of the fold change is depicted. Thus, this data confirms previous literature and extends it to other HPV16-transformed cells. It can be concluded that hypoxia leads to a strong decrease in the expression of the protein levels of the HPV oncoproteins E6 and E7 in HPV16-transformed cells. This change is consistently seen irrespective of the HPV16 variant lineage present in the cells.

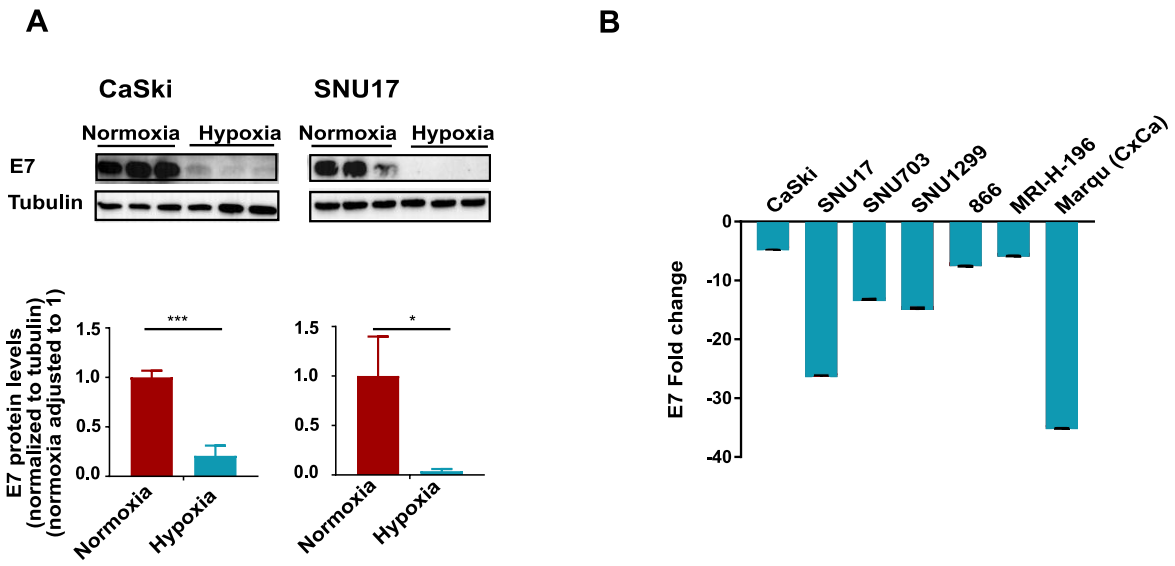

Figure 14. Decrease in E7 protein levels upon hypoxia
*Cells were cultured either in normoxia or hypoxia for 24 hours, in biological triplicates. The cells were lysed using E6/E7 lysis buffer. E7 levels in the cells were assessed using SDS-PAGE and Western blotting with anti-E7 antibody. α-tubulin was used as the loading control. A) Western blot images (upper panel) and quantification (lower panel) of E7 levels upon hypoxia in CaSki and SNU17 cells. For quantification, the E7 band intensities were normalized to α-tubulin in the corresponding lane. Subsequently, the α-tubulin normalized band intensity for each lane (normoxia and hypoxia) was divided by mean intensity (normoxia), thus adjusting band intensities in normoxia to 1, and accordingly adjusting the hypoxia band intensities. The mean of biological triplicates +/- SD is depicted. Statistical testing was done using paired t tests using GraphPad Prism v7. * p value<0.05, *** p value <0.001 n=3. (lower panels). B) Fold change in E7 levels upon hypoxia in CaSki and SNU17. Fold change was calculated as (mean α-tubulin normalized E7 band intensity normoxia/hypoxia). For ease of visualization of decreased levels, the fold change is depicted on the negative axis. Bars depict the fold change with error bars representing the error propagation Calculations were done in MS Excel 2016 and the graphs were plotted in GraphPad Prism v7.*

5.3 Timeline of E7 decrease upon hypoxia in CaSki cells.

Next, it was of interest to investigate the timeline of the decrease in the expression of E7 in the cell line of interest, CaSki. Cells were plated at one time point, then placed in hypoxia and harvested at the respective time points, along with their normoxic counterparts. A decrease in E7 protein levels was only observed from 24h onwards. After 24 hours of hypoxia treatment, the cells still have very low levels of E7 protein, which were undetectable at 48 hours (Figure 15a).

The fold change of E7 protein levels, at the different time points was calculated. The timeline of change in E7 protein levels upon increasing hypoxia duration (compared to normoxia) can be observed in Figure 15b.

From these results, it can be observed that while a mild decrease is seen in E7 protein levels under shorter hypoxia durations, it takes longer than 12 hours, and up to 24 hours of hypoxia exposure for a significant decrease in protein expression to be observed. Also, hypoxia treatment of 48 hours leads to a decrease in E7 protein levels below those detectable by Western blotting.

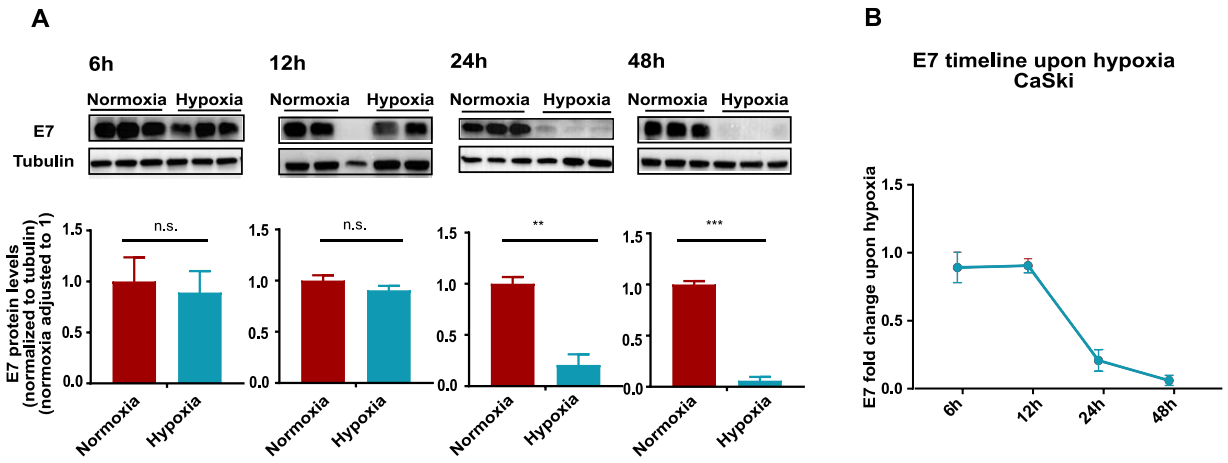

Figure 15. Timeline of E7 expression upon hypoxia in CaSki cells
*Cells were cultured either in normoxia or hypoxia for the mentioned time periods, in at least two biological replicates. The cells were harvested by trypsinization and lysed using E6 and E7 lysis buffer. E7 levels in the cells were assessed using SDS-PAGE and Western blotting with anti-E7 antibody. α-tubulin was used as the loading control A) Western blot images (upper panel) and quantification (lower panel) of E7 levels upon hypoxia in CaSki across different durations of hypoxia. For quantification, the E7 band intensities were normalized to α-tubulin in the corresponding lane. Subsequently, the α-tubulin normalized band intensity for each lane (normoxia and hypoxia) was divided by mean intensity (normoxia), thus adjusting band intensities in normoxia to 1, and accordingly adjusting the hypoxia band intensities. The mean of biological replicates +/- SD is depicted. Statistical testing was done using paired t tests using GraphPad Prism v7. n.s. non significant * p value<0.05,**p value <0.01 *** p value <0.001 n=3 (or 2, 12h hypoxia). (lower panels). B) Fold change in E7 protein was calculated as the ratio of the mean tubulin.normalized E7 band intensity in hypoxia to the mean tubulin normalized E7 protein level in normoxia. The fold change across the different time points is depicted, with error bars depicting error propagation. Calculations were done in MS Excel 2016 and the graphs were plotted in GraphPad Prism v7.*

5.4 Investigating the effect of hypoxia on the APM components

After observing that hypoxia leads to decreased expression of the main HPV16 oncoproteins E6 (Figure 13) and E7 (Figure 14 and Figure 15), which are the target of choice for most immunotherapies (section 1.3.2), the next question was to investigate the effect of hypoxia on the presentation of E6 and E7-derived epitopes on the cell surface. Given the critical role of antigen presentation for targeting of virus-infected or cancer cells by $CD8^+$ T cells, any effect of hypoxia on the APM might reflect in changes in recognition and targeting of hypoxic HPV16-transformed cells by $CD8^+$ T cells. Thus, it was of interest to investigate the effect of hypoxia on the various APM components. For this, a repertoire of APM components were selected, as representative candidates of the various steps of HLA-I antigen presentation (section 1.2.2.1). The selected components are listed in Table 10 below.

APM components	***Function***
PSMB5-10, PSME1, 2	*Proteasome subunits*
TAP1, TAP2	*Transporter molecules*
ERAP1, ERAP2, PDIA	*Enzymes*
CALR, CANX	*Chaperones*
MHC I (HLA I; HLA A), B_2M	*Surface presentation of peptide*

Table 10. APM components
A list of the APM components that were investigated in the study. A repertoire of proteins which represent all steps of antigen presentation, namely the proteasome subunits (degradation of the protein into peptides), transporter molecules (transport into the ER), enzymes (trim the peptides to the appropriate size of 8-10aa), chaperones (loading of peptides onto the MHC I), and the MHC I complex proteins themselves was selected.

To assess the effect of hypoxia on the APM component proteins Label free quantitation-based mass spectrometry was used. To ensure that the results were statistically robust, four replicates per condition (normoxia/hypoxia) per cell line were used. First, for the preparation of the cell lysates for analysis by liquid chromatography and mass spectrometry, in-gel trypsin digestion was compared with the SP3 sample preparation [141] (Figure 16).

As can be seen in Figure 16a, the total peptide count was higher in SP3 sample preparation as compared to in-gel trypsin digestion. This was true for both normoxic and hypoxic samples. Thus, this method was considered suitable. A crucial step for the suitability of this method was to ensure that the proteins of interest are detectable by the IDA mass spectrometry approach, following the LFQ analysis. Thus, in a test run, the number of unique+razor peptides for the detection of the proteins of interest was assessed. Unique+razor peptides are peptides unique to a particular protein, and assigned to it with the highest number of peptides. It was observed that most APM component proteins of interest could be detected with at least two unique+razor peptides (Figure 16b). Thus, this approach was deemed suitable for analysis and was used for analysis of all the HPV16-transformed cell lines and controls.

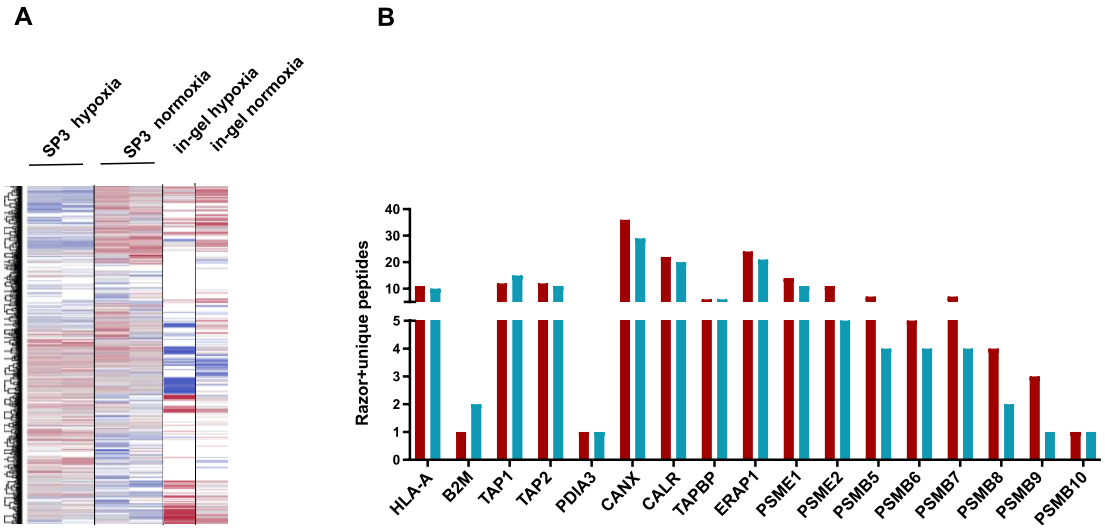

Figure 16 Comparison of sample preparation methods (Sophia Fohr).
CaSki RIPA lysates were used to assess whether SP3 or in-gel trypsin digestion sample preparation, followed by LFQ mass spectrometry (MS) analysis is more suitable for detection of the selected APM components. A) Using both normoxic and hypoxic test CaSki lysates, sample preparation for MS analysis was done using SP3, and in-gel trypsin digestion. LC-MS analysis was performed with the UltiMate 3000 LC and Q Exactive HF-X mass spectrometer. The results are depicted as a heatmap of total proteins detected in each sample. Two technical replicates were run for the SP3 sample preparation samples, and only one replicate for the in-gel digestion samples. B) Following LC-MS analysis, analysis was performed with MaxQuant software for the identification of unique+razor peptides per APM protein protein of interest. Number of unique+razor peptides are depicted in normoxic samples (red) and hypoxic samples (red). Graph was created using using GraphPad Prism v7.

Volcano plots for cell lines selected for in-depth analysis, C33A, CaSki and SNU17, depicting the log fold change (x axis) vs the –log of the adjusted p value for the fold change (y axis) in the entire proteome upon 24h hypoxia can be seen in Figure 17. None of the APM components is significantly affected by 24h hypoxia in any of the target cells of interest.

The effect of hypoxia was also investigated in cells transformed with other HPV16 variant lineages. It can be observed that hypoxia affects the whole proteome differentially amongst the different HPV16-transformed cells and controls (Figure 17 and Figure 18). Surprisingly, no significant changes were observed in any of the APM components upon 24h hypoxia treatment in any of the cell lines.

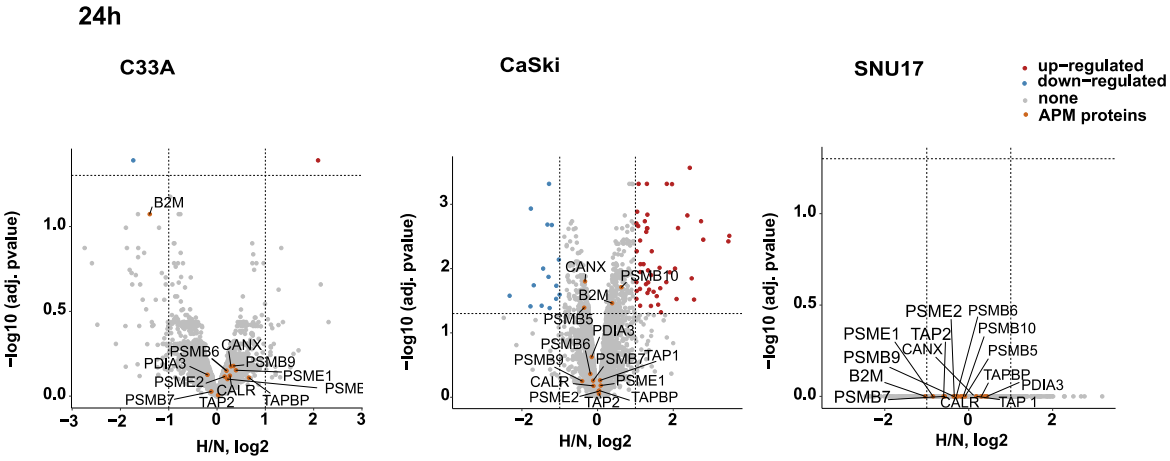

Figure 17. APM upon 24h hypoxia in selected cells.
Cells were treated to 24 hours normoxia and hypoxia, in four biological replicates. Cells were harvested and lysates were prepared by RIPA lysis. Sample preparation for mass spectrometry was done using SP3 sample preparation, and the samples were analysed by mass spectrometry, using the UltiMate 3000 LC coupled with the Orbitrap Exploris 480 mass spectrometer. Data analysis was performed with the MaxQuant software, followed by statistical analysis using the R script limma. Volcano plots were created using the –log10 (adjusted p values) vs the log2 fold change upon hypoxia vs. normoxia (H/N, log2). The volcano plots depict the changes in the whole proteome upon hypoxia, with the proteins of interest marked in orange. Upregulated proteins are shown in red, downregulated proteins in blue, and unchanged expression with grey. Figures prepared in collaboration with Karim Aljakouch. Significance thresholds (dashed lines) were used as published in literature, at log fold change of +/-1 and a p value cutoff of 0.05.

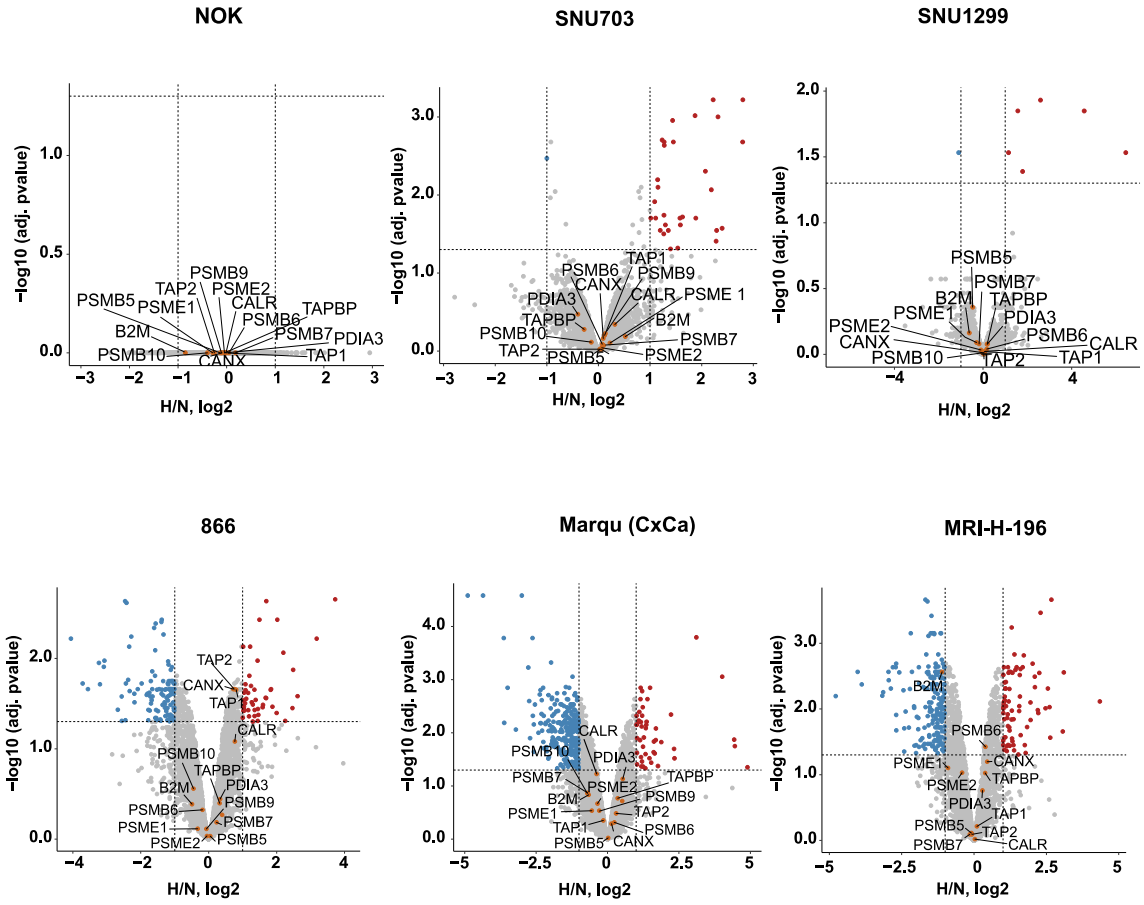

Figure 18. APM upon 24h hypoxia in other cells

Cells were treated to 24 hours normoxia and hypoxia, in four biological replicates. Cells were harvested and lysates were prepared by RIPA lysis. Sample preparation for mass spectrometry was done using SP3 sample preparation, and the samples were analysed by mass spectrometry, using the UltiMate 3000 LC coupled with the Orbitrap Exploris 480 mass spectrometer. Data analysis was performed with the MaxQuant software, followed by statistical analysis using the R script limma. Volcano plots were created using the –log10 (adjusted p values) vs the log2 fold change upon hypoxia vs. normoxia (H/N, log2). The volcano plots depict the changes in the whole proteome upon hypoxia, with the proteins of interest marked in orange. Upregulated proteins are shown in red, downregulated proteins in blue, and unchanged expression with grey. Figures prepared in collaboration with Karim Aljakouch. Significance thresholds (dashed lines) were used as published in literature, at log fold change of +/-1 and a p value cutoff of 0.05.

Since by 24h of hypoxia, extremely low levels of E7 protein in CaSki cells were still detectable, but the expression was completely lost upon 48h hypoxia treatment (Figure 15), we tested for the effect of longer hypoxia duration on the APM proteins in the control cells C33A, as well as two HPV16-transformed cells, CaSki and SNU17. The volcano plots are depicted in Figure 19, and similar to 24h hypoxia treatment, no significant change was observed on the expression of any of the APM components. Thus, these results suggest that the APM is unaffected in cervical (and oral) epithelial cells by hypoxia.

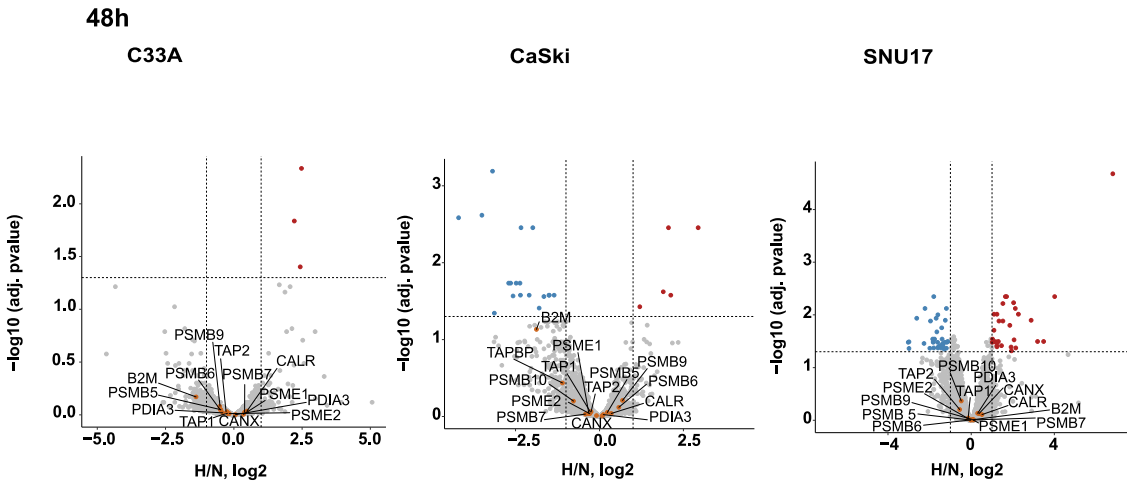

Figure 19. APM upon 48h hypoxia in selected cells
To investigate whether longer hypoxia treatment affects the APM, C33A, CaSki and SNU17 were treated to 48 hours normoxia and hypoxia, in four biological replicates. Cells were treated to 24 hours normoxia and hypoxia, in four biological replicates. Cells were harvested and lysates were prepared by RIPA lysis. Sample preparation for mass spectrometry was done using SP3 sample preparation, and the samples were analysed by mass spectrometry, using the UltiMate 3000 LC coupled with the Orbitrap Exploris 480 mass spectrometer. Data analysis was performed with the MaxQuant software, followed by statistical analysis using the R script limma. Volcano plots were created using the –log10 (adjusted p values) vs the log2 fold change upon hypoxia vs. normoxia (H/N, log2). The volcano plots depict the changes in the whole proteome upon hypoxia, with the proteins of interest marked in orange. Upregulated proteins are shown in red, downregulated proteins in blue, and unchanged expression with grey. Figures prepared in collaboration with Karim Aljakouch. Significance thresholds (dashed lines) were used as published in literature, at log fold change of +/-1 and a p value cutoff of 0.05.

5.5 Hypoxia treatment does not affect HLA-A2 expression levels .

The HLA-I expression on the cell surface is critical for recognition by $CD8^+$ T cells. The mass spectrometry-based approach suggested no change in the expression levels of the APM components upon hypoxia. However, this does not address the specific expression levels on the cell surface. HLA-A2+ cells were used for this study, since HLA-A2 is the most commonly expressed HLA-I allele in the Caucasian population. The effect of 24h hypoxia on HLA-A2 levels on cells, was addressed by flow cytometry. The histogram overlay of the representative normoxic and hypoxic replicates, along with the MFI values across 3 biological replicates can be seen in Figure 20a for the three selected cell lines of interest (C33A, CaSki and SNU17). It can be observed that HLA-A2 levels are not significantly changed in either the HPV-negative C33A cells or the HPV16-transformed CaSki or SNU17 cells. The fold change in the MFI upon 24h hypoxia (compared to normoxia) for all 9 cell lines, including controls was calculated. It can be observed that 24h hypoxia treatment did not strongly change the surface expression levels of HLA-A2 in any of the HPV16-positive cell lines or controls (Figure 20b)

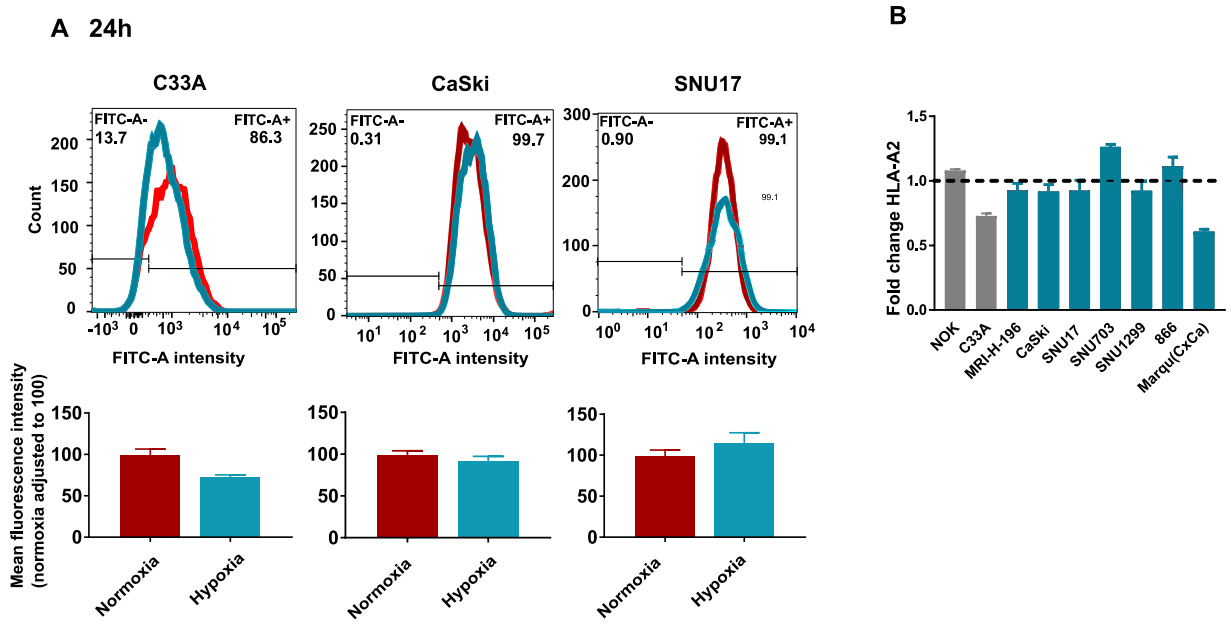

Figure 20. Effect of 24h hypoxia on HLA-A2
Cells were treated to normoxia or hypoxia for 24 hours in biological triplicates. Cells were harvested and stained for HLA-A2 levels, using a FITC-labelled antibody. Acquisition was performed on the BD FACS Canto II at the DKFZ Flow cytometry core facility. A) Representative histograms of FITC intensity on the x axis vs count of events on the y axis of one of the replicates are depicted. The normoxic (red) and hypoxic (blue) samples are overlayed. Bottom panels depict the MFI (mean fluorescence intensities) for normoxic and hypoxic cells +/- SD, normalized to normoxic MFI (which was adjusted to 100).
B)Fold change of HLA-A2 upon hypoxia was calculated for all the cells, by the ratio MFI hypoxia/average MFI normoxia. Error bars depict the error propagation. Analysis was performed using FlowJo v10.6, followed by MS Excel version 10. Graphs were made using GraphPad Prism v7.

Effect of longer hypoxia treatment (48h) was also explored in control cell line C33A and HPV16-transformed cells CaSki and SNU17. It was observed that long-term hypoxia also did not lead to a regulation of the HLA-A2 levels on the surface of these cells (Figure 21).

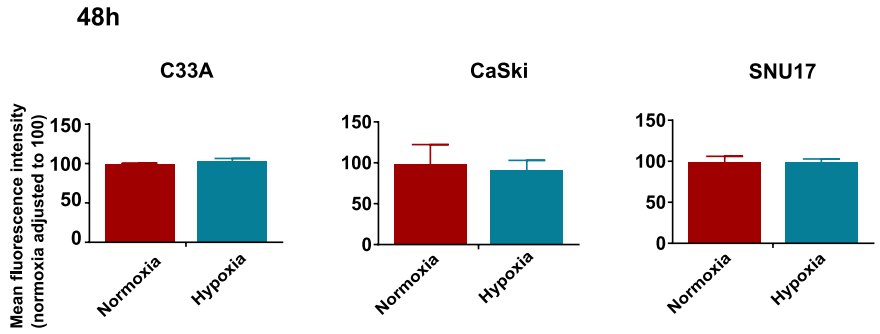

Figure 21. Effect of 48h hypoxia on HLA-A2 levels.
To investigate whether longer hypoxia has an effect on HLA-A2 levels, cells were treated to normoxia or hypoxia for 48 hours in biological triplicates. Cells were harvested and stained for HLA-A2 levels, using FITC-labelled antibodies. Acquisition was performed on the BD FACS Canto II at the DKFZ Flow cytometry core facility. The MFI (mean fluorescence intensities) for normoxic and hypoxic cells +/- SD, normalized to normoxic MFI (which was adjusted to 100) is depicted. Analysis was performed using FlowJo v10.6, followed by MS Excel 2016. Graphs were made using GraphPad Prism v7.

5.6 Mass spectrometry-based detection of HPV16-derived peptides.

So far, it was observed that the HPV16 oncoproteins E6 and E7 are decreased in expression upon hypoxia, but the APM machinery seems largely unperturbed. For the design of a therapeutic vaccine against HPV16-induced malignancies, the best candidate peptides would be those presented on the cell surface in a hypoxic microenvironment. With the eventual goal to investigate whether hypoxia affects the surface presentation of peptides, different steps of the targeted mass spectrometry-based epitope detection strategy developed in our group, were optimized to improve the sensitivity and reproducibility of the previously established IP process [106]. The main challenge for the IP protocol used for the detection of HPV16 E6- and E7-derived peptides is the need to start with extremely high cell numbers, because of the low abundance of these peptides. Since the IP protocol was established previously in CaSki cells, SNU17 cells were used to enhance the throughput of the IP protocol. An on-column IP was set up using SNU17 cells and was compared to the already established in-solution IP protocol [106].

Figure 22a shows the MRM spectra of an endogenous control peptide from both on-column IP and in-solution IP, with the synthetic peptide spectra displayed downwards. A good match between the RT (retention time) of elution, and the relative intensities of the different transitions between the IP and the synthetic peptide spectra, was used as an indication of a successful detection. Comparing the spectra between the in-solution IP and the on-column IP, it was concluded that the on-column IP was successfully

established (Figure 22b). Next, different elution protocols were compared in the on-column IP, for elution of the HLA-peptide complex from the antibody-beads, with the standard in-solution IP protocol. The endogenous control peptide intensity, from the MRM scan, was used as a readout. It was observed that elution with 10% acetic acid, or once with 0.1% TFA was slightly better than the other approaches (Figure 22b). It was also observed that re-IP using the run-through lysate did not yield many peptides, indicating good efficiency of the on-column IP. However, when these methods were compared with the in-solution IP, it was observed that the in-solution IP was performing better, and with overall usage of lesser antibody (Figure 22b). Thus, it was ultimately decided to continue with the in-solution IP.

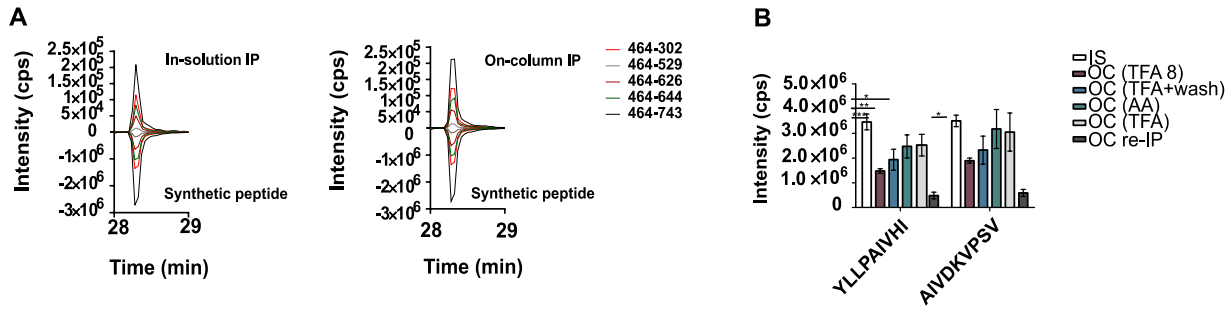

Figure 22. Comparison of on-column IP with in-solution IP.
*A) Representative MRM spectra of endogenous control peptide (AIVDKVPSV) detected in SNU17 cells using in-solution IP and on-column IP. B) SNU17 lysate was equally distributed to perform 5 IPs (4 on-column and one in solution IP (white)). The on-column IPs were eluted with different elution protocols, namely 8 successive elutions with 0.1% trifluoroacetic acid (purple); first elution with 0.1% TFA for 2 hours, followed by a final wash with 0.2% TFA (blue); elution with 10% acetic acid (green) or elution with 0.1% TFA for 2 hours (grey). A rerun of the lysate after on-column IP (purple), through a new column was used as a positive control to check for IP efficiency (dark grey). Intensity of endogenous control peptides YLLPAIVHI and AIVDKVPSV normalized to spike-in peptide FGPVNHEEL was compared across the different conditions (y axis). Statistical testing was performed using GraphPad v7 using one-way ANOVA testing. * p value<0.05, ** p value < 0.01 and ***p value < 0.001.*

For further improving the in-solution IP protocol, several parameters were tested. The first step towards enriching the HLA-A molecule is efficient cell lysis. Different detergents are used for cell lysis. Several detergents were selected from literature and compared for efficiency of lysis, namely 1% n-Octyl β-D-glucopyranoside (OGP), 1% Digitonin, 1% CHAPS, 1% n-Dodecyl-β-D-maltoside (DDM)/ 0.1% Cholesteryl hemisuccinate (CHM), 1% OGP/ 0.25% Sodium deoxycholate (SDC) and 1% DDM (

Figure 23a). Based on Western blotting of the lysates to assess for HLA-A levels, it was concluded that 1% OGP/ 0.25% Sodium deoxycholate (SDC) and 1% DDM are the best. A detailed analysis of these results is published in the Master's thesis of Catharina Lotsch, who was supervised by me. The next step that could affect the efficiency of the epitope purification protocol is sample preparation after IP and prior to LC-MS analysis. Ultrafiltration as well as reverse phase liquid chromatography are suitable for the removal of proteins and salts from the IP sample. Different desalting methods can influence the efficiency of peptide detection, as well as lead to losses during sample processing. Thus, different desalting methods were compared, to choose one which allows for the least loss of target peptides. A synthetic peptide mixture comprised of HLA-A2 binding peptides was used as input (Table 7). These were processed using different desalting and protein removal methods, such as ultrafiltration with 3kDa cutoff filters, reverse phase separation with self-packed columns with Zorbax™, or with commercial SepPak™ cartridges, or a SepPak™ 96 well desalting plate. These techniques were used sequentially in different combinations as described in Figure 23b. Results showed that desalting with Zorbax, followed by ultrafiltration (3kDa) was the best-suited technique (Figure 23b).

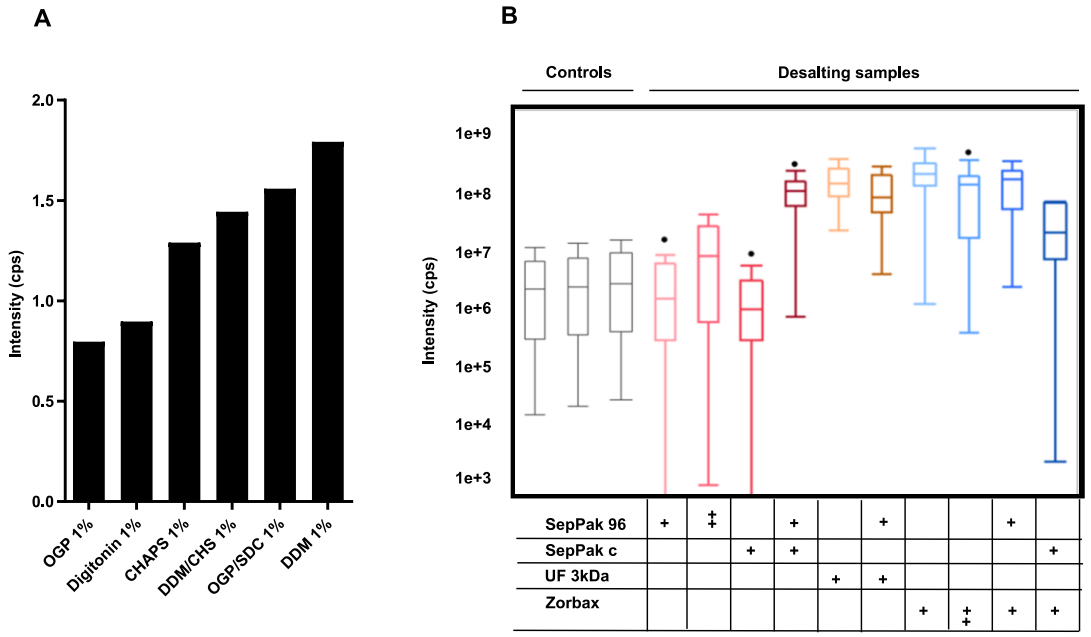

Figure 23. Optimizing the in-solution IP.
A) Equal numbers of CaSki cells (40 million) were lysed using different lysis buffers: 1% n-Octyl β-D-glucopyranoside (OGP), 1% Digitonin, 1% CHAPS, 1% n-Dodecyl-β-D-maltoside (DDM)/ 0.1% Cholesteryl hemisuccinate (CHM, 1% OGP/ 0.25% Sodium deoxycholate (SDC) and 1% DDM. HLA-A levels normalized to α-tubulin were assessed using Western blotting of the cell lysates. These results are published in the Master's thesis of Catharina Lotsch, supervised by me as a part of the PhD thesis. B) Different desalting methods, SepPak™96 well plate (SepPak 96), SepPak™ cartridge (SepPak c), ultrafiltration 3kDa (UF 3kDa), and Zorbax™, were compared using a synthetic peptide mixture of HLA-A2 binding cysteine-free peptides (Table 7). Intensity of peptides detected is depicted as boxplots (y axis) was taken as a readout to compare the different desalting methods (different colours). The control samples were the older runs of the synthetic peptide mixture. The desalting procedures used are indicated with + below the x axis. Two + symbols in the same technique imply the same desalting method was used twice. Samples were analysed on the UltiMate 3000 LC coupled with the Orbitrap Q Exactive HF-X instrument. MS analysis by Dr. Mogjiborahman Salek.

Using the targeted epitope detection strategy published previously, HLA-A2-binding peptides were successfully detected in CaSki cells (Figure 24a) [106] as well as in 866 cells, in samples prepared by Dr. Alina Steinbach, during her PhD (Figure 24b). Since no software exists to date for objective analysis of MS^3 data, three criteria to be met before the peptides would be considered truly detected were successfully established. These criteria were published in Blatnik, Mohan, Bonsack et al [106]. Briefly, a match between the liquid chromatography retention time, MRM spectra as well as MS^3 spectra (in terms of relative hierarchy of abundance of fragment ions) between the IP sample and the synthetic peptide spectra, was needed in three biological IP replicates, for a peptide to be considered detected. Peptides were considered Limit of detection (LOD) describes peptides detected using only the two most abundant fragments [106].

A

Peptide	Detected by MS^3 analysis (CaSki)	Detected by MS^3 analysis (866 cells)
E7/7-15	Detected	-
E7/11-19	Detected	-
E7/77-86	Detected	Detected
E7/77-87	Detected	Detected
E7/78-86	Detected	Detected
E7/80-90	Detected	-
E7/81-90	Detected	Detected
E7/82-90	Detected	-
E7/11-20	LOD	-
E7/11-21	LOD	-
E7/12-19	LOD	-

B

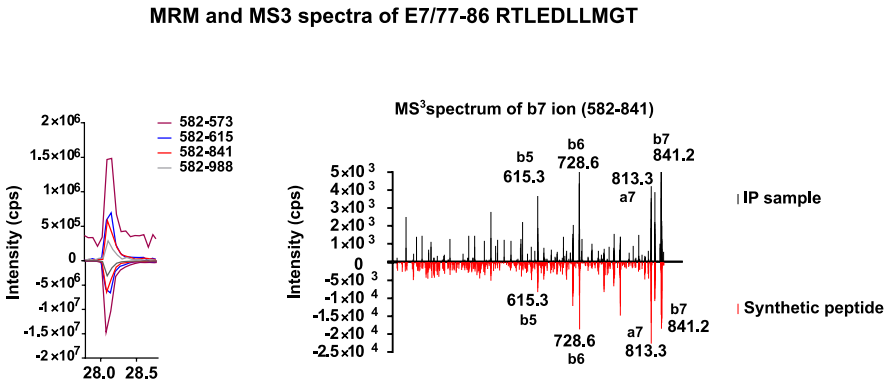

Figure 24. Peptides detected in HPV16-transformed cells
(IP by Dr. Alina Steinbach, MS acquisition by Dr. Renata Blatnik).
A) Summary of peptides detected in CaSki cells [106], and in 866 cells using the MS^3 mass spectrometry analysis method on the QTRAP6500 mass spectrometer coupled with the nanoAcquity LC (Waters). Detected peptides are those following the published detection or limit of detection (LOD) criteria [106].
B) MRM (left) and MS^3 (right) spectra of one of the four peptides detected in 866 cells.

After successfully detecting E6 and E7-derived HLA-A2 binding peptides on two HPV16-transformed cells (Figure 24), and having further optimized the IP protocol, the next exciting question was to assess how hypoxia affects the epitope repertoire on the cell surface. Unfortunately, however, we were unable to follow up on this question because of loss of communication between the NanoAcquity UPLC and the QTRAP6500 instrument, followed by further issues with the new Thermo Fisher Orbitrap QExactive HF X instrument. However, the optimizations to improve the sensitivity of peptide detection will hopefully help in addressing this question in the future.

An indirect way to address the effect of hypoxia on epitopes presented on the cells surface is by assessing the killing of HPV16-transformed cells by peptide-specific $CD8^+$ T cells. Thus, it was decided to switch to immunological assays.

5.7 Selection of HLA-A2 positive donors

Intending to find donors who show memory T cell responses to HPV16 E6- and E7-derived peptides, isolated PBMCs from women above 40 years of age were isolated. A screening of all the ordered donors was performed, and only HLA-A2+ donors were selected. In the RBC-depleted PBMCs, the lymphocytes were gated as the target cell population, as shown in Figure 25, left panels. The HLA-A2+ and HLA-A2- populations were set using staining of the cells with the isotype control antibody. An example of an HLA-A2 negative donor can be seen in Figure 25a, where the histograms from the isotype control and the antibody staining were completely overlapping. An example of an HLA-A2 positive donor, where the isotype control and HLA-A2 histograms are well separated, can be seen in Figure 25b. Only HLA-A2+ donors were subsequently used for further experiments.

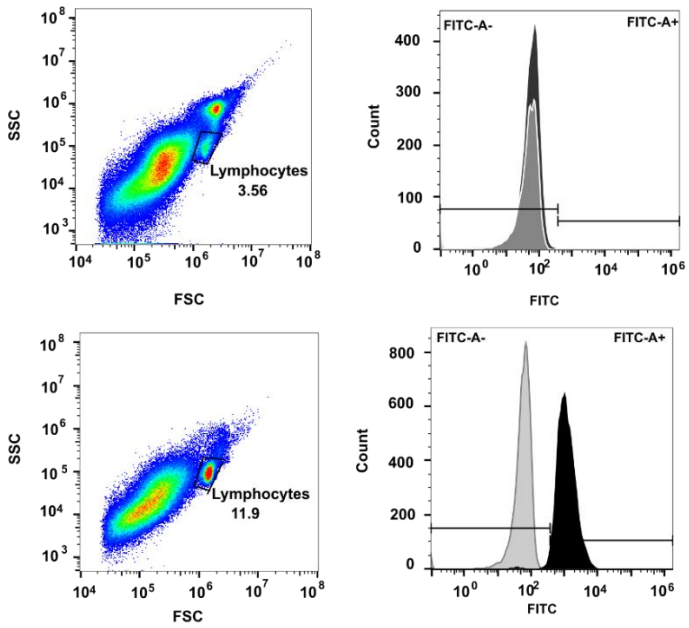

Figure 25. Flow cytometry-based selection of HLA-A2+ donors.
HLA-A2-positive donors were selected by flow cytometric staining of buffy coats. Left panels show gating of lymphocytes using forward scatter (FSC) and side scatter (SSC) properties. Upper panels show an example of an HLA-A2-negative donor, and lower panels shows an example of an HLA-A2-positive donor. The FITC+ gate was set using an isotype control staining. Data was acquired using the BD FACS Accuri™ Flow cytometer. Data analysis was done using FlowJo v10.6.

5.8 Effect of hypoxia T cell memory responses towards HPV16 E6- and E7-derived peptides.

The HLA-A2+ PBMCs isolated were then used to check for the effect of hypoxia on IFNγ secretion by memory T cells against HPV16 E6 and E7-derived peptides. Memory T cells present in the donors due to prior exposure to HPV16 were expanded using short-term T cell cultures (4.1.3), in the presence of the specific HPV16 HLA-A2 binding peptides. Then, an ELISpot assay was set up simultaneously in normoxia as well as in hypoxia, to assess the differences in the T cell responses. HPV16 HLA-A2-binding peptides were pooled into seven peptide pools (see Table 8) to be able to save on PBMC cell numbers. Memory T cell responses against the seven peptide pools, as well as the negative DMSO control and the CEF positive control, were assessed using 3 donors. Only the positive control, the CEF peptide pool, was responsive in all three donors, as assessed by an SFU greater than 200, and an SI greater than 2. In Figure 26, the SI values are plotted only for the pools where the SFU crossed the threshold of 200. Out of the peptide pools, pool 2 showed no responses in any of the donors.

Three of the peptide pools, pools 1, 3, and 6, showed responses in only 1 donor each, and only in normoxia, but not in hypoxia. Pools 4 and 7 showed responses in both normoxia as well as hypoxia, in one of the donors (Figure 26a). Thus, these pools were deconvoluted to further investigate whether there are differences in a peptide-specific manner between normoxia and hypoxia. Figure 26b depicts the peptides in which the SFU threshold of 200 was crossed in either normoxia or hypoxia, left panel. Combining this information with the SI values (Figure 26b, right panel), some interesting differences can be seen in these peptides. The peptides E7/18-28, E6 R17I/9-19 and E7/11-19 elicited responses only in hypoxia. On the other hand, E6/25-33, E7/80-90 and E7/81-91 elicited responses only in normoxia. One of the peptides, E7/86-93 activated T cells in both normoxia as well as hypoxia. While these results need further validation in more donors, they may suggest differences in T cell memory responses under hypoxia.

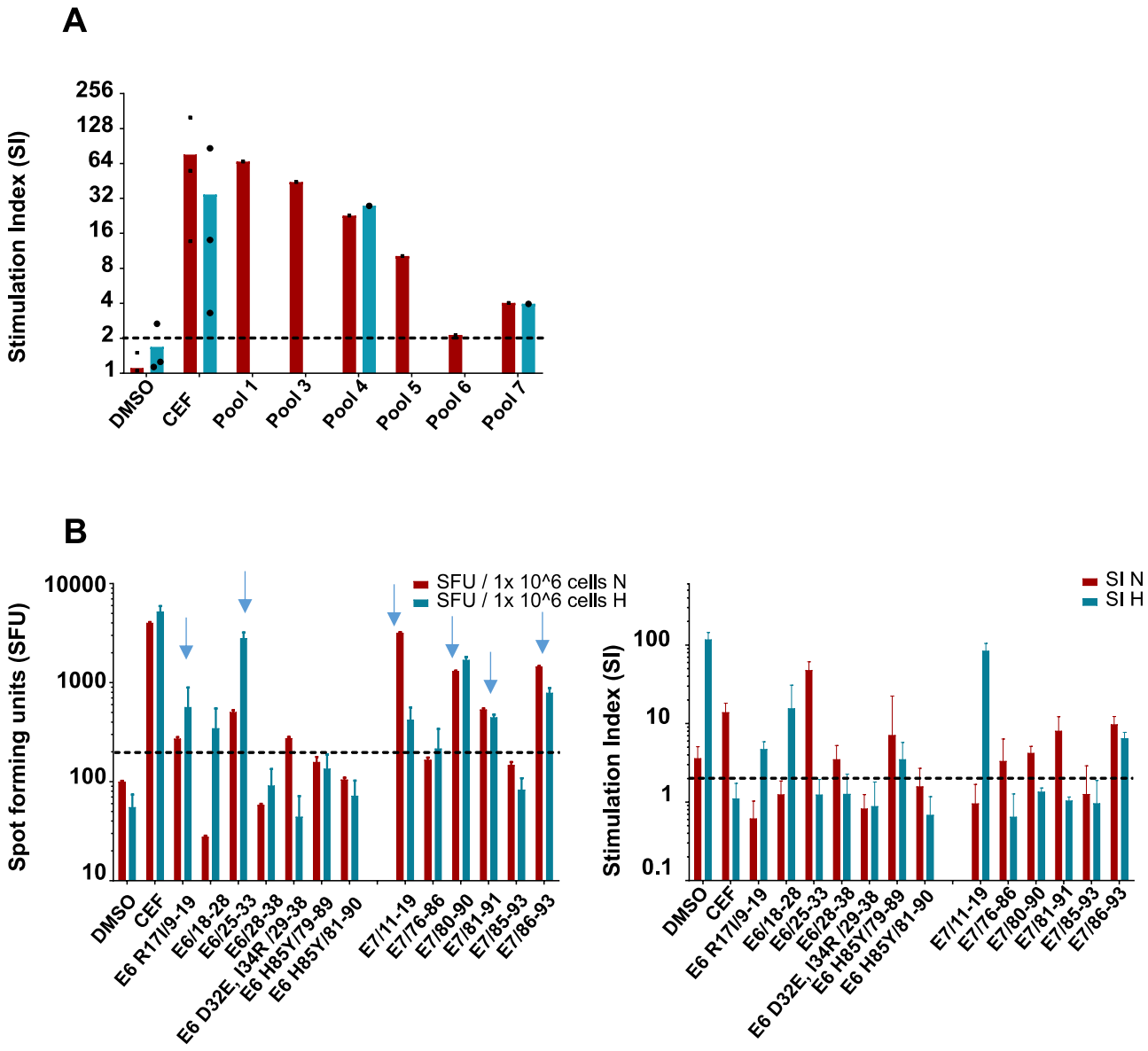

Figure 26. Effect of hypoxia on T cell memory responses.
A) Short-term T cell cultures were expanded from 3 donors and ELISpots were set up using peptide pools (Table 8). The plates were read using the CTL ELISpot reader, and the Stimulation Index (SI) was calculated in normoxia (red) and hypoxia (blue). B) For one of the donors, the 2 peptide pools which showed reactions in both normoxia (blue) in hypoxia (red) in (A), were deconvoluted. The spot forming units (SFU) per million cells (left), and the SI values (right) can be seen for all the peptides in these pools. Arrows in the left panel indicate peptides where the SFU was >200 in both normoxia and hypoxia, but peptide-specific differences were observed in SI values between normoxia and hypoxia (right panel). Experiments in collaboration with Kathrin Öhlenschläger and Nisha Veits.

5.9 Screening of donors for memory responses against HPV16 E6 and E7-derived peptides

Most of the donors, which yielded more than 300 million cells, were used to address the question which was of more relevance to us, which is whether T cell-mediated cytotoxicity towards HPV16-transformed cells is affected under hypoxia. Since literature shows both an immunosuppressive effect of hypoxia on $CD8^+$ T cells [125], as well as enhancement of their cytotoxicity upon incubation in hypoxia [126], it was intriguing to investigate how the targeting of HPV16-transformed cells by $CD8^+$ T cells is affected by hypoxia.

To this purpose, all the donors were screened for memory T cell responses against 46 HPV16 E6- and E7-derived HLA-A2-binding peptides (Table 7). The results are depicted in Figure 27. In Figure 27a, an example of the positive control CEF and the negative HIV-A2 control (Table 7) can be seen. Additionally, two immunogenic responses can be seen as an example, one strong (E7/80-90), and the other weak (E6/29-39). In Figure 27b, the SI values for all the peptides, where the SFU crossed 200, are depicted, across all donors tested. It is interesting to note that some peptides showed a very high SI value, but were immunogenic in only one donor tested, for example E6/25-33. Other peptides, such as E7/82-90, were frequently immunogenic across multiple donors. Memory responses were observed against 21 peptides out of the 46 HLA-A2 binders tested. Interestingly, most of the responses were seen against E7-derived peptides (Figure 27b). T cell memory responses were also observed against E6 variant peptides, across donors (Figure 27c). However, since our target cells CaSki do not contain most of these variants, we did not subsequently generate T cell lines against these variants.

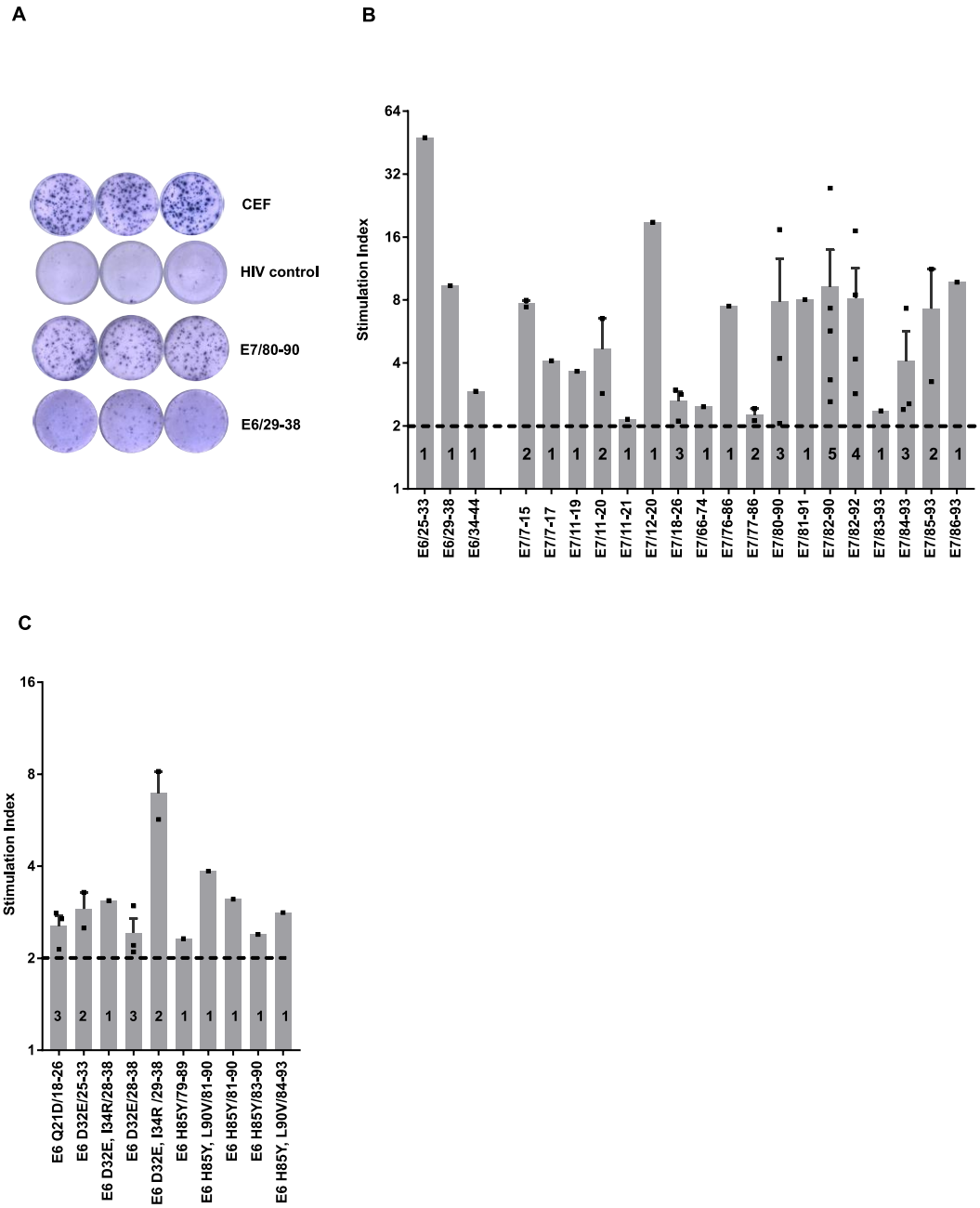

Figure 27. Screening donors for memory responses against HPV16 E6- and E7-derived peptides.
Short-term T cell cultures were set up from PBMCs, and used in IFNγ ELISpot assays against 46 HPV16-derived HLA-A2-binders, positive control CEF and negative control HIV-A2. A) Representative wells depicting the positive control (CEF), negative control (HIV-A2), a strongly positive peptide (E7/80-90), as well as a weakly positive peptide (E6/29-38). B) Stimulation index (SI) values of all HPV16 E6- and E7-derived HLA-A2 binding peptides which had an SFU equal to/greater than 200/million cells. C) Stimulation index (SI) values of all HPV16 E6-variant HLA-A2 binding peptides which had an SFU equal to/greater than 200/million cells. Mean SI (+/-SD) across donors is depicted in cases where the peptide was seen to be immunogenic in more than one donor. Individual spots depict different donors. The numbers within the bars represent the number of donors where T cell responses were observed.

5.10 Effect of hypoxia on $CD8^+$ T cell-mediated killing of HPV16-transformed cells.

After screening of the donors, a total of 18 peptide-specific $CD8^+$ T cell lines were generated, from 16 donors. After excluding T cell lines which showed alloreactive killing of HPV-negative C33A cells, 9 peptide specific $CD8^+$ T cell lines were remaining (Figure 28-30). The VITAL-FR cytotoxicity assays were set up in normoxia and hypoxia, with normoxic target HPV16-transformed target cells, CaSki, as depicted in Figure 10. In most of the cases (8 out of 9 T cell lines), cytotoxicity was seen to be enhanced upon hypoxia (Figure 28 and Figure 30). However, out of the seven peptide-specific $CD8^+$ T cells depicted in Figure 28, cytotoxicity was enhanced across all effector: target (E:T) ratios in three donors (Figure 28a), while it was observed to be enhanced at only high E:T ratios (40:1) in four donors (Figure 28b). An interesting observation is that even in T cell lines where cytotoxicity was very weak in normoxia, there was an increased specific killing evident upon hypoxia (Figure 28). However, in one of the T cell lines, from another donor, hypoxia was seen to supress specific killing of the same HPV16-transformed target cells, CaSki (Figure 29). While this result was surprising to us, it is in fact consistent with existing contradictory literature on the effects of hypoxia on $CD8^+$ T cells.

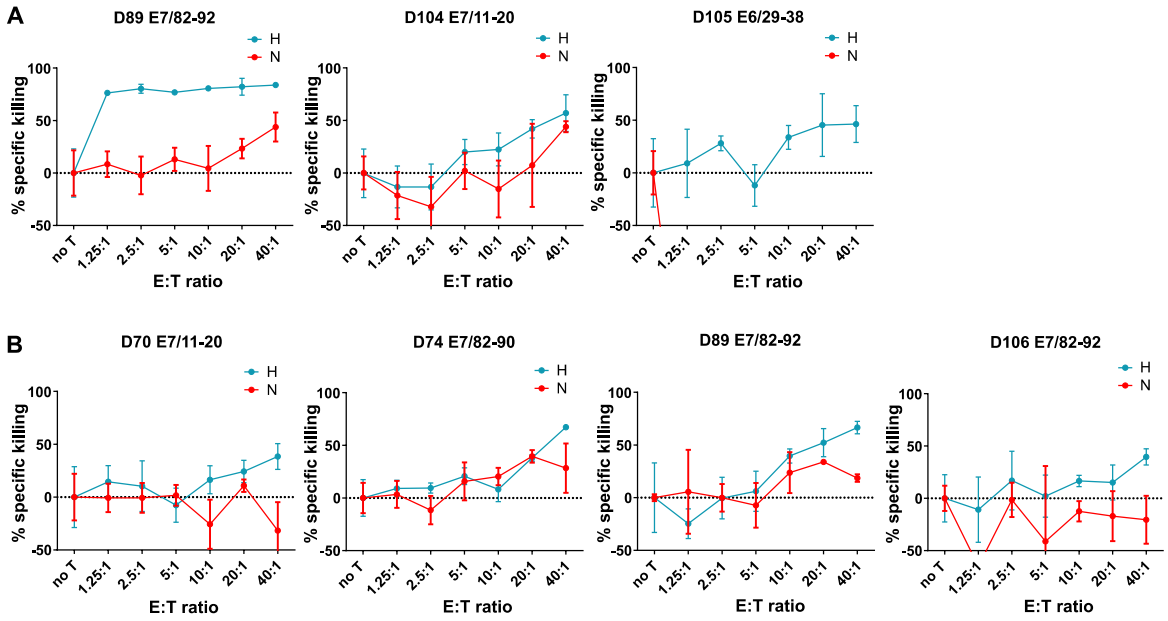

Figure 28. Hypoxia leads to increased killing of target cells.
Semi long-term T cell lines were generated from PBMCs (Figure 7). VITAL-FR cytotoxicity assays were performed in normoxia and hypoxia (Figure 10), with normoxic targets. Specific killing (y axis) was calculated across each E:T ratio (x axis). Based on the formula (section 4.7) negative specific killing can be obtained when the CaSki cells outgrow the C33A cells. A) Hypoxia led to increased specific killing of CaSki cells across all E:T ratios in three donors. B) Hypoxia led to increased specific killing of CaSki cells only in high E:T ratios (40:1) in four donors.

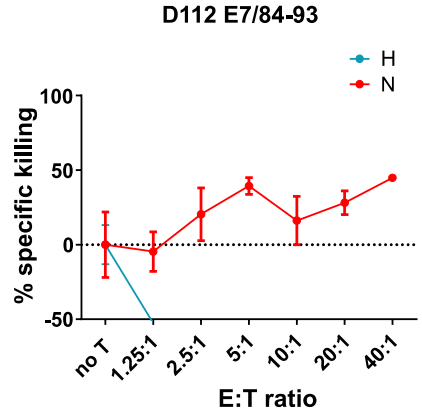

Figure 29. Hypoxia leads to decreased killing of target cells.
Semi long-term T cell lines were generated from PBMCs (Figure 7). VITAL-FR cytotoxicity assays were performed in normoxia and hypoxia (Figure 10), with normoxic targets. Specific killing (y axis) was calculated across each E:T ratio (x axis).Based on the formula (section 4.7) negative specific killing can be obtained when the CaSki cells outgrow the C33A cells. The T cell line derived from donor 112 showed decreased specific killing under hypoxia.

So far, most of the peptide-specific T cell lines showed enhanced specific killing upon hypoxia, especially at higher E:T ratios. In context of the previous data that the source oncoproteins are decreased in hypoxic conditions, it was of interest to investigate whether preincubation of the target cells in hypoxia decreases their being killed by the hypoxic $CD8^+$ T cells (despite their enhanced functionality under hypoxia). In Figure 30, a cytotoxicity assay is depicted, where in addition to the usual conditions, the hypoxic cytotoxicity assay was carried out with 72h-hypoxia-preincubated targets (see also Figure 10). A preincubation period of 72 hours was chosen to ensure that the source protein expression is completely decreased, which was observed to happen by 48 hours (Figure 15), and an additional 24 hours for recycling of any surface epitopes. Cells were counted and plated as per their doubling times, to ensure they do not grow to overconfluence in the hypoxia chamber, during preincubation. It was observed that while hypoxia led to increased specific killing of normoxic target cells by this $CD8^+$ T cell line, the specific killing was completely supressed in the case of the hypoxia-preincubated targets (Figure 30). As a conclusion, the results suggest that hypoxia might be enhancing the cytotoxic activity of HPV16-specific $CD8^+$ T cells, in a donor-specific manner. However, the effect of hypoxia on the suppression of the source protein expression can supersede the effects of enhanced cytotoxicity of hypoxic $CD8^+$ T cells.

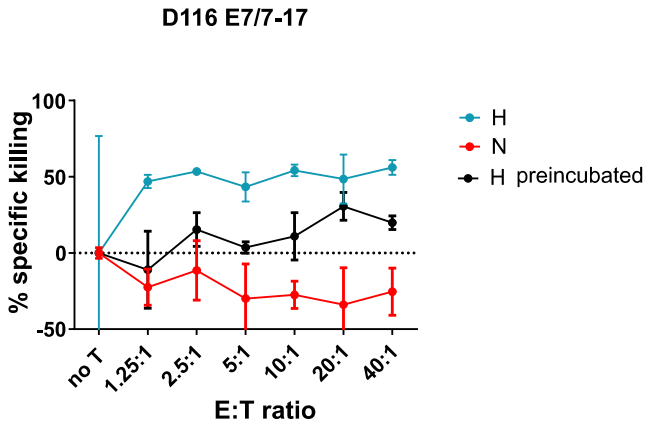

Figure 30. Pre-incubation of target cells in hypoxia leads to decreased killing under hypoxia.
Semi long-term T cell lines were generated from PBMCs (Figure 7). VITAL-FR cytotoxicity assays were performed in normoxia and hypoxia (Figure 10), with normoxic and hypoxia-preincubated targets. Specific killing (y axis) was calculated across each E:T ratio (x axis).Based on the formula (section 4.7) negative specific killing can be obtained when the CaSki cells outgrow the C33A cells.
VITAL FRs were set up in normoxia (red) with normoxic T cells and targets; in hypoxia (blue) with hypoxic T cells and normoxic targets; and in hypoxia (black) with hypoxic T cells and 72-h-hypoxia-preincubated targets.

6 Discussion

Despite prophylactic vaccines being commercially available since more than a decade, HPV-induced malignancies remain a major global health burden, with cervical cancer still being the 4th most common cancer [17]. One of the reasons is the lack of availability and implementation of these vaccines in poorer countries which account for 90% of annual cervical cancer cases. Analysis of global vaccine coverage up to 2014 revealed that only a small fraction of cervical cancer cases projected worldwide up to 2080 will be prevented (380,000/1,100,000) based on the current coverage. An alarmingly high number of cervical cancer cases (approx. 675,000) projected by 2080, can be attributed to lack of vaccines, or HPV types not included in the vaccines [85] (section 1.3.1). This highlights the need for a therapeutic vaccine for HPV-induced malignancies, followed by improved coverage of these vaccines worldwide.

A number of immunotherapies are currently being developed for HPV-induced malignancies. Therapeutic vaccines developed using several approaches (live vector-based, nucleic acid-based, cell-based and subunit-based) have been developed and have shown promising results in clinical trials [90] (section 1.3.2). Yet several others therapies are being explored in ongoing trials [89]. However, no therapeutic vaccines has become commercially available to date. One important aspect of tumors, which has been so far ignored, is the tumor microenvironment (section 1.4). The promising results highlight the need to investigate the other TME components in the context of developing therapeutics for improving the success of HPV immunotherapies.

6.1 Hypoxia as a challenge to therapies

Hypoxia is a major aspect of the TME of most solid tumors. Hypoxia is a major challenge for development of successful therapeutics, as it enhances the ability of tumors to escape from sites where the therapies are targeted (eg. the site of tumor radiation[149]), as well as enhancing their capacity for efflux of chemotherapy drugs [115]. This occurs via a plethora of mechanisms, which, especially in the case of resistance to radiation therapy[149] have been linked to HIF1α [115]. From the perspective of immunotherapies, the enhancement of tumor invasiveness, metastasis, immunosuppression and immune escape under hypoxic conditions are of particular concern. (section 1.4). Thus, hypoxia poses a major challenge to the success immunotherapies. [132].

6.1.1 Importance of targeting hypoxia for successful therapies

In the recent past, hypoxia has been successfully used as a target to improve sensitivity to chemotherapy and radiation in the context of several tumors [115, 149]. These drugs fall into three main classes hypoxia prodrugs, HIF1α targeting drugs, and anti-angiogenic drugs. Anti-angiogenic therapies target the tumor vasculature, which is closely linked with the supply of oxygen to the tumors. The success of these strategies suggests an bright future for the incorporation of hypoxia targeting strategies into immunotherapies. However, a very limited number of clinical trials have occurred to investigate the effect of hypoxia in immunotherapies [132]. The reason for this hesitancy might be the fact that the downstream effects of hypoxia are so diverse, including effects on the immune cells. As an exciting advancement in this year, a CAR T cell therapy was developed which elegantly used hypoxia to their advantage, to selectively target ovarian (SKOV3) and head and neck (HN3) tumors, and spare healthy tissues in mice [150]. In the context of cervical cancer, the clinical importance of the TME, and indirectly hypoxia, is highlighted by the marked improvement of prevalent chemotherapeutic protocols observed upon combination with the anti-angiogenic drug bevacizumab, as compared to chemotherapy alone [134, 135].

In the context of development of a therapeutic vaccine for HPV16-induced malignancies, effects of hypoxia have been reported on HPV16 oncoprotein expression, $CD8^+$ T cell functions in different tumors, as well as HLA-I expression in different cancers (section 1.4 and 1.4.1), highlighting its potential as a therapeutic target. However, for effectively targeting hypoxia to improve the success of cervical cancer immunotherapies, it is important to gain a deeper understanding on its effect on HPV16-transformed cells, and their targeting by cytotoxic T cells.

6.2 Effect of hypoxia on HPV16-transformed cells

6.2.1 Hypoxia decreases HPV oncoproteins expression

Most immunotherapies for HPV16-induced malignancies target the the E6 and E7 oncoproteins. These are considered optimal targets, given their elaborate requirement in the life cycle of HPV (section 1.1.4). Thus, it is extremely concerning that their expression is lost upon hypoxic conditions, which are known to be prevalent in solid tumors, including cervical cancers. A decreased expression of HPV oncoproteins in several HPV16-transformed cells was observed upon 24-hour hypoxia treatment. This confirms existing literature on the effect of hypoxia on HPV16 E6 and E7 expression [137, 139, 151].

6.2.1.1 E7 is decreased across cell lines transformed with different HPV16 variant lineages

E7 protein levels were observed to be starkly decreased in all seven HPV16-transformed cell lines tested (Figure 14). These results demonstrate that cervical cancer cells transformed with different variant lineages of HPV16 (Table 5) all respond similarly to hypoxia, with a decrease in expression of E7 oncoprotein. Differential geographical distribution and pathogenicity has been suggested for the different HPV16 variant lineages in literature non European (NE, or B, C and D) vs European (E) (section 1.1.2, Table 2). Further, downregulation of E7 expression has been suggested as a mechanism for the virus to enter dormancy and persist in the host, forming sleeper cells which can transform into cancerous cells upon reoxygenation [137, 152].

Thus, the results suggest that different variant lineages are all capable of responding to hypoxia in a similar way, and enter a dormant state, irrespective of differences in their geographical distribution and pathogenicity. If this is indeed the case, it is promising from the perspective of developing therapeutics, since no differential treatments for the different variant lineages would need to be developed.

6.2.1.2 Decrease in E7 protein levels only occurs after 12 hours of hypoxia

On further investigating the timeline of decrease of E7 protein expression upon hypoxia, it was observed that in CaSki cells, E7 protein levels are not decreased by 12 hours of hypoxia, and even up to 24 hours of hypoxia, some protein could still be detected by Western blotting (Figure 15).

Given the importance of E6 and E7 as targets for immunotherapy, a decrease in these proteins upon conditions prevalent in a cervical tumor microenvironment is of concern. However, since at least 24 hour hypoxia treatment is required for complete loss of E7 protein expression, some peptides might still be presented on the cell surface. Several tumors, including cervical cancer [153] have a fluctuating oxygen supply caused by abberant vasculature, creating a condition known as cycling hypoxia. Thus, it is likely that the oncoprotein expression is restored upon reoxygenation of the cervical cancer tissue [138].

6.2.2 No effect of hypoxia on the APM

While the E6 and E7 proteins are still being expressed, and soon after their degradation, epitopes derived from these proteins would be presented on the cell surface in the context of HLA-I, to cytotoxic T cells, after processing through the APM (section 1.2.2.1,

Figure 2). Not many studies have explored the effect of hypoxia on the APM. Importantly, in mesenchymal stem cells, hypoxia was observed to upregulate the immunoproteasome components (PSMB 8, 9 and 10), while decreasing expression of the regulatory subunits (PSMB 4, 11) and the proteasome core subunits

(PSMB 4, 5 and 6). Hypoxia was also seen to increase the expression of HLA II in these cells [54]. In the context of tumor cells, hypoxia has been reported to dysregulate some components of the APM *in vitro* and *in vivo* in the context of sarcoma and pulmonary mouse tumors [129]. Regulation of the APM could potentially affect the presentation of antigens on the cell surface, thus it was of interest to explore the effects of hypoxia on APM in cervical cancer cells.

6.2.2.1 Using the right normalization strategies while investigating the effects of hypoxia

A high throughput method was needed to investigate the effect of hypoxia on the APM. Since hypoxia affects numerous cell processes, especially in cancer cells, finding an appropriate normalization control is difficult. Quantitative PCR would have been one option.

However, it has been reported that most commonly used housekeeping genes for quantitative PCR are themselves regulated by hypoxia, making them unsuitable for normalization [154]. This dilemma was solved by using a label free quantification (LFQ) mass spectrometry-based strategy, MaxLFQ [143], that uses intrinsic normalization, thereby making it the optimal strategy for assessing the effects of a treatment like hypoxia which has such pleiotropic effects.

6.2.2.2 Using the right sample preparation strategy for mass spectrometry

It was important to ensure sample processing was as similar as possible, in the 9 cell lines being assessed for the effect of hypoxia on the APM samples. This was especially important amongst biological replicates. Thus, the SP3 sample preparation was chosen for its advantages of high throughput, speed and reproducibility [141]. The superior performance of this method was also demonstrated by the results comparing it to the in-gel trypsin digestion method (Figure 16).

6.2.2.3 Hypoxia does not affect the APM

The results, interestingly, showed no significant effect of 24-hour hypoxia treatment on the APM in any of the HPV16-transformed cell lines, as well as the 2 HPV-negative control cells (Figure 17 and Figure 18). Additionally, an even longer duration of hypoxia treatment of 48h, did not affect the APM proteins in C33A, CaSki and SNU17 cells (Figure 19). The effect of hypoxia on cell surface presentation of HLA-A2, was also assessed by flow cytometry (Figure 20 and Figure 21). Unlike what is reported in the literature about increase [127, 128] or decrease [129] in HLA-I levels upon hypoxia, no significant change in HLA-A2 levels upon 24-hour hypoxia treatment (Figure 20), was observed in any of the cell lines, irrespective of HPV variant lineage (Figure 15). Additionally, even a 48h hypoxia treatment showed no change in expression of HLA-A2 levels in C33A, CaSki and SNU17 cells (Figure 21). From a perspective of developing therapeutics,

this is promising, as it suggests that the presentation of epitopes from E6 and E7, in hypoxic HPV16-transformed cells, would not be perturbed.

6.2.3 Effect of hypoxia on CD8$^+$ T cell-mediated killing of HPV16-transformed cells

In light of the information that the source oncoproteins were decreased in expression upon hypoxia, with no change on the APM, it was of intriguing to explore the effect of hypoxia on recognition and killing of these cells by hypoxic CD8$^+$ T cells.

6.2.3.1 Enhanced cytotoxicity upon hypoxia in the majority of T cell lines

Interestingly, increased cytotoxicity upon hypoxia was observed in 7/8 peptide-specific cell lines (Figure 23). On the other hand, in one out of these eight CD8$^+$ T cell lines, a stark decrease in cytotoxicity upon hypoxia was observed (Figure 29). While these contradictory results were puzzling, they could mean that the effects of hypoxia on CD8$^+$ T cells depend on some other factors as well, which would need further exploration. It is also important to note that these results are consistent with the contradictory literature which has shown both upregulation of cytotoxic T cell activity by hypoxia [126], and well as the immunosuppressive effects of hypoxia on these cells [125]. Since these CD8$^+$ T cell lines were generated against different HPV16 E6- and E7-derived peptides, an alternate explanation of these contradictory results could also be that the repertoire of peptides presented on the surface of hypoxic CaSki cells is altered as compared to normoxic CaSki. However, given that no effect of hypoxia on the APM was observed, this seems unlikely.

6.2.3.2 Enhanced cytotoxicity in high E:T ratios

Increased killing in a majority of the donors is interesting given the prior results showing decreased target protein expression upon hypoxia (Figure 13 and Figure 14). It is possible that the killing is happening during the first 24 hours of the cytotoxicity assay, while E7 is still being expressed (Figure 15). An interesting observation amongst the 7 peptide-specific CD8$^+$ T cell lines with increased cytotoxicity upon hypoxia was that in 3 of the cell lines, increased cytotoxicity upon hypoxia was evident in all effector: target (E:T) ratios (Figure 28a). On the other hand, in 4 cell lines, enhanced cytotoxicity upon hypoxia was only observed in high E:T ratios (Figure 28b). This might suggest that the enhanced killing at higher E:T ratios (Figure 28b) is due to the fact that a higher number of T cells is required for killing of the hypoxic targets when the source protein is decreased under hypoxia (Figure 13 and Figure 14).

6.2.3.3 Suppressed killing of hypoxia-preincubated target cells

To delineate between the effects of hypoxia on the targets cells vs the $CD8^+$ T cells, target cells were preincubated in hypoxia, prior to the cytotoxicity assay (Figure 10). These hypoxia-preincubated cells, in addition to normoxic cells, were then used as targets for hypoxic T cells.

The normoxic targets were killed more efficiently by the hypoxic T cells, but there was no killing of the hypoxia-preincubated targets (Figure 30). The half life of the peptide E7/7-17 on the HLA-A2 molecule is much lower than 24h, as predicted using the NetMHCstabpan1.0 prediction server [155], thus, this indicates that there would not be any more residual peptide present on the cells, after loss of expression of the source protein upon 48h hypoxia. This indicates that hypoxia indeed leads to decreased presentation of epitopes on the surface of hypoxic HPV16-transformed cells, and can hinder their targeting by specific T cells.

On the whole, the results from the cytotoxicity assays suggest that the activity of $CD8^+$ T cells is enhanced upon hypoxia (Figure 28), in most cases. These results are promising from a perspective of development of immunotherapies for cervical cancer. However, this enhanced cytotoxicity is dependent on source protein expression, which is decreased upon hypoxia.

A lack of effect of hypoxia on the APM suggests that restoring the expression of E6 and E7 proteins could enable epitope presentation on the cell surface. This suggest the potential success of a combination of immunotherapies with hypoxia relieving strategies.

6.3 Conclusion

In conclusion, this work provides insight into the effect of hypoxia on seven HPV16-transformed cell lines, in the context of expression of HPV16 oncoproteins as well as the APM proteins. Enhanced killing of HPV16-transformed cells by hypoxic peptide-specific $CD8^+$ T cells, was observed in all cases but one. The results also suggest that this enhanced killing is dependent on the expression of the source proteins. Since the results also show that the source protein is decreased in expression upon hypoxia, this is of concern from the point of view of generating effective therapeutic vaccines.

To address this and to enable the development of successful immunotherapies, the results from this study highlight the importance of using combination therapies in the future, such as published methods such as relieving ECM pressure or normalizing tumor vasculature, to relieve hypoxia [132], or specifically targeting hypoxia [115]. Such combination therapies may hold promise in enhancing the efficacy of therapeutic vaccines targeting HPV16-induced malignancies. Another aspect that needs to be explored is the concept

of cycling hypoxia, which is prevalent in the cervical cancer microenvironment. If the expression of the HPV16 oncoproteins E6 and E7 is upregulated upon reoxygenation, as shown for the HPV18 E6 and E7 [137], in the context of cycling hypoxia[138, 153], it may provide a window of treatment dependent upon live monitoring of the hypoxia status of the tumor using PET imaging [156] or dyes [157, 158].

6.4 Open questions

While addressing the effects of hypoxia on HPV16-transformed cells, and their targeting by $CD8^+$ T cells, the results from this thesis also raise some questions relevant for future investigations.

6.4.1 Effect of hypoxia on other HLA-I allotypes

It is important to note that the focus of this study was on the most frequently expressed HLA-I allotype in the Caucasian population, namely HLA-A2. This HLA-I allotype was focused on from the perspective of developing a therapeutic vaccine for HPV16-induced malignancies. However, it remains an open, but unlikely possibility that hypoxia affects HLA-I expression in an allotype-dependent manner, on the other allotypes. This would be interesting to address in future studies.

Further, it has been reported in the literature that the effects of hypoxia on HLA-I expression were more pronounced on cells in 3D culture systems as compared to 2D cultured counterparts in murine sarcoma cells [129]. Since all experiments for this thesis were carried out in 2D cultures of cervical cancer cells, it would be interesting to investigate these effects in a cervical cancer 3D culture or organoid system which has been recently developed [159, 160].

6.4.2 Irreversible effects of hypoxia on $CD8^+$ T cells

An additional point of interest is that the $CD8^+$ T cells were preincubated for 48 hours in hypoxia, before the cytotoxicity assay setup. In literature, it has been reported that "long-term" preincubation of $CD8^+$ T cells in hypoxia led to increased cytotoxicity not only in hypoxia but also towards normoxic targets [126]. Given that most effects of hypoxia are quickly reversed since HIF1α is rapidly degraded upon exposure to O_2, the persistent effect of hypoxia on T cells needs further investigation. It would be interesting, and relevant to explore, how long the $CD8^+$ T cells need to be preincubated in hypoxia, to enhance their cytotoxicity against normoxic targets. Due to a paucity of $CD8^+$ T cell numbers, some of these interesting questions could not be addressed in the context of this thesis.

6.4.3 Effect of hypoxia on other immune cell subsets in the cervical cancer TME

Another important parameter to remember in the context of development of immunotherapies is the complexity of the TME. While the studies in this thesis were performed *in vitro* with purified $CD8^+$ T cells,

in the cervical cancer TME there are other immune cells (section 1.2.3), each of which could be affected by hypoxia which will collectively determine the outcome of combination therapies of immunotherapy with hypoxia relieving strategies. A recent study has shown promising results that hypoxic $CD8^+$ T cells can retain their superior cytotoxic functions *in vivo,* using mouse models of melanoma [126]. In addition to this, other aspects such as the effect of hypoxia on antigen presentation by APCs, or on other cells which play a pro-tumorigenic role, would be interesting to explore. The results from this thesis set the base for addressing these additional questions in the future using co-culture of immune cells with the recently developed organoid model of cervical cancer system [159, 160].

In conclusion, the results obtained in this thesis, provide novel insights into the effect of hypoxia on HPV16-transformed cells and their killing by cytotoxic T cells. This work provides new avenues for research for improved immunotherapies, while also raising new questions for further research into this topic.

7 References

1. zur Hausen, H., *The search for infectious causes of human cancers: Where and why.* Virology, 2009. **392**(1): p. 1-10.
2. zur Hausen, H., *Papillomaviruses and cancer: from basic studies to clinical application.* Nat Rev Cancer, 2002. **2**(5): p. 342-50.
3. Harden, M.E. and K. Munger, *Human papillomavirus molecular biology.* Mutat Res Rev Mutat Res, 2017. **772**: p. 3-12.
4. Gheit, T., *Mucosal and Cutaneous Human Papillomavirus Infections and Cancer Biology.* Front Oncol, 2019. **9**: p. 355.
5. McBride, A.A., *The papillomavirus E2 proteins.* Virology, 2013. **445**(1-2): p. 57-79.
6. de Villiers, E.M., et al., *Classification of papillomaviruses.* Virology, 2004. **324**(1): p. 17-27.
7. Bernard, H.U., et al., *Classification of papillomaviruses (PVs) based on 189 PV types and proposal of taxonomic amendments.* Virology, 2010. **401**(1): p. 70-9.
8. Bzhalava, D., C. Eklund, and J. Dillner, *International standardization and classification of human papillomavirus types.* Virology, 2015. **476**: p. 341-344.
9. Van Doorslaer, K., et al., *The Papillomavirus Episteme: a central resource for papillomavirus sequence data and analysis.* Nucleic Acids Res, 2013. **41**(Database issue): p. D571-8.
10. Burk, R.D., A. Harari, and Z. Chen, *Human papillomavirus genome variants.* Virology, 2013. **445**(1-2): p. 232-43.
11. Doorbar, J., et al., *The biology and life-cycle of human papillomaviruses.* Vaccine, 2012. **30 Suppl 5**: p. F55-70.
12. Egawa, N., et al., *Human Papillomaviruses; Epithelial Tropisms, and the Development of Neoplasia.* Viruses, 2015. **7**(7): p. 3863-90.
13. Chen, Z., et al., *Non-human Primate Papillomaviruses Share Similar Evolutionary Histories and Niche Adaptation as the Human Counterparts.* Front Microbiol, 2019. **10**: p. 2093.
14. de Martel, C., et al., *Worldwide burden of cancer attributable to HPV by site, country and HPV type.* Int J Cancer, 2017. **141**(4): p. 664-670.
15. Cornet, I., et al., *HPV16 genetic variation and the development of cervical cancer worldwide.* Br J Cancer, 2013. **108**(1): p. 240-4.
16. Chesson, H.W., et al., *The estimated lifetime probability of acquiring human papillomavirus in the United States.* Sex Transm Dis, 2014. **41**(11): p. 660-4.
17. Arbyn, M., et al., *Estimates of incidence and mortality of cervical cancer in 2018: a worldwide analysis.* The Lancet Global Health, 2020. **8**(2): p. e191-e203.
18. Gheit, T., et al., *Risks for persistence and progression by human papillomavirus type 16 variant lineages among a population-based sample of Danish women.* Cancer Epidemiol Biomarkers Prev, 2011. **20**(7): p. 1315-21.
19. Schiffman, M., et al., *A population-based prospective study of carcinogenic human papillomavirus variant lineages, viral persistence, and cervical neoplasia.* Cancer Res, 2010. **70**(8): p. 3159-69.
20. Xi, L.F., et al., *Risk for high-grade cervical intraepithelial neoplasia associated with variants of human papillomavirus types 16 and 18.* Cancer Epidemiol Biomarkers Prev, 2007. **16**(1): p. 4-10.
21. Riemer, A.K.G.a.A.B., *The Invisible Enemy – How Human Papillomaviruses Avoid Recognition and Clearance by the Host Immune System.* The Open Virology Journal, 2012: p. 249-256.
22. Herfs, M., et al., *A discrete population of squamocolumnar junction cells implicated in the pathogenesis of cervical cancer.* Proc Natl Acad Sci U S A, 2012. **109**(26): p. 10516-21.
23. Bergvall, M., T. Melendy, and J. Archambault, *The E1 proteins.* Virology, 2013. **445**(1-2): p. 35-56.
24. Vande Pol, S.B. and A.J. Klingelhutz, *Papillomavirus E6 oncoproteins.* Virology, 2013. **445**(1-2): p. 115-37.

25. Roman, A. and K. Munger, *The papillomavirus E7 proteins.* Virology, 2013. **445**(1-2): p. 138-68.
26. Graham, S.V., *The human papillomavirus replication cycle, and its links to cancer progression: a comprehensive review.* Clin Sci (Lond), 2017. **131**(17): p. 2201-2221.
27. Spriggs, C.C. and L.A. Laimins, *Human Papillomavirus and the DNA Damage Response: Exploiting Host Repair Pathways for Viral Replication.* Viruses, 2017. **9**(8).
28. Klingelhutz, A.J. and A. Roman, *Cellular transformation by human papillomaviruses: lessons learned by comparing high- and low-risk viruses.* Virology, 2012. **424**(2): p. 77-98.
29. SMOTKIN, D., *Oncogenic and Nononcogenic Human Genital Papillomaviruses Generate the E7 mRNA by Different Mechanisms.* JOURNAL OF VIROLOGY, 1989: p. 1441-1447.
30. Tan, M.J., et al., *Cutaneous beta-human papillomavirus E6 proteins bind Mastermind-like coactivators and repress Notch signaling.* Proc Natl Acad Sci U S A, 2012. **109**(23): p. E1473-80.
31. Brimer, N., et al., *Cutaneous papillomavirus E6 oncoproteins associate with MAML1 to repress transactivation and NOTCH signaling.* Oncogene, 2012. **31**(43): p. 4639-46.
32. Doorbar, J., *The E4 protein; structure, function and patterns of expression.* Virology, 2013. **445**(1-2): p. 80-98.
33. Buck, C.B., et al., *Maturation of papillomavirus capsids.* J Virol, 2005. **79**(5): p. 2839-46.
34. Vinokurova, S., et al., *Type-dependent integration frequency of human papillomavirus genomes in cervical lesions.* Cancer Res, 2008. **68**(1): p. 307-13.
35. Coleman, M.P.a.N., *Integration of high-risk human papillomavirus: a key event in cervical carcinogenesis?* Journal of Pathology, 2007: p. 356–367.
36. LAMBERT, S.J.A.P.F., *Integration of human papillomavirus type 16 DNA into the human genome leads to increased stability of E6 and E7 mRNAs: Implications for cervical carcinogenesis.* Proc. Natl. Acad. Sci. USA, 1995: p. 1654-1658.
37. Isaacson Wechsler, E., et al., *Reconstruction of human papillomavirus type 16-mediated early-stage neoplasia implicates E6/E7 deregulation and the loss of contact inhibition in neoplastic progression.* J Virol, 2012. **86**(11): p. 6358-64.
38. DEAN, E.M.B.a.C.L., *Human Papillomavirus.* Microbiology Spectrum, 2016.
39. DiMaio, D. and L.M. Petti, *The E5 proteins.* Virology, 2013. **445**(1-2): p. 99-114.
40. Ren, S., et al., *HPV E2, E4, E5 drive alternative carcinogenic pathways in HPV positive cancers.* Oncogene, 2020. **39**(40): p. 6327-6339.
41. Kenneth Murphy with acknowledgment to Paul Travers, M.W.w.c.b.A.M., Casey T. Weaver, *Janeway's immunobiology.* Garland Science, Taylor & Francis Group, LLC, an informa business. **8th Edition**.
42. Richard A. Goldsby, T.J.K., Barbara A. Osborne, Janis Kuby, *Immunology.* W.H. Freeman, New York, 2003. **5th Edition**.
43. Iwasaki, A., *A virological view of innate immune recognition.* Annu Rev Microbiol, 2012. **66**: p. 177-96.
44. Italiani, P. and D. Boraschi, *From Monocytes to M1/M2 Macrophages: Phenotypical vs. Functional Differentiation.* Front Immunol, 2014. **5**: p. 514.
45. Hangartner, L., R.M. Zinkernagel, and H. Hengartner, *Antiviral antibody responses: the two extremes of a wide spectrum.* Nat Rev Immunol, 2006. **6**(3): p. 231-43.
46. Sumpter, T.L., S.C. Balmert, and D.H. Kaplan, *Cutaneous immune responses mediated by dendritic cells and mast cells.* JCI Insight, 2019. **4**(1).
47. Golubovskaya, V. and L. Wu, *Different Subsets of T Cells, Memory, Effector Functions, and CAR-T Immunotherapy.* Cancers (Basel), 2016. **8**(3).
48. Jameson, S.C. and D. Masopust, *Understanding Subset Diversity in T Cell Memory.* Immunity, 2018. **48**(2): p. 214-226.
49. Hoyer, S., et al., *Concurrent interaction of DCs with CD4(+) and CD8(+) T cells improves secondary CTL expansion: It takes three to tango.* Eur J Immunol, 2014. **44**(12): p. 3543-59.

50. Rosendahl Huber, S., et al., *T cell responses to viral infections - opportunities for Peptide vaccination.* Front Immunol, 2014. **5**: p. 171.
51. Wang, M. and M.H. Claesson, *Classification of human leukocyte antigen (HLA) supertypes.* Methods Mol Biol, 2014. **1184**: p. 309-17.
52. Sidney, J., et al., *HLA class I supertypes: a revised and updated classification.* BMC Immunol, 2008. **9**: p. 1.
53. Tanaka, K., *The proteasome: Overview of structure and functions.* Proc. Jpn. Acad., Ser. B, 2009. **85**.
54. Abu-El-Rub, E., et al., *Hypoxia-induced shift in the phenotype of proteasome from 26S toward immunoproteasome triggers loss of immunoprivilege of mesenchymal stem cells.* Cell Death Dis, 2020. **11**(6): p. 419.
55. Eskandari, S.K., et al., *The immunoproteasome: An old player with a novel and emerging role in alloimmunity.* Am J Transplant, 2017. **17**(12): p. 3033-3039.
56. Leone, P., et al., *MHC class I antigen processing and presenting machinery: organization, function, and defects in tumor cells.* J Natl Cancer Inst, 2013. **105**(16): p. 1172-87.
57. Steinbach, A., et al., *ERAP1 overexpression in HPV-induced malignancies: A possible novel immune evasion mechanism.* Oncoimmunology, 2017. **6**(7): p. e1336594.
58. Takeuchi, A. and T. Saito, *CD4 CTL, a Cytotoxic Subset of CD4(+) T Cells, Their Differentiation and Function.* Front Immunol, 2017. **8**: p. 194.
59. Smola, S., *Immunopathogenesis of HPV-Associated Cancers and Prospects for Immunotherapy.* Viruses, 2017. **9**(9).
60. Hibma, M.H., *The Immune Response to Papillomavirus During Infection Persistence and Regression.* The Open Virology Journal, 2012(6): p. 241-248.
61. Barros, M.R., Jr., et al., *Activities of stromal and immune cells in HPV-related cancers.* J Exp Clin Cancer Res, 2018. **37**(1): p. 137.
62. Christopher B. Buck, P.M.D., Cynthia D. Thompson*, Jacek Lubkowski†, Wuyuan Lu‡, Douglas R. Lowy*, and John T. Schiller, *Human alpha-defensins block papillomavirus infection.* PNAS, 2005. **103**: p. 1516–1521.
63. Moerman-Herzog, A. and M. Nakagawa, *Early Defensive Mechanisms against Human Papillomavirus Infection.* Clin Vaccine Immunol, 2015. **22**(8): p. 850-7.
64. Wiens, M.E. and J.G. Smith, *alpha-Defensin HD5 Inhibits Human Papillomavirus 16 Infection via Capsid Stabilization and Redirection to the Lysosome.* mBio, 2017. **8**(1).
65. Gulati, N.M., et al., *alpha-Defensin HD5 Stabilizes Human Papillomavirus 16 Capsid/Core Interactions.* Pathog Immun, 2019. **4**(2): p. 196-234.
66. Amador-Molina, A., et al., *Role of innate immunity against human papillomavirus (HPV) infections and effect of adjuvants in promoting specific immune response.* Viruses, 2013. **5**(11): p. 2624-42.
67. Black, A.P., et al., *Human keratinocyte induction of rapid effector function in antigen-specific memory CD4+ and CD8+ T cells.* Eur J Immunol, 2007. **37**(6): p. 1485-93.
68. Trina J. Stewart, M.J.S., Germain J. P. Fernando, Ian H. Frazer, and Graham R. Leggatt, *Inhibition of Early Tumor Growth Requires J alpha18-positive (Natural Killer T) Cells.* Cancer Research, 2003. **63**: p. 3058–3060.
69. Joseph J. Carter, S.K.L., James P. Hughes, Laura A. Koutsky, Jane Kuypers, James P. Hughes, Nancy Kiviat, and Denise A. Galloway, *Comparison of Human Papillomavirus Types 16, 18, and 6 Capsid Antibody Responses Following Incident Infection.* Journal of Infectious Diseases, 2000. **181**: p. 1911–9.
70. Wang, S.S., et al., *Seroprevalence of human papillomavirus-16, -18, -31, and -45 in a population-based cohort of 10000 women in Costa Rica.* Br J Cancer, 2003. **89**(7): p. 1248-54.
71. Steinbach, A. and A.B. Riemer, *Immune evasion mechanisms of human papillomavirus: An update.* Int J Cancer, 2018. **142**(2): p. 224-229.

72. Hong, S. and L.A. Laimins, *Manipulation of the innate immune response by human papillomaviruses.* Virus Res, 2017. **231**: p. 34-40.
73. Oliveira, L.B., I.R. Haga, and L.L. Villa, *Human papillomavirus (HPV) 16 E6 oncoprotein targets the Toll-like receptor pathway.* J Gen Virol, 2018. **99**(5): p. 667-675.
74. Evans, M., et al., *Antigen processing defects in cervical carcinomas limit the presentation of a CTL epitope from human papillomavirus 16 E6.* J Immunol, 2001. **167**(9): p. 5420-8.
75. Demoulin, S.A., et al., *Cervical (pre)neoplastic microenvironment promotes the emergence of tolerogenic dendritic cells via RANKL secretion.* Oncoimmunology, 2015. **4**(6): p. e1008334.
76. Chen, X.J., et al., *Clinical Significance of CD163+ and CD68+ Tumor-associated Macrophages in High-risk HPV-related Cervical Cancer.* J Cancer, 2017. **8**(18): p. 3868-3875.
77. Mattarollo, S.R., et al., *Invariant NKT cells in hyperplastic skin induce a local immune suppressive environment by IFN-gamma production.* J Immunol, 2010. **184**(3): p. 1242-50.
78. Mattarollo, S.R., et al., *NKT cells inhibit antigen-specific effector CD8 T cell induction to skin viral proteins.* J Immunol, 2011. **187**(4): p. 1601-8.
79. R. KIRNBAUER*, F.B., N. CHENGt, D. R. LowY*, AND J. T. SCHILLER, *Papillomavirus Li major capsid protein self-assembles into virus-like particles that are highly immunogenic.* Proc. Nati. Acad. Sci. USA, 1992. **89**.
80. Harper, D.M., et al., *Efficacy of a bivalent L1 virus-like particle vaccine in prevention of infection with human papillomavirus types 16 and 18 in young women: a randomised controlled trial.* The Lancet, 2004. **364**(9447): p. 1757-1765.
81. Villa, L.L., et al., *Prophylactic quadrivalent human papillomavirus (types 6, 11, 16, and 18) L1 virus-like particle vaccine in young women: a randomised double-blind placebo-controlled multicentre phase II efficacy trial.* The Lancet Oncology, 2005. **6**(5): p. 271-278.
82. Joura, E.A., et al., *A 9-valent HPV vaccine against infection and intraepithelial neoplasia in women.* N Engl J Med, 2015. **372**(8): p. 711-23.
83. Harper, D.M. and L.R. DeMars, *HPV vaccines - A review of the first decade.* Gynecol Oncol, 2017. **146**(1): p. 196-204.
84. Hildesheim, A., *Effect of Human Papillomavirus 16/18 L1 Viruslike Particle Vaccine Among Young Women With Preexisting Infection.* JAMA, 2007: p. 743-753.
85. Bruni, L., et al., *Global estimates of human papillomavirus vaccination coverage by region and income level: a pooled analysis.* The Lancet Global Health, 2016. **4**(7): p. e453-e463.
86. Bedell, S.L., et al., *Cervical Cancer Screening: Past, Present, and Future.* Sex Med Rev, 2020. **8**(1): p. 28-37.
87. Schneider, V., *Criticism of the Pap Smear as a Diagnostic Tool in Cervical Cancer Screening.* Acta Cytol, 2017. **61**(4-5): p. 338-344.
88. Bishop, J.A. and P.K. Ha, *Human papillomavirus detection in a "Digital" age.* Cancer, 2016. **122**(10): p. 1502-4.
89. Smalley Rumfield, C., et al., *Therapeutic Vaccines for HPV-Associated Malignancies.* Immunotargets Ther, 2020. **9**: p. 167-200.
90. Chabeda, A., et al., *Therapeutic vaccines for high-risk HPV-associated diseases.* Papillomavirus Res, 2018. **5**: p. 46-58.
91. Shanmugasundaram, S. and J. You, *Targeting Persistent Human Papillomavirus Infection.* Viruses, 2017. **9**(8).
92. Khallouf, H., A.K. Grabowska, and A.B. Riemer, *Therapeutic Vaccine Strategies against Human Papillomavirus.* Vaccines (Basel), 2014. **2**(2): p. 422-62.
93. Ho, N.I., et al., *Adjuvants Enhancing Cross-Presentation by Dendritic Cells: The Key to More Effective Vaccines?* Front Immunol, 2018. **9**: p. 2874.

94. Kaufmann., A.M., et al., *Safety and Immunogenicity of TA-HPV, a Recombinant Vaccinia Virus Expressing Modified Human Papillomavirus (HPV)-16 and HPV-18 E6 and E7 Genes, in Women with Progressive Cervical Cancer.* Clinical Cancer Research, 2002: p. 3676–3685.
95. Baldwin., P.J., S.H.v.d. Burg., and C.M. Boswell., *Vaccinia-Expressed Human Papillomavirus 16 and 18 E6 and E7 as a Therapeutic Vaccination for Vulval and Vaginal Intraepithelial Neoplasia*. Clin Cancer Res, 2003. **9**: p. 5205–5213.
96. Rosales, R., et al., *Regression of human papillomavirus intraepithelial lesions is induced by MVA E2 therapeutic vaccine.* Hum Gene Ther, 2014. **25**(12): p. 1035-49.
97. Kim, T.J., et al., *Clearance of persistent HPV infection and cervical lesion by therapeutic DNA vaccine in CIN3 patients.* Nat Commun, 2014. **5**: p. 5317.
98. Trimble, C.L., et al., *Safety, efficacy, and immunogenicity of VGX-3100, a therapeutic synthetic DNA vaccine targeting human papillomavirus 16 and 18 E6 and E7 proteins for cervical intraepithelial neoplasia 2/3: a randomised, double-blind, placebo-controlled phase 2b trial.* The Lancet, 2015. **386**(10008): p. 2078-2088.
99. Santin, A.D., et al., *Human papillomavirus type 16 and 18 E7-pulsed dendritic cell vaccination of stage IB or IIA cervical cancer patients: a phase I escalating-dose trial.* J Virol, 2008. **82**(4): p. 1968-79.
100. Rahma., O.E., et al., *Pre-immature dendritic cells (PIDC) pulsed with HPV16 E6 or E7 peptide are capable of eliciting specific immune response in patients with advanced cervical cancer.* Journal of Translational Medicine, 2014. **12**.
101. Nagarsheth, N.B., et al., *TCR-engineered T cells targeting E7 for patients with metastatic HPV-associated epithelial cancers.* Nat Med, 2021. **27**(3): p. 419-425.
102. Daayana, S., et al., *Phase II trial of imiquimod and HPV therapeutic vaccination in patients with vulval intraepithelial neoplasia.* Br J Cancer, 2010. **102**(7): p. 1129-36.
103. Kenter., G.G., M.J.P. Welters., and A.R.P.M. Valentijn., *Vaccination against HPV-16 Oncoproteins for Vulvar Intraepithelial Neoplasia.* The New England Journal of Medicine, 2009.
104. Muderspach., L., S. Wilczynski., and L. Roman, *A Phase I Trial of a Human Papillomavirus (HPV) Peptide Vaccine for Women with High-Grade Cervical and Vulvar Intraepithelial Neoplasia Who Are HPV 16 Positive.* 2000: p. 3406–3416.
105. Grabowska, A.K., A.M. Kaufmann, and A.B. Riemer, *Identification of promiscuous HPV16-derived T helper cell epitopes for therapeutic HPV vaccine design.* Int J Cancer, 2015. **136**(1): p. 212-24.
106. Blatnik, R., et al., *A Targeted LC-MS Strategy for Low-Abundant HLA Class-I-Presented Peptide Detection Identifies Novel Human Papillomavirus T-Cell Epitopes.* Proteomics, 2018. **18**(11): p. e1700390.
107. Riemer, A.B., et al., *A conserved E7-derived cytotoxic T lymphocyte epitope expressed on human papillomavirus 16-transformed HLA-A2+ epithelial cancers.* J Biol Chem, 2010. **285**(38): p. 29608-22.
108. Lill, J.R., et al., *Minimal Information About an Immuno-Peptidomics Experiment (MIAIPE).* Proteomics, 2018. **18**(12): p. e1800110.
109. Wang, R., et al., *Human papillomavirus vaccine against cervical cancer: Opportunity and challenge.* Cancer Lett, 2020. **471**: p. 88-102.
110. Hanahan., D. and R.A. Weinberg, *The Hallmarks of Cancer.* Cell, 2000. **100**: p. 57–70.
111. Hanahan, D. and R.A. Weinberg, *Hallmarks of cancer: the next generation.* Cell, 2011. **144**(5): p. 646-74.
112. Burgos-Panadero, R., et al., *The tumour microenvironment as an integrated framework to understand cancer biology.* Cancer Lett, 2019. **461**: p. 112-122.
113. Ribeiro Franco, P.I., et al., *Tumor microenvironment components: Allies of cancer progression.* Pathol Res Pract, 2020. **216**(1): p. 152729.

114. Roma-Rodrigues, C., et al., *Targeting Tumor Microenvironment for Cancer Therapy.* Int J Mol Sci, 2019. **20**(4).
115. Jing, X., et al., *Role of hypoxia in cancer therapy by regulating the tumor microenvironment.* Mol Cancer, 2019. **18**(1): p. 157.
116. Petrova, V., et al., *The hypoxic tumour microenvironment.* Oncogenesis, 2018. **7**(1): p. 10.
117. Sun., Y., H. Qu., and T. Jing, *Interactions between hypoxia-inducible factor-1α and other molecules in cancer: a literature review.* Int J Clin Exp Med, 2019. **12**: p. 9158-9166.
118. Wigerup, C., S. Pahlman, and D. Bexell, *Therapeutic targeting of hypoxia and hypoxia-inducible factors in cancer.* Pharmacol Ther, 2016. **164**: p. 152-69.
119. Vito, A., N. El-Sayes, and K. Mossman, *Hypoxia-Driven Immune Escape in the Tumor Microenvironment.* Cells, 2020. **9**(4).
120. Taylor, C.T., et al., *Hypoxia-dependent regulation of inflammatory pathways in immune cells.* J Clin Invest, 2016. **126**(10): p. 3716-3724.
121. Elia, A.R., et al., *Human dendritic cells differentiated in hypoxia down-modulate antigen uptake and change their chemokine expression profile.* J Leukoc Biol, 2008. **84**(6): p. 1472-82.
122. Mancino, A., et al., *Divergent effects of hypoxia on dendritic cell functions.* Blood, 2008. **112**(9): p. 3723-34.
123. Parodi, M., et al., *Hypoxia Modifies the Transcriptome of Human NK Cells, Modulates Their Immunoregulatory Profile, and Influences NK Cell Subset Migration.* Front Immunol, 2018. **9**: p. 2358.
124. Krzywinska, E., et al., *Loss of HIF-1alpha in natural killer cells inhibits tumour growth by stimulating non-productive angiogenesis.* Nat Commun, 2017. **8**(1): p. 1597.
125. Vuillefroy de Silly, R., et al., *Phenotypic switch of CD8(+) T cells reactivated under hypoxia toward IL-10 secreting, poorly proliferative effector cells.* Eur J Immunol, 2015. **45**(8): p. 2263-75.
126. Gropper, Y., et al., *Culturing CTLs under Hypoxic Conditions Enhances Their Cytolysis and Improves Their Anti-tumor Function.* Cell Rep, 2017. **20**(11): p. 2547-2555.
127. Kukita, K., et al., *Cancer-Associated Oxidase ERO1-alpha Regulates the Expression of MHC Class I Molecule via Oxidative Folding.* J Immunol, 2015. **194**(10): p. 4988-96.
128. Kajiwara, T., et al., *Hypoxia augments MHC class I antigen presentation via facilitation of ERO1-alpha-mediated oxidative folding in murine tumor cells.* Eur J Immunol, 2016. **46**(12): p. 2842-2851.
129. Sethumadhavan, S., et al., *Hypoxia and hypoxia-inducible factor (HIF) downregulate antigen-presenting MHC class I molecules limiting tumor cell recognition by T cells.* PLoS One, 2017. **12**(11): p. e0187314.
130. Olin, M.R., et al., *Superior efficacy of tumor cell vaccines grown in physiologic oxygen.* Clin Cancer Res, 2010. **16**(19): p. 4800-8.
131. Olin, M.R., et al., *Oxygen is a master regulator of the immunogenicity of primary human glioma cells.* Cancer Res, 2011. **71**(21): p. 6583-9.
132. Dewhirst, M.W., et al., *Rationale for hypoxia assessment and amelioration for precision therapy and immunotherapy studies.* J Clin Invest, 2019. **129**(2): p. 489-491.
133. Curty, G., P.S. de Carvalho, and M.A. Soares, *The Role of the Cervicovaginal Microbiome on the Genesis and as a Biomarker of Premalignant Cervical Intraepithelial Neoplasia and Invasive Cervical Cancer.* Int J Mol Sci, 2019. **21**(1).
134. Alldredge, J.K. and K.S. Tewari, *Clinical Trials of Antiangiogenesis Therapy in Recurrent/Persistent and Metastatic Cervical Cancer.* Oncologist, 2016. **21**(5): p. 576-85.
135. Longoria, T.C. and K.S. Tewari, *Pharmacologic management of advanced cervical cancer: antiangiogenesis therapy and immunotherapeutic considerations.* Drugs, 2015. **75**(16): p. 1853-65.
136. Spurgeon, M.E. and P.F. Lambert, *Human Papillomavirus and the Stroma: Bidirectional Crosstalk during the Virus Life Cycle and Carcinogenesis.* Viruses, 2017. **9**(8).

137. Hoppe-Seyler, K., et al., *Induction of dormancy in hypoxic human papillomavirus-positive cancer cells.* Proc Natl Acad Sci U S A, 2017. **114**(6): p. E990-E998.
138. Hoppe-Seyler, K., et al., *Virus/Host Cell Crosstalk in Hypoxic HPV-Positive Cancer Cells.* Viruses, 2017. **9**(7).
139. Bossler, F., et al., *Repression of Human Papillomavirus Oncogene Expression under Hypoxia Is Mediated by PI3K/mTORC2/AKT Signaling.* mBio, 2019. **10**(1).
140. Kruse, S., et al., *Therapeutic vaccination using minimal HPV16 epitopes in a novel MHC-humanized murine HPV tumor model.* Oncoimmunology, 2019. **8**(1): p. e1524694.
141. Hughes, C.S., et al., *Single-pot, solid-phase-enhanced sample preparation for proteomics experiments.* Nat Protoc, 2019. **14**(1): p. 68-85.
142. Tyanova, S., T. Temu, and J. Cox, *The MaxQuant computational platform for mass spectrometry-based shotgun proteomics.* Nat Protoc, 2016. **11**(12): p. 2301-2319.
143. Cox, J., et al., *Accurate proteome-wide label-free quantification by delayed normalization and maximal peptide ratio extraction, termed MaxLFQ.* Mol Cell Proteomics, 2014. **13**(9): p. 2513-26.
144. Ritchie, M.E., et al., *limma powers differential expression analyses for RNA-sequencing and microarray studies.* Nucleic Acids Res, 2015. **43**(7): p. e47.
145. Tyanova, S. and J. Cox, *Perseus: A Bioinformatics Platform for Integrative Analysis of Proteomics Data in Cancer Research.* Methods Mol Biol, 2018. **1711**: p. 133-148.
146. Benjamini., Y. and Y. Hochberg, *Controlling The False Discovery Rate - A Practical And Powerful Approach To Multiple Testing.* Journal of the Royal Statistical Society, 1995.
147. Stanke, J., et al., *A flow cytometry-based assay to assess minute frequencies of CD8+ T cells by their cytolytic function.* J Immunol Methods, 2010. **360**(1-2): p. 56-65.
148. Palazon, A., et al., *HIF transcription factors, inflammation, and immunity.* Immunity, 2014. **41**(4): p. 518-28.
149. Kabakov, A.E. and A.O. Yakimova, *Hypoxia-Induced Cancer Cell Responses Driving Radioresistance of Hypoxic Tumors: Approaches to Targeting and Radiosensitizing.* Cancers (Basel), 2021. **13**(5).
150. Kosti, P., et al., *Hypoxia-sensing CAR T cells provide safety and efficacy in treating solid tumors.* Cell Rep Med, 2021. **2**(4): p. 100227.
151. Bossler, F., K. Hoppe-Seyler, and F. Hoppe-Seyler, *PI3K/AKT/mTOR Signaling Regulates the Virus/Host Cell Crosstalk in HPV-Positive Cervical Cancer Cells.* Int J Mol Sci, 2019. **20**(9).
152. Szalmas, A., *Commentary: Induction of Dormancy in Hypoxic Human Papillomavirus-Positive Cancer Cells.* Front Oncol, 2018. **8**: p. 77.
153. Ellingsen, C., et al., *pO(2) fluctuation pattern and cycling hypoxia in human cervical carcinoma and melanoma xenografts.* Int J Radiat Oncol Biol Phys, 2012. **83**(4): p. 1317-23.
154. Caradec, J., et al., *'Desperate house genes': the dramatic example of hypoxia.* Br J Cancer, 2010. **102**(6): p. 1037-43.
155. Rasmussen, M., et al., *Pan-Specific Prediction of Peptide-MHC Class I Complex Stability, a Correlate of T Cell Immunogenicity.* J Immunol, 2016. **197**(4): p. 1517-24.
156. Khan, R. and M. Seltzer, *PET Imaging of Tumor Hypoxia in Head and Neck Cancer: A Primer for Neuroradiologists.* Neuroimaging Clin N Am, 2020. **30**(3): p. 325-339.
157. Kumari, R., et al., *Azodyes as markers for tumor hypoxia imaging and therapy: An up-to-date review.* Chem Biol Interact, 2019. **307**: p. 91-104.
158. Xue, T., et al., *Strategies for Tumor Hypoxia Imaging Based on Aggregation-Induced Emission Fluorogens.* Chemistry, 2020. **26**(12): p. 2521-2528.
159. Lohmussaar, K., et al., *Patient-derived organoids model cervical tissue dynamics and viral oncogenesis in cervical cancer.* Cell Stem Cell, 2021.
160. Chumduri, C., et al., *Opposing Wnt signals regulate cervical squamocolumnar homeostasis and emergence of metaplasia.* Nat Cell Biol, 2021. **23**(2): p. 184-197.

8 Supplementary Figures

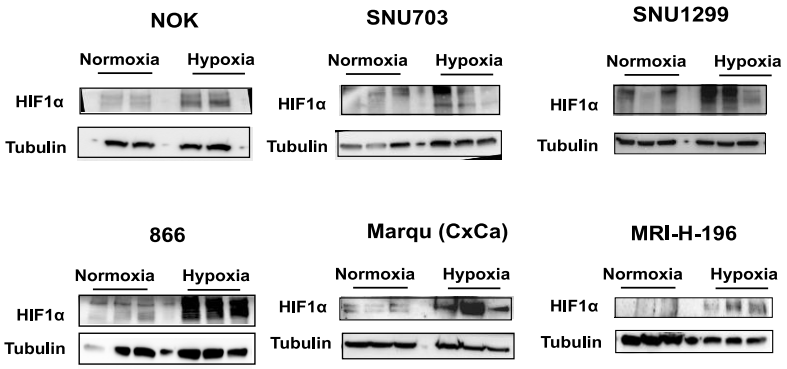

Supplementary figure 1. Hypoxia responsivity of other HPV16-transformed cells.
Western blot images of HIF1alpha levels in 24h normoxia and hypoxia treated HPV16-transformed cells (panels labelled), for which the fold change was reported in Figure 11b. All cells were treated to normoxia or hypoxia in biological triplicates, except for NOK cells where duplicates were used.

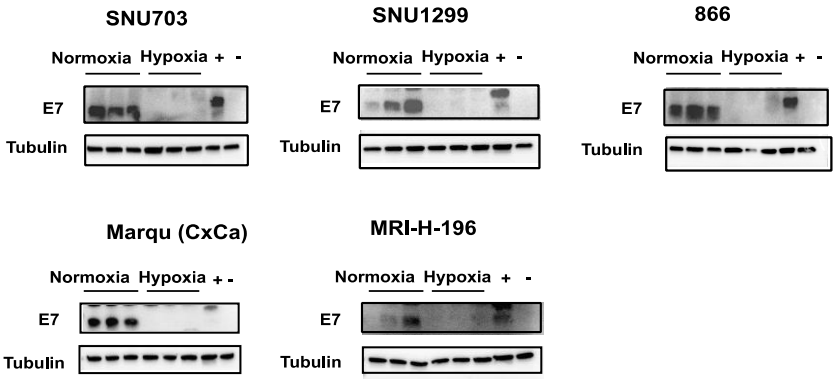

Supplementary figure 2. Decrease in E7 expression upon hypoxia exposure.
Western blots depicting E7 protein levels in 24h normoxia and hypoxia treated HPV16-transformed cells. Fold changes are depicted in Figure 14b. PAP-A2 cell lysates were used as positive controls for E7 expression (+), and 2277NS cell lysates were used as negative controls (-). The E7 molecular weight in PAP-A2 cells (20kDa) is different from HPV16-transformed cells (18kDa), since PAP-A2 express the strep-tagged version of the E7 protein [140].